Modeling and Control of Combustion Instability

by

Jean-Pierre Hathout

B.Sc., Cairo University, Egypt (1992)
M.Sc., Cairo University, Egypt (1995)

Submitted to the Department of Mechanical Engineering
in partial fulfillment of the requirements for the degree of

Doctor of Science

at the

MASSACHUSETTS INSTITUTE OF TECHNOLOGY

June 2000

Author .....
Department of Mechanical Engineering
May 18, 2000

Certified by .....
Anuradha M. Annaswamy
Principal Research Scientist and Lecturer
Thesis Supervisor

Certified by .....
Ahmed F. Ghoniem
Professor
Thesis Supervisor

Accepted by .....
Ain A. Sonin
Chairman, Department Committee on Graduate Students

Modeling and Control of Combustion Instability

by

Jean-Pierre Hathout

Submitted to the Department of Mechanical Engineering
on May 18, 2000, in partial fulfillment of the
requirements for the degree of
Doctor of Science

Abstract

Combustion instability poses substantial threat to environmentally-friendly lean-premixed combustors used for power generation and transportation, and to high-powered propulsion systems. While its global mechanism has been explained using energy arguments and encapsulated in the Rayleigh criterion, subtle interactions between the acoustic field and the "heat-release" dynamics remain unknown. Instability mitigation using passive solutions has been successful. This, however, is not without sacrificing performance as measured by emission, power or payload. Active feedback control of combustion instability has been demonstrated. However, limitations manifested by small operating envelopes, secondary resonances, and limited stability margins hinder the implementation of active control in practical systems. In this thesis, we have carried out extensive analytical and experimental studies with the objective of developing reduced-order models for combustion dynamics, and designing model-based control strategies for unstable combustors. The models capture two distinct mechanisms of combustion dynamics within the system including mixture inhomogeneity and flame kinematics. While the former has been observed previously, the latter contributed significantly to the driving mechanism. Both couple with the resident acoustics giving rise to time-delay based and phase-lag induced instabilities, respectively. The same models are used to explain observations in a number of experimental studies. Nonlinearities leading to limit-cycles are shown to arise due to phase lag between velocity and heat-release oscillations, and not due to saturation as claimed before. Active control strategies, which exploit the structure of the models, optimize an associated cost function (e.g., using an LQG-LTR controller), and are effective in the presence of time-delays (e.g., using a Posi-Cast controller), are implemented in simulations and experiments, showing superiority over empirical approaches. Bandwidth constraints, authority limitations and nonlinearities in the actuation are challenging aspects of control which are addressed for two classes of actuators that include speakers and fuel injectors.

Thesis Supervisor: Anuradha M. Annaswamy
Title: Principal Research Scientist and Lecturer

Thesis Supervisor: Ahmed F. Ghoniem
Title: Professor

To my lucky charm, Sherine.

Acknowledgments

I would like to start by thanking Professor Anuradha Annaswamy and Professor Ahmed Ghoniem who have guided me through the past five years, always impelling me to accomplish more and making me realize that I can make a valuable contribution to my field. Their role in my education, most importantly in making me mature as a researcher, has been invaluable to me. I would also like to thank Professor Harry Asada and Professor James Paduano for their support and valuable suggestions during our discussions together.

I owe a great deal to Professor Stephen Crandall who gave me the opportunity to visit MIT for the first time in the summer of 1994, as a visiting engineer, and later encouraged me to pursue a graduate education at the institute.

I am grateful to Dr. Mahmoud Fleifil with whom I collaborated, for spending time discussing my research and giving me valuable advice. It was also a great pleasure working with Jennifer Rumsey, Brent Brunell, and Ravi Prasanth.

I would like to thank my colleagues; Youssef Marzouk, Costa Petrov, Issam Lakkis, Sungbae Park, Shankar Subramaniam, Aleksandar Kojic, Ashish Krupadanam, and Mehmet Yunt for their continued support.

Finally, I would like to thank Leslie Regan and her team at the graduate student office for all their help. Thanks are also due to Kate Melvin, Susan McLean and Karla Stryker.

I owe a debt of gratitude to my wife, Sherine, who has always been there for me. I am very grateful to my parents, Virginia and Youssef, and my sister, Nathalie, for their moral support during these five years.

This work has been sponsored by the National Science Foundation, contract no. ECS 9713415, and in part by the Office of Naval Research, contract no. N00014-99-1-0448.

Contents

List of Figures

Chapter 1

Introduction

An important requirement of lean-premixed combustion systems, designed for low emission and high efficiency, as well as near-stoichiometric, high-power, high-speed propulsion systems, is stable performance over a wide range of operating conditions. Pressure oscillations which persist if stability is lost endanger the structural integrity of the engine and impact its components life-time. Practical solutions to avoid or suppress combustion instabilities have been difficult to provide, since the underlying mechanisms of the latter are not well understood and are challenging to predict in new engine designs. While combustion dynamics are governed by the acoustic characteristics, including geometry and operating conditions, as well as properties of the burning zone such as flame anchoring mechanism and combustion zone structure, scale-up rules which allow laboratories results to assist in prototype designs are not available. Clearly, there is an urgent need to examine and model the mechanisms responsible for combustion instability.

Passive and active control technologies have been explored to combat combustion instability. Passive means, including changing the flame anchoring plane, flame stabilization mechanism, and boundary conditions, and installing baffles or acoustic dampers have been used successfully. However, they may require major hardware redesign, could limit the operability of the engine, and may shift the operating conditions away from the conditions of lowest emission in lean systems [45, 56]. In such cases, active control becomes an attractive alternative.

Until recently, active control designs have been empirical and have succeeded within limited operating conditions. In fact, controllers have been shown to fail when operating conditions were shifted [20, 102]. In addition, empirically designed controllers, of the phase-shift type, could exhibit the undesirable behavior of exciting secondary instabilities [20, 75, 92, 33, 7], and no optimization framework can be implemented when these are utilized. Very little model-based control has been implemented for abating combustion instability because of the lack of accurate models.

The motivation for this thesis is to develop a system's framework for modeling and control of combustion instability [4, 27, 37, 29, 40, 38]. A physically-based, reduced-order dynamics model for an essentially laminar combustion process was derived, and model-based control designs were developed. The modeling approach was successful in revealing the mechanism leading to the instability, determining the importance of interaction between acoustic modes during actuation, explaining the origin of secondary resonance encountered with empirically designed controllers, understanding the stabilizing effect of controlled actuation, revealing the impact of actuator dynamics on the control design, and obtaining optimal control designs.

In the coming sections, a historical background of combustion instability will be presented, followed by a literature survey of the major efforts in studying combustion instabilities in experimental rigs and through full-scale numerical simulations, actuation and sensing devices in these facilities, reduced-order modeling, and control.

1.1 Historical Background

In a typical continuous combustion process, a highly-flammable fuel-air mixture is ignited, and the hot gases generated due to the chemical transformation of the mixture are used to perform certain functions. In its simplest form, the combustion process can be considered as a reacting mixture flowing in a constant area duct with a flame anchored at a specific location in the duct. The latter ignites the reactants, releasing their chemical energy in the form of heat, thus raising their temperatures and reducing their density. Combustion chambers can be viewed as organ pipes in which acoustic pressure and velocity oscillations can be sustained. Flames, which are essentially surfaces across which reactants are converted

into products, not only possess their own inherent instabilities, but are also known to respond readily to imposed fluctuations. The potential coupling between the unsteady components of pressure and heat-release rate can lead to their resonant coupling, thus growth, and has long been referred to as thermoacoustic instability.

Historically, the first observation of combustion oscillation was the "singing flame" which was discovered by Higgins in 1777 [95]. This phenomenon caught the interest of several researchers [24, 16] and they described that high levels of sound can be produced by placing a flame, anchored on a small diameter fuel supply tube in a larger diameter tube. The flame was found to excite the fundamental mode or one of the harmonics of the larger tube. The "dancing flame" was discovered later by Le Conte [16] where a flame pulses in synchronization with the audible beats of music. "It was exceedingly interesting to observe how perfectly even the trills [1] of the musical instrument were reflected on the sheet of the flame. A deaf man might have seen the harmony!", he quoted.

Concomitantly, Rijke [73] showed that sound can be generated in a vertical tube open at both ends by placing a heated metal gauze inside the tube. The sound was heard only when the heating element was placed in the lower half of the tube, specifically at a distance of a quarter the tube length from the bottom. Rayleigh [80] was the first to hypothesize the onset of the instability, and define a criterion for positive coupling based on a phenomenological, heuristic, description of the instability, his explanation was as follows: "If heat be periodically communicated to, and abstracted from, a mass of air vibrating in a cylinder bounded by a piston, the effect produced will depend upon the phase of the vibration at which the transfer of heat takes place. If heat be given to the air at the moment of greatest condensation or to be taken from it at the moment of greatest rarefaction, the vibration is encouraged. On the other hand, if heat be given at the moment of greatest rarefaction, or abstracted at the moment of greatest condensation, the vibration is discouraged". This can also be compared to a thermodynamic cycle (e.g. the Carnot engine). In a continuous combustion process, the engine will be doing work against the acoustic field instead of the piston.

Afterwards, many researchers [79, 103, 9, 10, 23], restated the context of Rayleigh's

[1] The alternation of two musical tones a scale degree apart.

criterion indicating the importance of the phase between the pressure oscillations and the unsteady heat addition in encouraging the instability. The "famous" Rayleigh criterion is best described as this phenomenological inequality [81]

$$\int_0^\tau \int_0^V p'(x,t)q'(x,t)dvdt \;\; > \;\; \int_0^\tau \int_0^V \Phi(x,t)dvdt, \tag{1.1}$$

where p' and q', are the perturbation in pressure and the heat release, respectively, τ, V and Φ are the period of oscillation, the control volume (the combustor volume) and the wave energy dissipation, respectively.

Thermoacoustic instability occurs when the inequality, Eq. (1.1), is satisfied. The LHS and RHS of the inequality describe the total mechanical energy added to the oscillations by the heat addition process per cycle and the total energy dissipated by the oscillation per cycle, respectively. Normally, the acoustic dissipation in combustors can be assumed very small (RHS$\sim$ 0). The LHS of Eq. (1.1) indicates that to satisfy the Rayleigh criterion a specific relationship between p' and q' must exist. Assuming that p' and q' have a periodic time dependence, the sign of the time integral of their product will depend on the ratio $\frac{\tau_o}{\tau}$ where τ_o is the phase difference between p' and q'. A simple evaluation of the integral shows that it is a maximum (positive) when $\frac{\tau_o}{\tau} = 0, 1, 2..$ and minimum (and even negative) when $\frac{\tau_o}{\tau} = \frac{1}{2}, \frac{3}{2}, ..$ This agrees with Rayleigh's hypothesis; p' and q' in phase will lead to instability. On the other hand, when p' and q' are out of phase, the effect will be a stabilizing one. Note that the integrals are also spatial, which means that both effects, destabilizing and stabilizing, can occur in different locations of the combustor, and at different times, and the stability of the combustor will be decided by the net mechanical energy added to the combustor. Since compressions in the acoustic field are essentially isentropic [23], i.e. pressure, temperature and density oscillate in phase in the field, the inequality can become valid also if the integral in the LHS involves the dynamics between the heat release fluctuations and either of these variables.

Thermoacoustic instability occurs because of the two-way coupling between combustion exothermicity and acoustics. A dynamics point of view for explaining the instability is that the acoustic field and the heat release source (the flame) are connected dynamically in

positive feedback [4].

In most cases, combustion instabilities are undesirable since, as observed in large scale engines, they are manifested by growing heat release and pressure oscillations. These severe fluctuations are dangerous since they can lead to excessive vibrations resulting in mechanical failures, high levels of acoustic noise, high burn and heat transfer rates, and possibly component melting. The oscillations are not a menace in all systems. In fact, the operation of pulsed combustors and ramjet engines inherently depend on the presence of sustained oscillations [103].

Recently, the problem is becoming more relevant because of the stringent low emission and high-power requirements. Modern, low NO_x emission equipment as well as high-power near stoichiometric operated engines are prone to these instabilities due to the nature of the flame stabilization mechanisms, the premixing of fuel and air prior to combustion, and the staging of the combustion process. Interest in understanding the physics involved in the instability has grown, and is being used to abate it through passive control means and most recently through the use of active feedback control (for more information, see [13, 57, 37]).

In the following sections, we focus on the efforts that were recently performed with the goal of abating combustion instability in both lean-premixed, near-blowout combustion and near-stoichiometric, close-to-flashback combustion. These include experimental investigation, computational fluid dynamics (CFD) simulations, reduced-order models, actuation and sensing techniques, and control design.

1.2 Literature Survey

1.2.1 Experimental Investigations

Experiments were carried out with the objective of investigating combustion dynamics and the different coupling mechanisms between flow, acoustics and heat release dynamics [45, 56, 75, 46, 9, 96]. A 2-D dump combustor operating at equivalence ratios of $0.8 < \phi < 0.86$ was studied in [45]. Three modes of instability, at three different frequencies were identified;

"humming", "buzzing" and "chucking". Transitioning between different modes was achieved by changing the boundary or the equivalence ratio, and the flame structure exhibited what appeared to be modulations in response to organized large-scale vortical structures. Forcing using a loudspeaker led to similar flame modulations. A similar geometry was used in [56] with $0.48 < \phi < 0.7$, where CH radical emissions was measured to quantify the heat release rate. Under forced conditions, the flame structure exhibited a variety of length scales, with the dominant frequency corresponding to the quarter wave acoustic mode. Forcing at frequencies higher than the naturally resonant mode stabilized the combustor. Modulation at the unstable or lower frequencies drove the system to instability. A similar combustor operating near stoichiometric conditions was used in [75]. Flame oscillations driven by a very large vortical structure, shed regularly at the step, controlled the instability, with large changes in the velocity. Increasing the mean velocity did not affect the amplitude of the velocity oscillations, but decreased the amplitude of the pressure oscillation, without changing the frequency. Changing the boundary conditions shifted the frequency. The Rayleigh index was seen to be positive in regions where the vortices were growing, and negative reaching minimum at the point of wall impingement.

In a related paper, Candel and co-workers considered a premixed-dump combustor with a square cross section and five reactants jets at $\phi = 0.8$. A low-frequency instability, occurring at the eigen frequencies of the system, was shown to be acoustically coupled. For stable combustion, $\phi < 0.8$, interaction between the middle jet and the outer jets was noticed, while for unstable combustion, $\phi > 0.8$, the jet remained parallel to the centerline and large recirculation zones formed in the wake of the other jets suggesting flame vortex interaction. In [9], a "reheat buzz" instability that occurs in an afterburner was studied in an axisymmetric combustor with a flame stabilized behind a conical gutter, under lean conditions. The fundamental quarter wave mode was unstable, with larger pressure oscillations level at the higher equivalence ratio. System identification was used to obtain heat release dynamics models.

In [96], a lean-premixed axisymmetric coaxial dump combustor was investigated. The flame was stabilized in the wake of a swirler and a bluff center body. The equivalence ratio was varied from lean blow-out to stoichiometric. Observations indicated that under

stable conditions, a narrow flame, collapsed near the centerline, did not interact with the large vortices in the recirculation zones. On the other hand, an axially spread flame led to instability. These observations were corroborated by high positive Rayleigh index at the outer shear layer. Vortex-flame interaction supported the instability when increasing the mean flow (contrary to [75]), decreasing the swirl number, decreasing the swirl number, decreasing the equivalence ratio, lowering the recess between the bluff body and the dump plane, or increasing the mixture inhomogeneity. Moreover, the flame surface area fluctuations were found to be in phase with pressure fluctuations, supporting the result in [25], and in phase with the equivalence ratio fluctuations [39]. The latter was shown to cause instability in certain combustors [74, 15].

Several experimental investigations have been reported pertaining to active control of thermoacoustic instability, which can be grouped under the following four categories. In the first, the idea was to use the concept of anti-sound and phase-shift control strategy, and has been used in [56, 20, 102, 75, 92, 33, 96, 15, 88, 87, 55, 36, 35]. In all these cases except [15, 87], the combustor rig was a laboratory-scale, while in these an industrial rig was used, with pulsed-fuel injection as the actuation device. In the second category, a low-frequency open-loop control strategy was used to pulse the fuel injector between two operating points that correspond to stable oscillations [82]. In [47, 42], it was observed that changing the equivalence ratio could create a hysteresis loop with two branches, one stable and the other unstable, and that forcing causes jumps from the unstable to the stable branch. In the final category [66], an on-line observer was used to identify the amplitudes and frequencies of the pressure oscillations and a phase-shift control strategy is used to suppress the oscillations.

The above discussion shows the richness of the dynamics involved in combustion instability. The focus in this thesis is to study the dominant dynamics causing the heat-release/acoustics coupling. In order to accomplish this, we neglect vortex shedding and vortex-flame interaction, and assume weak to moderate turbulence conditions in the combustion system. As shown in Chapter 2, we focus on two main mechanisms that can drive to instability, namely, (i) coupling of the flame area, hence the heat-release, with the acoustics through velocity perturbations, and (ii) coupling of the heat release with the pressure perturbations through equivalence ratio perturbations.

1.2.2 Numerical Simulations

Numerical CFD simulations have been used to gain insight into some of the intrinsic mechanisms of combustion instability using different physical models and numerical schemes [92, 76, 64, 51, 59, 44]. In [64], a cavity-type combustor with an intake duct and an exhaust pipe was used. The flow in the combustor section, assumed to be low-Mach number, compressible, viscous and 2D, was obtained by solving the unsteady Navier-Stokes equations, and a thin flame whose burning velocity depended on the local curvature was adopted. The flow in the exhaust duct was taken to be inviscid, compressible and 1D. The solution revealed strong interactions between the convective instabilities of the separating shear layer, the flame and the acoustic field. Velocity and pressure oscillations at five different frequencies were recorded, with the strongest peak at the lowest frequency which was near that of the convective instability of the recirculation zone. The interaction between the flame and the vortical structures downstream the dump plane caused the heat release unsteadiness. Response to high and low-frequency forcing confirmed the results in [56].

In [92, 76] a dump combustor with a flame stabilized at the recirculation zone was simulated. In [76], the flow was assumed to be compressible, inviscid and 2D, and a thin flame model was employed with a burning velocity which varied with the local pressure. Results showed that a short duct with open-open ends was stable, while the long duct with closed-open ends was unstable at the quarter wave mode frequency. Although the simulation predicted the unstable acoustic mode, flame wrinkles due to vortical structures were not captured. The simulation was repeated using more elaborate numerical techniques in [92]. In this case, the flow was assumed to be viscous and the flame was artificially thickened which proved more accurate. By forcing the combustor at the inlet section at 500 Hz, flashback was predicted.

A simulation of the instability in an axisymmetric dump combustor was done in [59]. The flow was considered viscous, and compressible and the flame was assumed to be thin. The evolution of the latter was modeled using the G-equation with a local flame velocity which depended on the local turbulence intensity. It was shown that the half-wave acoustic mode was unstable. Simulations were carried out at different Mach numbers. The frequency of

the unstable mode increased with increasing the Mach number up to 0.45 where it remained at the inlet duct acoustic mode. This study showed that both the convective and acoustic resonant modes were present in the flow, but only one mode dominated at any given condition. In [50], combustion was modeled as a Well-Stirred reactor (WSR) and the feedline characteristics imposed perturbations in the equivalence ratio. The model predicted roll-off frequencies of the order of 500 to 1000 Hz, but did not capture instability. This may be because at the acoustic frequency, no phase lag is present in the WSR model. The link between equivalence-ratio perturbations and heat release has also been made elsewhere [15, 74].

In [44] a coaxial dump combustor of an idealized ramjet engine was simulated. The flow was assumed to be compressible and inviscid. A simplified two-step parametric model was used to compute the heat release. In cold flow, forcing at the first longitudinal mode of the combustor which was in the range of the locally most amplified frequency near the dump plane produced periodic coherent vortex structures, suggesting that the low-frequency oscillation in the combustor was induced by a vortex-merging mechanism resulting from the interaction between vortex-rollup frequency and acoustic frequency in the inlet duct. The low-frequency instability was shown to depend on the length as well as the sonic speed in the inlet duct. In a reacting flow, the energy release altered the flow field by destroying the pattern of vortex merging, and a new pattern dominated by a large vortex appeared. the dominant mode frequency was close to that observed in the cold flow, which was near to the quarter-wave mode inlet duct.

Although the CFD simulations are a good tool to gain insight into the dynamics of the instability, they lack the amenability for use in model-based control design. Numerical simulations are mostly used for diagnostic reasons when information is hard to obtain from experiments. Therefore, the need for accurate reduced-order models that capture combustion instability is pertinent for model-based control. The state of the art in reduced-order modeling will be presented next.

1.2.3 Models

Most of the modeling efforts so far have focused on the system's acoustics [46, 9, 47, 66, 76, 100], with the heat-release dynamics represented by a phase-lag relationship as suggested by Crocco [17]. Linear heat release dynamics models were also obtained by system identification [9], or by modeling the heat release dynamics as a time delay [20]. The model in [9] along with a single-frequency acoustic model led to a successful design of a stabilizing controller. Time delay was applied in another study [66] to model the mixing of cold reactants with hot gases by large scale fluid motions, In [46] the expansion due to heat release was modeled as a volume mass source, with the strength of the latter obtained from a measured spectrum for the heat release. Combining this with a single-frequency acoustic model, the unstable modes were predicted.

Nonlinear models of the combustor dynamics have also been obtained. In [82] a control volume approach was used to get a set of ODEs that govern the dynamics of the fuel nozzle, combustion chamber, and tailpipe region. The combustion process was modeled as a WSR governed by a one-step reaction. The model was used successfully to predict instability. In other studies, it was recognized that flame dynamics was the primary source of nonlinearity [20, 74]. In [20], a nonlinear heat-release model based on saturation in the flame surface area due to flow reversal at large flow perturbations was developed and used to predict limit cycle in a bluff-body combustor. In [74] a nonlinear model of the heat release dynamics, based on saturation in the flame response to large equivalence ratio perturbations, was used to predict limit cycles. On-line system identification was applied, e.g., in [66], and the frequencies, amplitudes, and phases of the dominant modes of the combustor were tracked. This method was used to design a controller that could deliver additional heat release out of phase with the unstable pressure mode, using a secondary fuel injector.

Despite such large effort to model combustion instability analytically, most of these models fail to predict the relationship among the heat-release dynamics, the mixing dynamics, the mixing and the burning rate, and the acoustic field. Although the single-mode acoustic model [46, 9, 47, 66, 100] may be sufficient for prediction of instability, it may not be accurate for control design. On-line system identification of heat-release dynamics [9] suffers

from the fact that it is valid only at the particular condition at which system identification was performed, and may not readily be generalizable to different operating conditions and geometries. On-line identification of an unstable system [66] is not robust and its validity is yet to be determined. the validity of the WSR assumption to model the combustion process dynamics under moderate turbulence intensity is yet to be determined [82]. Nonlinear heat-release models based on saturation [20, 74] still need to be verified and it remains to be seen if saturation is indeed the dominant nonlinear mechanism. Actually, we show in Chapter 5 that yet another mechanism pertaining to an amplitude-dependent phase lag between heat release and acoustics is crucial in a establishing the limit cycles.

Recently, at MIT, a heat-release dynamics model for a wrinkled premixed flame, stabilized on a perforated plate, forced by perturbations in the acoustics and the equivalence ratio, a multi-mode acoustic dynamics model, and actuator dynamics models were developed [25, 4, 27, 37, 39, 29, 40, 38]. We used the coupled models to design low order as well as optimal controllers, which are successfully used to suppress instability in a laboratory combustor [37, 5]. The merits of these models and how they were used in gaining much more more insight into the combustion instability and designing optimal control will be presented in this thesis.

1.2.4 Actuation and Sensing

The feasibility of active control depends on the performance of sensors and actuators. High-bandwidth sensors are available in the form of pressure transducers and microphones, and heat release sensors, in the form of photodiodes, photomultipliers, and radiometers. More recently, optical planar mapping and equivalence ratio sensors have become available. Actuation has been more challenging due to bandwidth and authority requirements. Successful actuators include speakers [75], oscillating center bodies [9], moving airfoils or flaps, and stream-wise or cross-stream reactants jets [56]. Direct means for varying the heat release through fuel or air stream oscillation, i.e., equivalence ratio oscillations can be achieved acoustically [7], or using solenoid injectors [9, 102, 88, 55, 82, 15].

Actuators have been hindered by limitations in the bandwidth, as well as saturation.

For instance, in [4, 37, 27], saturation was a primary limitation, which was overcome by using optimal control techniques that decreased the required control effort. Most often, fuel injectors are solenoid operated, and the hardware imposes limitations on the bandwidth of the valve. Fast-response valves are becoming available (e.g., Moog Direct-Drive Valve, which is a proportional valve, has shown an operational bandwidth of 450 Hz [36]). On-off injectors that allow a constant flow rate preset by the differential pressure across the valve when it is set *on* are the most common [9, 102, 88, 55, 82, 15]. Modulation of the fuel flow can be achieved by controlling the opening time in open loop [82, 102, 88]. Alternatively, the valve is controlled by feedback of the pressure/heat release output [102, 9]. The former approach makes no use of the knowledge of either the amplitude or the frequency of the instability, while the latter makes use only of the frequency and positive parts of the output signal. Logical operators that set/modulate the pulse and/or the frequency of injection in closed-loop were also tested. A scheme to actuate at the instability frequency while changing periodically the pulse width, proportional to the amplitude of the measured output signal, was presented in [55]. In [102], injection at higher harmonics of the instability were discussed.

In [37, 5], it was shown that the incorporation of the loudspeaker dynamics plays a crucial role in designing optimal controllers. The impact of actuation on the system dynamics was investigated in [39], the impact of actuation from flow sources (e.g., speakers) and heat sources (e.g., injectors) was studied from an energy viewpoint. More insight on how work exchange between actuators and the combustor is modulated for decreasing the acoustic energy in the combustor, was extracted, and this clarified as to how energy exchanges translate into damping in the combustor. The above aspects will be discussed in details in the thesis.

1.2.5 Control

Over the years, two different approaches have been suggested for designing an active controller: an experimental strategy, and an approach based on a theoretical model. Examples of the first category include [48, 9, 75, 49, 33, 34, 56, 8]. Typically, the approach therein is to design an electronic circuit that consists of a filter and phase-shifter, tune the parameters of this circuit so that the amplitude of the unstable frequency is attenuated. However, in many

of these studies, it has been found that this may introduce secondary peaks in the closed-loop system. These peaks occur at frequencies which may not correspond to the natural acoustic modes, indicating that it is a result of the control design.

Model-based active control solutions have been suggested in [9, 8, 32, 31, 100, 93]. Here, the laws that govern thermal acoustics are employed to obtain a description of the underlying dynamics. Conservation equations and constitutive relations make it possible to analyze combustor dynamics, quantify its properties in relation to various parameters such as its geometry, operating conditions (equivalence ratio, flow rate, etc), and design principles (for flame stabilization, cooling, etc.), and predict its behavior as the system parameters are changed. In [9], a model-based control design is discussed while the analysis is limited to the unstable frequency. It is shown that the controller stabilizes the system using a Nyquist criterion. In [8], a theoretical approach such as the LMS [97] is used. The model is determined using an input-output system identification approach by sweeping the input frequency over the desired range. The same approach is used in [93] as well, except that the μ-synthesis method is employed for control.

A control design methodology based on a physically derived model, first and foremost, provides: (1) The guidelines for efficient design that should generate satisfactory performance with minimal control effort. (2) Information regarding the dynamic range and bandwidth of the actuators and sensors, as well as the respective locations that can yield an optimal performance. (3) A better insight into the process itself by showing how the active controller modulates the gain-phase characteristics between the pressure and the heat release. The latter provides insight into the choice of the design parameters such as the flame stabilizing mechanisms, geometry, etc., and the coupling mechanisms in the combustion process and their dependence on the boundary conditions. For example, we can explain why "secondary peaks" appear for certain boundary conditions [27].

In [32, 31, 100], the authors use a physical-law-based model and a control design strategy drawn from modern control theory. While we use a similar approach, our contribution in this paper is distinguished by three points: (1) We employ a heat release dynamics model based on flame kinematics to describe the relationship between the amplitude and phase of the heat release rate and the acoustic field [26]. (2) We retain the coupling between acoustic

modes. While ignoring the coupling of the mode has a small effect on predicting the growth rate, it is inadequate for designing a controller [4] since it may not accurately determine the phase lag between the control input and the pressure response for certain actuator-sensor locations. (3) We provide an insight into how the active controller modulates the gain-phase characteristics of the combustor thereby stabilizing it.

1.3 Summary and Goals

In the Sec. 1.2, we presented an extensive literature survey of most of the efforts pertaining to understanding, modeling and controlling combustion instabilities. As discussed previously, experiments and CFD simulations represent diagnostical tools to understand the underlying combustion dynamics. Physically-based modeling supported by observations taken from experimental data will be the main tool used in this thesis to shed more light on the physics, derive a reduced-order model and use the latter for designing model-based control.

The richness of dynamics in combustion instabilities and the myriad of mechanisms including acoustics, fluid mechanics, flame kinematics, chemical kinetics, and other system related phenomena such as feedline dynamics, actuators dynamics and the concomitant coupling mechanisms make the task of modeling and control of such systems challenging and complex. Our aim here is to focus on the dominant processes and their interactions.

To achieve our goals, we will (i) decompose the problem into various processes that contribute to the dynamics, mainly heat release and acoustics, (ii) identify the interactions between these processes, (iii) model the individual processes and the interactions using physically-based and model reduction methods, (iv) validate the models with available experimental data, (v) model the effect of actuators on the combustion dynamics, (vi) model the intrinsic dynamics of actuators (vii) design appropriate control strategies, implement them and compare them to experimental results when available.

Chapter 2

Modeling of Combustion Instability

The two prongs of a combustion instability, the acoustic field which acts as the host oscillator and the combustion heat-release dynamics process which acts as the driver, must be carefully modeled to provide the framework for developing the active control strategy. In this chapter, we will first derive a model describing the heat-release dynamics in a combustor, then the acoustics in the combustor chamber will be modeled when either longitudinal or bulk modes are excited. The unsteady heat release drives the acoustics to instability through different coupling mechanisms. One possibility is through area fluctuations which was measured in [9], and modeled in [25]. The other possibility is through mixture inhomegeneity (reactants' equivalence-ratio fluctuations), observed as early as in [79], and modeled in [29, 40]. It has been observed that the area fluctuations destabilize longitudinal modes in general [4, 48], whereas equivalence-ratio fluctuations destabilize the bulk mode of the combustor [15, 29] as well as longitudinal modes [83], this will be discussed in Sec 2.4 where the stability of the overall model is studied.

2.1 Heat-Release

The heat-release dynamics will be studied for a generic flame anchored at its base. Two methodologies are used, a flame kinematics approach which uses the G-equation [25], and a lumped-model approach which relies on conservation equations arguments. We study the

effect of forcing fluctuations in the velocity as well as in the equivalence ratio on the unsteady heat release. The model is reduced to a dynamic ODE which is amenable for control design.

2.1.1 Flame Kinematics Model

The goal of this section is to derive an analytical model for the heat-release rate in response to simultaneous perturbations in the flow velocity, u, and the equivalence ratio, ϕ. The two effects were modeled separately in [25] and [29]. In the latter, a similar attempt was made, albeit using a lumped parameter model derived from the conservation of mass and energy. Here, we use the flame kinematics equation.

We make the following assumptions: (i) The flame is a thin interface separating reactants and products and is insensitive to pressure perturbations [9]. The flame can model turbulent premixed combustion if conditions of high Damkohler number and weak to moderate turbulence intensity prevail [64]-[22]. (ii) The flame is weakly convoluted, i.e., it can be described by a single-valued function, $\xi(r,t)$, describing the instantaneous location of its surface. In this case, ξ and the heat release, Q, are given by[1]

$$\frac{\partial \xi}{\partial t} = u - v\frac{\partial \xi}{\partial r} - S_u(\phi)\sqrt{\left(\frac{\partial \xi}{\partial r}\right)^2 + 1}, \tag{2.1}$$

$$Q = \kappa(\phi)\int_0^R \sqrt{1+\left(\frac{\partial \xi}{\partial r}\right)^2}\,dr, \tag{2.2}$$

where S_u is the burning velocity, $\kappa(\phi) = 2\pi\rho_u S_u(\phi)\Delta h_r(\phi)$, ρ_u is the density of the unburnt mixture, and Δh_r is the enthalpy of reaction per unit mass of the mixture.

Assuming negligible velocity component in the radial direction, and linearizing around nominal values $\overline{u}$, $\overline{S}_u$, and $\overline{\xi}(r)$, denoting $\overline{(.)}$ and $(.)'$ as steady and perturbation, respectively, we get

$$\frac{\partial \xi'}{\partial t} = u' + \overline{S}_u\frac{\partial \xi'}{\partial r} + \frac{\partial \overline{\xi}}{\partial r}\left.\frac{dS_u}{d\phi}\right|_{\overline{\phi}}\phi', \tag{2.3}$$

[1]We consider here a flame stabilized over a perforated plate, R is the radius of the perforation.

with boundary conditions[2]

$$\xi'(R,t) = 0 \ \forall\, t, \qquad \xi'(r,0) = 0 \ \forall\, r,$$

while

$$Q'(t) = \overline{\kappa}\int_0^R \xi'(r,t)dr + d_1\phi', \tag{2.4}$$

where[3]

$$\overline{\kappa} = 2\pi\rho_u S_u \Delta\overline{h}_r, \text{ and } d_1 = 2\pi\rho_u \left(\overline{S}_u \left.\frac{d\Delta h_r}{d\phi}\right|_{\overline{\phi}} + \Delta\overline{h}_r \left.\frac{dS_u}{d\phi}\right|_{\overline{\phi}}\right)\left(\int_0^R r\overline{\xi}dr\right).$$

It is worth noting that the flame area fluctuation, A'_f, is given by $A'_f(t) = 2\pi\int_0^R \xi'(r,t)dr$. This with Eq. (2.3) shows that the flame area is affected by both u' and ϕ', and the area in turn impacts Q' as shown in Eq. (2.4). This also shows that ϕ' affects directly Q' and indirectly through the area fluctuations.

Equation (2.3) can be manipulated further and solved for ξ' in the Laplace domain as:

$$\xi'(r,s) = \left(\frac{u'(s)}{s} + \frac{\partial\overline{\xi}}{\partial r}\left.\frac{dS_u}{d\phi}\right|_{\overline{\phi}}\frac{\phi'(s)}{s}\right)\left(1 - e^{-(R-r)\frac{s}{\overline{S}_u}}\right), \tag{2.5}$$

where s is the Laplace operator. Differentiating Eq. (2.4) with respect to time, and using Eq. (2.3), we get

$$\dot{Q}' = \overline{\kappa}\int_0^R \left(u' + \overline{S}_u\frac{\partial\xi'}{\partial r} + \frac{\partial\overline{\xi}}{\partial r}\left.\frac{dS_u}{d\phi}\right|_{\overline{\phi}}\phi'\right)dr + d_1\dot{\phi}', \tag{2.6}$$

which is integrated over r, as

$$\dot{Q}' = \overline{\kappa}\left(Ru' - \overline{S}_u\xi'(0,t) + \int_0^R \frac{\partial\overline{\xi}}{\partial r}\left.\frac{dS_u}{d\phi}\right|_{\overline{\phi}}\phi' dr\right) + d_1\dot{\phi}'. \tag{2.7}$$

[2]It should be noted that with the appropriate change in coordinates and boundary conditions, Eq. (2.3) can also represent flames stabilized behind a gutter [19], or a dump [74].

[3]The factor $\left.\frac{d\Delta h_r}{d\phi}\right|_{\overline{\phi}}$ is positive and $\left.\frac{dS_u}{d\phi}\right|_{\overline{\phi}}$ is also positive when $\phi \leq 1$.

Taking the inverse Laplace of Eq. (2.5) at $r = 0$, and substituting in Eq.(2.7), after some manipulations, we get

$$\dot{Q}' = \overline{\kappa}\left(Ru' - \overline{S}_u \int_{t-\tau_f}^{t} u'(\tau)d\tau + \overline{S}_u d_2 \int_{t-\tau_f}^{t} \phi'(\tau)d\tau + d_3\phi'\right) + d_1\dot{\phi}', \tag{2.8}$$

where $d_2 = \frac{d\bar{\xi}}{dr}\Big|_0 \frac{dS_u}{d\phi}\Big|_{\overline{\phi}}$, $d_3 = -\overline{\xi}(0)\frac{dS_u}{d\phi}\Big|_{\overline{\phi}}$, and $\tau_f = R/S_u$ is the characteristic propagation delay of the flame surface into the reactants flow. Note that for the class of flames considered here, the slope at the flame tip, which is typically conical, is zero, therefore the third term in the RHS of Eq. (2.8) can be omitted. Therefore, the model simplifies to

$$\dot{Q}' = e_1 u' + e_2 \int_{t-\tau_f}^{t} u'(\tau)d\tau + e_3\phi' + d_1\dot{\phi}', \tag{2.9}$$

where for compactness we denote $e_1 = \overline{\kappa}R$, $e_2 = -\overline{\kappa}\overline{S}_u$, and $e_3 = \overline{\kappa}d_3$. The implications of the infinite dimensional dynamics exhibited in Eq. (2.9) on the acoustics will be discussed in details in Sec. 2.4. In the latter, stability will be studied when velocity and/or equivalence ratio fluctuations exist.

Next, we present a lumped-parameter approach for modeling the burning zone dynamics. Although, the approach uses a more simplified analysis, we will show that the result is qualitatively similar to the result shown in Eq. (2.9).

2.1.2 Lumped Heat Release Model

Modeling of the heat release dynamics is a challenge that has been clouded by the intricacy of turbulent combustion. One way of alleviating the complexity is by modeling turbulent premixed combustion, at high Damkohler numbers and weak to moderate turbulence intensity, as wrinkled laminar flames [64]. Thus, the rate of heat release, Q_f, is governed by the flame area, A_f, and the local burning rate per unit area along the flame surface, the laminar burning velocity, S_u, as

$$Q_f = \int_{A_f} \Delta h_r \rho_u S_u dA. \tag{2.10}$$

A flame front in premixed gaseous reactants behaves like a wave which is advected by the local flow velocity while propagating into the reactants in the direction normal to itself at a velocity S_u. Its shape is defined by the flow field in which it propagates as well as its self propagation velocity. It follows that S_u has two effects on the heat-release rate: a direct effect, and an indirect effect through its contribution to A_f. In turn, S_u depends on the thermodynamic conditions, i.e., pressure and temperature, the dynamic conditions, i.e., strain and rate of curvature, and the mixture properties, i.e., equivalence ratio. Δh_r is also strongly dependent on the equivalence ratio. In addition, S_u is dependent on the heat loss, which is a function of the flame stabilization environment and the flow conditions, especially at lean, near-flammability conditions. An accurate model of the heat-release dynamics should be able to correctly represent all these dynamics and predict the interaction among them.

A rigorous derivation of the response of a flame surface to velocity perturbation using the kinematics of a wrinkled laminar flame has been presented in [25], and augmented for equivalence ratio perturbations in Sec. 2.1.1. An alternate simpler yet more revealing derivation of the heat release dynamics is derived in this section based on mass and energy conservation arguments. The strength of this methodology lies in its flexibility in accommodating additional effects from other significant factors that might vary with time, including the burning velocity, the equivalence ratio, the mixing intensity and the density, besides the velocity that was addressed in [25].

The total heat release rate can be expressed as

$$Q_f = \beta A_f, \tag{2.11}$$

where $\beta = \rho_u S_u \Delta h_r$, note that S_u here is thought to be averaged along the flame surface. Equation (2.11) illustrates that the heat release rate depends on two basic components: mixture conditions, β, and surface area, A_f. The strength of this separation will be apparent below where we will show that heat release perturbations can be caused by surface area changes which can be affected by either the velocity field perturbations or S_u, and mixture conditions changes.

Applying mass conservation to a control volume bounded by the flame surface and a

virtual surface at the flame anchoring plane, and assuming a constant ρ_u, we get

$$\frac{dV_f}{dt} + S_u A_f = A_d u, \tag{2.12}$$

where V_f is the volume of accumulated reactants in the control volume, $A_d = \pi R^2$, and R is the flame base radius. For a general flame shape, one can assume that $V_f = \alpha A_f$, where α is a kinematics parameter function of the flame geometry, and dependent on the velocity field, the mixture condition and can be derived by the flame kinematics as in Sec. 2.1.1. By substitution, Eq.(2.12) becomes

$$\dot{A}_f + \omega_f A_f = A_d \frac{u}{\alpha} \tag{2.13}$$

which represents the evolution of the flame area. The flame characteristic frequency is $\omega_f = \frac{S_u + \dot{\alpha}}{\alpha}$. The heat release dynamics, using Eq. (2.11), can be derived as

$$\dot{Q}_f + \omega_q Q_f = A_d \frac{\beta}{\alpha} u. \tag{2.14}$$

where $\omega_q = \omega_f - \frac{\dot{\beta}}{\beta}$ is the heat release characteristic frequency. Equations (2.13) and (2.14) show that the flame surface area and the heat release behave as first order filters with characteristic frequencies which depend on the burning velocity and the flame geometry. The frequencies also depend on the time rate of change of the flame geometry and the flow condition.

Linear Heat Release Model

To assess the linear stability of the combustor, we linearize Eqs. (2.13) and (2.14) by assuming small perturbations around the mean parameters:

$$\dot{A'}_f + \overline{\omega}_f A'_f = A_d \frac{\overline{u}}{\overline{\alpha}} \left(\frac{u'}{\overline{u}} - \frac{S'_u}{\overline{S}_u} - \frac{\dot{\alpha}'}{\overline{\omega}_f \overline{\alpha}} \right), \tag{2.15}$$

$$\text{and } \dot{Q'}_f + \overline{\omega}_q Q'_f = A_d \frac{\overline{\beta}}{\overline{\alpha}} \overline{u} \left(\frac{u'}{\overline{u}} + \frac{\rho'_u}{\overline{\rho}_u} + \frac{\Delta h'_r}{\overline{\Delta h}_r} - \frac{\dot{\alpha}'}{\overline{\omega}_f \overline{\alpha}} + \frac{\dot{\beta}'}{\overline{\omega}_f \overline{\beta}} \right), \tag{2.16}$$

where $\overline{\omega}_q = \overline{\omega}_f = \frac{\overline{S}_u}{\overline{\alpha}}$, and $(.)'$ is the perturbation around the mean, $\overline{(.)}$.

The above equations show that while the flame surface area responds to changes in the burning velocity, S_u, the rate of heat release responds only to fast changes in S_u, as described by $\dot{\beta}'$. The reason is that the effect of the slow changes in S_u on the flame area counteracts the effect of changes in S_u. This latter is due to the dependence of Q'_f on S'_u through β', directly, and A'_f, indirectly (see Eq. (2.15)). This cancellation can be shown analytically from Eq. (2.11), assuming constant ρ_u and Δh_r, thus, $Q'_f = \rho_u \Delta h_r (\overline{A}_f S'_u + \overline{S}_u A'_f)$. Using Eq. (2.12), and neglecting the time and flow variations, $\overline{A}_f S'_u + \overline{S}_u A'_f = 0$, i.e., $Q'_f = 0$. On the other hand, the fast effect is retained in $\dot{\beta}'$.

Equations (2.15) and (2.16) represent the linearized surface area and heat-release dynamics. We consider the latter for the purpose of analysis since it is the heat release that couples with the acoustics and triggers the instability. After some manipulations and recognizing that $\beta = \beta(\phi, u)$ and $\alpha = \alpha(\phi, u)$, where ϕ is the equivalence ratio, Eq. (2.16) can be written as

$$\dot{Q}'_f + \overline{\omega}_f Q'_f = A_d \frac{\overline{\beta}}{\overline{\alpha}} \overline{u} \left(\frac{u'}{\overline{u}} + \frac{\rho'_u}{\overline{\rho}_u} + \mu \frac{\phi'}{\overline{\phi}} + \Lambda_\phi \frac{\dot{\phi}'}{\overline{\omega}\overline{\phi}} + \Lambda_u \frac{\dot{u}'}{\overline{\omega}_f \overline{u}} \right), \tag{2.17}$$

where for lean conditions: $\Delta h_r = \frac{\Delta H_r^o \phi}{\phi + a_{st}}$, $\mu = \frac{a_{st}}{\phi + a_{st}}$, ΔH_r^o is the enthalpy of reaction per unit mass of fuel, a_{st} is the stoichiometric fuel to air ratio by mass, $\Lambda_\phi = \frac{\partial \ln \beta}{\partial \ln \phi} - \frac{\partial \ln \alpha}{\partial \ln \phi} = \frac{\partial \ln (Q_f/V)}{\partial \ln \phi}$, and $\Lambda_u = \frac{\partial \ln \beta}{\partial \ln u} - \frac{\partial \ln \alpha}{\partial \ln u} = \frac{\partial \ln (Q_f/V)}{\partial \ln u}$. Λ_ϕ and Λ_u are sensitivity coefficients. This equation can be further simplified by neglecting perturbations in the density which scale as $O(\frac{(\rho'_u/\overline{\rho}_u)}{(u'/\overline{u})}) \approx \overline{M}$, where $\overline{M}$, is the mean Mach number and is much smaller than one in this family of combustors. Also, the last term in the RHS which represents the dependence of the heat-release rate per unit volume on u can be neglected. It is only significant in case of strong turbulence, hence its effect is localized in regions of high mixing rate such as wakes and recirculation zones. In general, these regions are only small portions of the flame surface and thus their effect can be minimal [4]. The simplified heat-release equation which retains

[4]For a conical flame: $\alpha = \frac{R}{3}\sqrt{1 - \left(\frac{S_u}{u}\right)^2} \approx \frac{R}{3}\left(1 - \frac{1}{2}\epsilon^2\right)$, $\epsilon = \frac{S_u}{u} < 1$, and thus $\frac{\partial \alpha}{\partial u} = \frac{R}{3u}\left(\epsilon - \frac{\partial S_u}{\partial u}\right)\epsilon$, and $\frac{\partial \alpha}{\partial \phi} = -\frac{R}{3u}\frac{\partial S_u}{\partial \phi}\epsilon$. For small ϵ, $\frac{\partial \alpha}{\partial u}$ can be neglected, to order ϵ^2 when $\frac{\partial S_u}{\partial u} < 1$.

only the important dynamics in moderately turbulent combustors is

$$\dot{Q}'_f + \overline{\omega}_f Q'_f = A_d \frac{\overline{\beta}}{\overline{\alpha}} \overline{u} \left(\frac{u'}{\overline{u}} + \mu \frac{\phi'}{\overline{\phi}} + \Lambda_\phi \frac{\dot{\phi}'}{\overline{\omega}_f \overline{\phi}} \right). \tag{2.18}$$

In this case, we can see from Eq. (2.18) that the heat release dynamics is affected primarily by the flame response to velocity and equivalence ratio perturbations.

The above equation exhibits phase-lag dynamics which characterize the system as finite-dimensional, whereas in Eq. (2.9) flame dynamics are captured by both phase-lag and a propagation delay, τ_f. We can show that the latter is qualitatively similar to Eq. (2.18) which is derived studying the kinematics of the flame surface by approximating the latter equation which is infinite dimensional to a finite dimensional ODE using Padé approximants [6], which results in the form shown in Eq. (2.18) [29].

2.2 Acoustics

The acoustics describing longitudinal as well as bulk-mode instability are studied in this section. Bulk-mode acoustics can be considered as a subset of the longitudinal case when the wave length of the acoustics mode is much greater than the combustor characteristic length [15, 38]. In this case the acoustics in the combustor can be modeled as a lumped-acoustic system [23]. We begin by formulating the general acoustics in an organ-type combustor, and then present a lumped-model approach of the acoustics in a combustor hosting a bulk mode.

2.2.1 Longitudinal Modes

In this section, we present the formulation of the thermoacoustic combustion instabilities in the form of a feedback system whose stability characteristics can be analyzed using system dynamics tools. We focus on the longitudinal modes and hence reduce the problem to one-dimensional reactive gas dynamics. Equations governing the acoustic pressure and velocity are obtained in the presence of unsteady heat addition within the field. These equations are then reduced to the case when the mean heat release is negligible, i.e., approximately

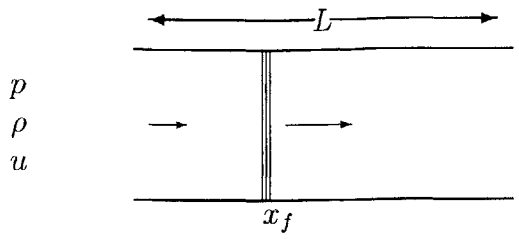

Figure 2-1: One dimensional reacting fluid flow with flame at $x = x_f$

homogeneous field, and when the mean flow is also negligible. These simplifications are used to illustrate the salient features of the analysis of multi-mode interactions.

Reactive-gas dynamics are described using the conservation equations under assumptions of negligible transport processes and one dimensional flow (see Fig. 2-1), as [98]

$$\frac{\partial \rho}{\partial t} + \frac{\partial (\rho u)}{\partial x} = 0 \tag{2.19}$$

$$\rho \frac{\partial u}{\partial t} + \rho u \frac{\partial u}{\partial x} + \frac{\partial p}{\partial x} = 0 \tag{2.20}$$

$$\rho \frac{\partial e}{\partial t} + \rho u \frac{\partial e}{\partial x} = -p \frac{\partial u}{\partial x} + q \tag{2.21}$$

where t and x are time and space, respectively, ρ, u, and p are the density, velocity, and pressure, respectively, and q is the heat release rate per unit volume. We assume that the gases on both sides of the combustion zone behave as perfect gases, and separate the system variables into their mean and perturbation components, e.g. $p(x,t) = \overline{p}(x) + p'(x,t)$. We also assume that the mean flow is steady. If the perturbation components are small variations about the mean flow, we obtain the governing linear equations for the perturbations as

$$\overline{\rho} \frac{\partial u'}{\partial t} + \overline{\rho u} \frac{\partial u'}{\partial x} + \overline{\rho} u' \frac{d\overline{u}}{dx} + \rho' \overline{u} \frac{d\overline{u}}{dx} + \frac{\partial p'}{\partial x} = 0 \tag{2.22}$$

$$\frac{\partial p'}{\partial t} + \overline{u} \frac{\partial p'}{\partial x} + u' \frac{d\overline{p}}{dx} + \gamma \overline{p} \frac{\partial u'}{\partial x} + \gamma p' \frac{d\overline{u}}{dx} = (\gamma - 1) q'. \tag{2.23}$$

We also assume that the flame zone is spatially localized at x_f, i.e.,

$$q'(x,t) = q'_f(t) \delta(x - x_f) \tag{2.24}$$

where q'_f denotes the heat release rate per unit area and $\delta(\cdot)$ denotes the Dirac delta function. This implies that the mean variables are essentially constant over the length of the combustor except for a step change at x_f. A further investigation of the problem shows that for low-Mach number flows, the step change in the pressure is negligible compared to the change in the mean velocity or mean density (see Ref. [4] for details). This enables us to simplify the relations (2.22) and (2.23) to

$$\left(\frac{\partial^2 p'}{\partial t^2} - \left(\overline{c}^2 - \overline{u}^2\right)\frac{\partial^2 p'}{\partial x^2}\right) + 2\overline{u}\frac{\partial^2 p'}{\partial x \partial t} = (\gamma - 1)\left(\frac{\partial q'}{\partial t} + \overline{u}\frac{\partial q'}{\partial x}\right) \tag{2.25}$$

$$\frac{\partial p'}{\partial t} + \overline{u}\frac{\partial p'}{\partial x} + \gamma\overline{p}\frac{\partial u'}{\partial x} = (\gamma - 1)q'. \tag{2.26}$$

Equations (2.25) and (2.26) describe the acoustic pressure and velocity field driven by unsteady heat release q' located at a point within the oscillator in the case when $\overline{q} \neq 0$ and $\overline{u}$ (or $\overline{M}$) $\neq 0$.

If the mean flow Mach number is negligibly small, Eqs. (2.25) and (2.26) can be obviously simplified as

$$\left(\frac{\partial^2 p'}{\partial t^2} - \overline{c}^2\frac{\partial^2 p'}{\partial x^2}\right) = (\gamma - 1)\frac{\partial q'_f}{\partial t}\delta(x - x_f) \tag{2.27}$$

$$\frac{\partial p'}{\partial t} + \gamma\overline{p}\frac{\partial u'}{\partial x} = (\gamma - 1)q'_f\delta(x - x_f) \tag{2.28}$$

where $\overline{c}$ is the average speed of sound in the combustor.

Using an expansion in basis functions

$$p'(x,t) = \overline{p}\sum_{i=1}^{n}\psi_i(x)\,\eta_i(t), \tag{2.29}$$

where in most cases, $\psi_i(x) = \sin(k_i x + \phi_{i0})$, k_i and ϕ_{i0} determined from the boundary conditions, and performing a weighted spatial averaging, the modal amplitudes can be shown to follow [4]:

$$\ddot{\eta}_i + 2\zeta\omega_i\,\dot{\eta}_i + \omega_i^2\eta_i = \sum_{i=1}^{n}\widetilde{b}_i\,\dot{q'_f}, \tag{2.30}$$

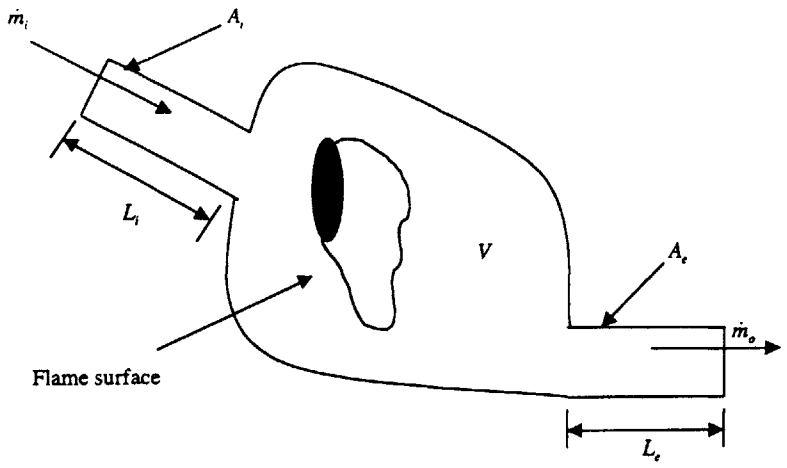

Figure 2-2: Schematic diagram of a combustor exhibiting a Helmholtz-type resonance

where $\tilde{b}_i = \gamma a_o \psi_i(x_f)/E$, $E = \int_0^L \psi_i^2(x)\,dx$, γ is the specific ratio, $a_o = \frac{\gamma-1}{\gamma\bar{p}}$, ζ represents the passive damping ratio in the combustor[5], L is its length, and $\omega_i = k_i\bar{c}$.

2.2.2 Bulk Mode

Helmholtz-type combustion instabilities (also known as bulk-mode instabilities) are characterized by low frequencies and no spatial dependence for the pressure, unlike longitudinal modes which resonate at higher frequencies and vary with the span of the combustor depending on the boundary conditions [4]. Combustors exhibit low frequency instabilities, e.g. [74, 15], blamed on bulk modes. The origin of a Helmholtz-type resonance [23] is the coupling between a compressible volume of gas in a large cavity creating a restoring potential energy for an oscillating mass of slug flow gas in a narrow neck attached to the cavity. The slug flow could occur either at the inlet or exit piping to the combustor chamber where the flame resides and which can be considered as the cavity (see Fig. 2-2).

In order to derive the acoustics dynamics of the bulk combustor, we start by using the following assumptions: (i) The flow is assumed one-dimensional and incompressible in the ducts. (ii) The volume of the combustor chamber is larger than that of each duct. (iii) The

[5]Dissipation in a combustor can be caused by heat losses in the flame zone and friction due to viscous effects.

gas behaves as a perfect gas, and is inviscid.

Applying the mass and energy conservations in the combustor portrayed in Fig. 2-2, and using the perfect gas state equation, the perturbation of the pressure in the combustor cavity around the steady mean can be evaluated as

$$\frac{dp'}{dt} = \frac{1}{V}\left(c_i^2\,\dot{m}'_i - c_e^2\,\dot{m}'_e + (\gamma-1)Q'_f\right), \tag{2.31}$$

where V is the volume of the cavity, $\dot{m}$ is the mass flow rate of gas, c is the speed of sound, and the subscripts i and e denote inlet and exit, respectively.

Using momentum and mass conservation, the perturbed incompressible flow in the ducts satisfies

$$\frac{d\,\dot{m}'_j}{dt} = -A_j\frac{\partial p'_j}{\partial x}(L_j,t), \tag{2.32}$$

where A and L are the cross-sectional area and length of the slug flow in the j^{th} duct, and $j = i$ or e. By substitution in Eq. (2.31), we get

$$\frac{d^2p'}{dt^2} + \frac{1}{V}\left(c_i^2A_i\frac{\partial p'_i}{\partial x}(L_i,t) - c_e^2A_e\frac{\partial p'_e}{\partial x}(L_e,t)\right) = \frac{\gamma-1}{V}\frac{dQ'_f}{dt}. \tag{2.33}$$

Assuming that the inlet and the exit ducts are acoustically open to the atmosphere, i.e., the pressure distribution in the ducts is negligible, hence, $\frac{\partial p'_j}{\partial x}(L_j,t) = \frac{p'}{L_j}$, and this results in the following oscillator equation for the pressure in the combustor:

$$\frac{d^2p'}{dt^2} + 2\zeta\omega\frac{dp'}{dt} + \omega^2p' = \frac{\gamma-1}{V}\frac{dQ'_f}{dt}, \tag{2.34}$$

where $\omega = \sqrt{\frac{c_i^2A_i}{L_iV} + \frac{c_e^2A_e}{L_eV}}$ is the effective Helmholtz frequency [23] associated with a combustor connected to ducts. The passive damping in the combustor due to different dissipation sources, e.g. heat-loss and friction, is accounted for in the natural damping ratio, ζ.

We should note here that the oscillator form in Eq. (2.34) is qualitatively similar to the oscillators in Eq. (2.30) where longitudinal modes are considered.

2.3 Coupling Mechanisms

In this section, the coupling dynamics that connect the heat-release and the acoustics in positive feedback, thus driving the combustion system to resonance are derived. Although we consider a combustor hosting several longitudinal modes, the same derivations with appropriate consideration for the spatial independence of the bulk mode are also applicable for a combustor hosting a bulk mode.

Perturbations in the flame area and the equivalence ratio which couple in a resonant way with the acoustic field are caused by velocity or pressure oscillations. Perturbations in the velocity and pressure are related to the perturbation in acoustic field via the energy equation [4]

$$\frac{\partial p'}{\partial t} + \gamma \overline{p} \frac{\partial u'}{\partial x} = (\gamma - 1) q', \tag{2.35}$$

which can be integrated over the combustor length to obtain (using Eq. (2.29))

$$u' = \sum_{i=1}^{n} \widetilde{c}_i \, \dot{\eta}_i + \theta a_o q', \tag{2.36}$$

where $\widetilde{c}_i = \frac{1}{\gamma k_i^2} \frac{d\psi_i}{dx}(x_f)$, $a_o = (\gamma - 1)/\gamma \overline{p}$, and θ represents the effect of the velocity ahead and behind the flame on q' [4]. This equation can be used with Eq. (2.8) to couple the heat release to the velocity perturbations.

Perturbations in the equivalence ratio at the fuel source due to coupling with the acoustics can be modeled starting from the mass conservation at the mixing section which results in

$$\frac{\phi_s}{\overline{\phi}} \cong 1 \mp \frac{u'}{\overline{u}}, \tag{2.37}$$

for fluctuations in the air flow only (fuel inlet is choked) or in the fuel flow only (air inlet is choked). Now using the momentum equation:

$$\overline{\rho} \frac{\partial u'}{\partial t} + \frac{\partial p'}{\partial x} = 0, \tag{2.38}$$

and p' as in Eq. (2.29), after some manipulations, we get

$$\dot{\phi_s}' \cong \pm\overline{\phi}\frac{\overline{p}}{\overline{\rho u}}\sum_{i=1}^{n}\frac{d\psi_i(x)}{dx}\eta_i, \tag{2.39}$$

according to fluctuations in the air flow only or in the fuel flow only. The equivalence ratio at the burning zone is related to that at the fuel source by a convective delay, $\tau_s = L_s/\overline{u}$, as

$$\phi' = \phi'_s(t-\tau_n), \tag{2.40}$$

where $\tau_n = \tau_s + \tau_{comb}$, and the latter is the combustion time delay. In most cases $\tau_s >> \tau_{comb}$, and $\tau_n \sim \tau_s$ is an acceptable approximation. We should also mention that in this analysis the radial distribution of the local equivalence ratio is assumed to be constant.

It is worth noting also that instability can arise in combustors where flue-gas recirculation is used to reduce NO_x formation, e.g. [2]. The recirculated products may couple with the acoustics and cause perturbations in the equivalence ratio which can be described in a similar manner as in Eqs. (2.39) and (2.40). Also, when injection is used as actuation, it introduces an additional term to appear in the RHS of Eq. (2.40) and is discussed in Chapter 3.

2.4 The Overall Combustion Instability Model

In this section, we examine the structure of the overall unforced combustion model. We consider a combustor hosting several acoustic modes, we incorporate the heat-release dynamics and the coupling dynamics between the latter and the acoustics. It should be noted that for a combustor hosting a bulk mode follows that of the longitudinal modes when only only one mode is present.

Combining the acoustics, heat-release dynamics, and convective-lag effects in Eqs. (2.30), (2.9) and (2.40), respectively, we obtain the following equations:

$$\ddot{\eta}_i + 2\zeta_i\omega_i\,\dot{\eta}_i + \omega_i^2\eta_i = e_1u' + e_2\int_{t-\tau_f}^{t}u'(\tau)d\tau + e_3\phi'_s(t-\tau_s)\} + d_1\,\dot{\phi}'_s\,(t-\tau_s). \tag{2.41}$$

Here, the parameters e_1, e_2, e_3, and d_1 are all divided by the cross-sectional area of the

combustor A_c. Equation (2.41) shows that two different time delays, τ_f and τ_s, can lead to instability, one arising from flame propagation effects, and the other from fuel convection.

The overall model of the combustor is represented by Eqs. (2.41), (2.36), and (2.39) when multiple modes are present. For ease of exposition, we restrict our discussion to the case when only one mode is present, a similar approach can be extended to the multi-mode case. If the variations are mainly in u', then Eqs. (2.41) and (2.36) can be combined to obtain the relation

$$\ddot{\eta} + (2\zeta\omega - \gamma_1)\dot{\eta} + (\omega^2 + \gamma_2)\eta - \gamma_2\eta(t - \tau_f) \;=\; 0, \tag{2.42}$$

where $\gamma_1 = e_1\tilde{c}$ and $\gamma_2 = e_2\tilde{c}$.

On the other hand, if ϕ'-perturbations only exist, then Eqs. (2.41) and (2.39), can be combined to obtain

$$\ddot{\eta} + 2\zeta\omega\dot{\eta} + \omega_i^2\eta - \beta_1\eta(t - \tau_s) + \beta_2\eta_i(t - \tau_s) \;=\; 0, \;\text{ and } \eta_i(t) = \int_0^t \eta(\zeta)d\zeta \tag{2.43}$$

where $\beta_1 = \pm d_1\overline{\phi}\frac{\bar{p}}{\overline{\rho u}}\frac{d\psi(x)}{dx}$, and $\beta_2 = \pm e_3\overline{\phi}\frac{\bar{p}}{\overline{\rho u}}\frac{d\psi(x)}{dx}$.

At the acoustic frequency, the impact of the fourth term on the RHS of Eq. (2.43) is typically smaller than the fifth term since $O(\beta_1) \approx O(\beta_2)$ and $\dot{\eta}$ scales as $|\omega|\eta$ around the unstable frequency Hence a simplified version of (2.43) can be analyzed in the form

$$\ddot{\eta} + 2\zeta\omega\dot{\eta} + \omega^2\eta - \beta_1\eta(t - \tau_s) \;=\; 0. \tag{2.44}$$

It is interesting to note that the structure of (2.44) is identical to that of (2.42) with the differences only due to the parameters. This implies that time-delay effects are present both in the presence of u'- and ϕ'-perturbations, with the distinction that with u', the time-delay is due to τ_f, which is due to flame propagation, and with ϕ', the delay is due to τ_s, a convective effect. The other distinction is in the damping effect; in the former, if γ_1 is positive, even in the absence of any time-delay, instabilities can be present. In the latter, on the other hand, instability is only due to the time-delay τ_c; the damping effect is stabilizing since its due to the dissipation in the combustor solely.

The above discussions indicate that the general class of models that describe the combustion instability are of the form of

$$\ddot{\eta} + 2\zeta_0\omega\dot{\eta} + (\omega^2 - \Gamma_1)\eta + \Gamma_2\eta(t-\tau) \;=\; 0 \tag{2.45}$$

with ζ_0, ω, Γ_1, Γ_2 and τ taking different values depending on whether the instability is due to u' or ϕ'.

When $2\zeta_o\omega > 0$, and for most practical cases, we have $|\Gamma_2| < \omega^2$ [29]. When $\tau = 0$, the system is stable. As τ increases, the system becomes unstable if $\tau^- \leq \tau \leq \tau^+$, where

$$\tau^{\mp} = \frac{1/\omega}{\sqrt{1 - 2\zeta_o^2 \pm \sqrt{\Gamma_2^2/\omega^4 - 4\zeta_o^2(1-\zeta_o^2)}}} cos^{-1}\left(\pm\frac{\sqrt{\Gamma_2^2/\omega^4 - 4\zeta_o^2(1-\zeta_o^2)} - 2\zeta_o^2}{\Gamma_2/\omega^2}\right), \tag{2.46}$$

while

$$2\zeta_o\sqrt{1-\zeta_o^2} < \frac{|\Gamma_2|}{\omega^2} < 1. \tag{2.47}$$

If $|\Gamma_2| > \omega^2$, there exists only one switch to instability at τ^-.

When $\zeta_o \sim 0$, the conditions simplify to [29, 40]:

$$\text{for} \qquad 0 < \Gamma_2 < \omega^2, \; \frac{n+1}{2} < \frac{\tau}{\tau_a} < \frac{n+2}{2} \quad n = 0, 2, 4..., \tag{2.48}$$

and for $\Gamma_2 > \omega^2$, $\frac{\tau}{\tau_a} > \frac{1}{2}$, where $\tau_a = 2\pi/\omega$. A time-delay system instability depends on the distance between the source of ϕ'_s, the convective velocity, and the acoustic frequency.

The presence of "stability bands", in terms of τ/τ_a, was used to predict instability conditions in experimental combustors caused by equivalence-ratio and velocity fluctuations, and is a central feature that can be exploited for control designs [40]. A comparison with experimental results will be discussed next.

2.4.1 Comparison with Experimental Results

Instability due to ϕ' fluctuations

We now compare the instability characteristics predicted by the model in (2.45) with the four experimental results [84, 51, 15, 60]. In the first three cases, the feedline consisted of a choked fuel-line and an unchoked air-feed. In [51], they also studied the case when the fuel-line was unchoked and the air-feed was choked. In [60], the corresponding details are not given, though fluctuations were observed to be present at the outlet of the fuel-line. Such feedline characteristics in turn introduce ϕ'-fluctuations as shown in section 2.3. Below, we consider each of these four results and show how the instability characteristics as predicted by the model in (2.45) compare with the results reported in [84, 51, 15, 60].

In [51], measurements of the pressure amplitude from different experiments where the position of the unchoked fuel inlet was changed, hence changing the convective delay τ_c, were collected as a function of τ_c/τ_{ac}. τ_{ac} is the acoustic mode time-constant, it follows that $\tau_{ac} = 2\pi/\omega$. The unstable regimes cluster around $\tau_c/\tau_{ac} = 0.65$ and 1.6 which is in agreement with our model. We neglected the effect of damping in all four cases, since it is small, and difficult to quantify. Therefore ζ was set to zero in Eq. (2.45). The results in [69] show that instability occurs when

$$\frac{n+1}{2} < \frac{\tau_c}{\tau_{ac}} < \frac{n+2}{2} \quad \text{for } n = 0, 2, 4... \tag{2.49}$$

which encompasses the unstable regions in [51]. In addition, in [84], instability occurred at $0.5 < \tau_c/\tau_{ac} < 1.0$, when the fuel inlet was unchoked in perfect agreement with our model (see Fig. 2-3). It is worth noting that the acoustic mode was that of a quarter-wave in [84], and a half-wave in [51].

The instability mode in [15] corresponds to that of a bulk-mode with $\omega = 200$ Hz where ϕ'-fluctuations were observed to be present. Based on the experimental data provided in [15], we calculated $\tau_c = 3.1ms$, leading to $\tau_c/\tau_{ac} = 0.62$, which matches the model predictions from Eq. (2.49).

Our final comparison is with the results of [60], where the instability characteristics were

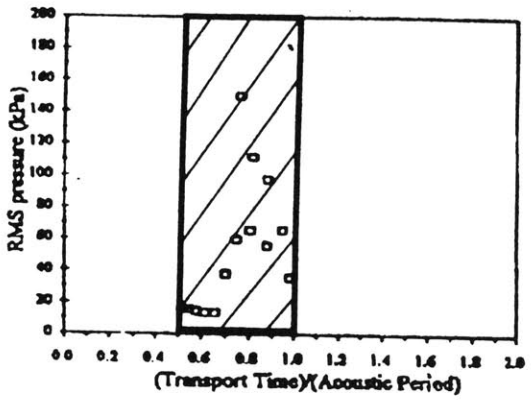

Figure 2-3: Instability band measured in [19] vs. our model predictions (shaded area).

observed to vary with L, the distance of the fuel-injector from the burning zone (see Fig. 7 in [60]). The paper shows that instability is also dependent on the value of $\overline{\phi}$. As the latter decreases, the instability vanishes. Our model can predict this behavior since $\overline{\phi}$, affects β_1 in Eq. (26). According to [69], as $\overline{\phi}$, and hence β_1 decreases, and below a critical value for the latter, the system will be stable irrespective of the amount of delay.

Instability due to u' fluctuations

In several of the experimental studies, the feedline dynamics was decoupled from the burning zone, but the pressure instabilities were still observed to be present. In [5, 48, 34], though the fuel inlet is choked and the air inlet is unchoked, the pressure fluctuations at the mixing section are small compared to those at the burning zone, which in turn suggests that the ϕ'-fluctuations are negligible as well. In [88], the fuel and air-streams are introduced using similar means with neither being choked resulting in an unperturbed equivalence-ratio. In [82], a premixer upstream of the cold-section of the combustor was introduced to ensure thorough mixing. In [96], a similar arrangement is made to decouple the feed-line perturba-

tions. These observations indicate that a mechanism different from ϕ'-fluctuations is indeed responsible for introducing the resonance. One such possible candidate is u'-perturbations.

In [4, 37], a model has been derived under such an assumption, and shown to compare favorably with experimental results in [5, 48, 34] for laminar flow conditions. For a certain class of flames τ_f is small when $\overline{S}_u$ is large (e.g., in a turbulent flow), and when the characteristic size of the flame, R, is small, the RHS of Eq. (2.42) can be simplified further by neglecting the fourth term in the LHS. Thus, when perturbations in the flame area change the equivalent damping in the combustor, defined as $2\zeta_o\omega = 2\zeta\omega - \gamma_1$, such that $2\zeta_o\omega < 0$, the oscillator is always unstable. In this case, γ_1 represents a "negative" damping added by the flame area fluctuations[6]. This condition arises when the flame is located in a position where the modal amplitude of the pressure and the velocity (represented by $\tilde{b}$ and $\tilde{c}$) are of the same sign. For example, in a closed-open combustor with fixed equivalence ratio, a quarter-wave mode is always stable whereas a three-quarter-wave mode gets destabilized when the flame is located between the node and the anti-node of the pressure mode [4]. Further comparisons with experimental combustors will be presented next.

On the other hand, the results in [88, 96, 87, 82], the flow velocities were in the turbulent regime. The question here is, whether the model in (2.45) can predict the instability reported in these four papers. In both [96, 82], the quarter-wave mode of the hot-section is driven into resonance. This implies that γ_1 in (2.42) is negative and hence ζ_0 in (2.45) is positive. But as indicated by the results in [69], instability can still occur due to the propagation delay τ_f. In particular, as τ_f increases, bands on instability occurs as indicated in Eq.(2.49). One of the quantities that can cause τ_f to change is $\overline{\phi}$, since $\tau_f = R/S_u$ and both R and S_u change with $\overline{\phi}$. It is interesting to note that in [82], it is observed (see Fig. 6 in [82]) that instability bands indeed occur as $\overline{\phi}$ changes. As pointed above, in this particular experimental set-up care was taken to decouple any ϕ'-perturbations from the burning zone.

It appears that similar mechanisms are present in [96, 87, 88] as well, though more experimental studies need to be carried out to support our hypothesis.

[6]The notion of "negative" and "positive" damping is used here to indicate heat-release perturbation which is out-of-phase and in-phase with the pressure oscillation, respectively. We have shown in previous work [39] that the effect of flame-area perturbation can be modeled as a negative damping term. Heat release can be modulated using active forcing to produce a positive damping term, as shown in [40]

Instability with Diffusion flames

In a number of experiments, a diffusion flame rather than a premixed flame is present and still known to result in instability (for example, [55, 53, 62, 102]). Our model presented in this paper is not applicable due to the assumption that the flame is premixed. A more in-depth study of a diffusion flame-model may be necessary in order to identify the possible mechanisms of instability.

Yet another assumption in our model is that the flame-perturbations are localized spatially. Therefore in rigs where the perturbations are present in a distributed form (as in [9]), the model presented here may not be appropriate. In [20] relevant models have been presented by assuming a certain spatial distribution of the flame.

Chapter 3

Actuation

Designing actuators depends on a clear insight into the dynamics of the system, while optimizing its operation relies on the availability of accurate models of the dynamics as well as for how the actuator impacts it under a range of conditions.

The problem is critical in combustion instability since: (1) It is important to minimize the input energy through the actuator while recognizing certain practical limitations on its design such as the bandwidth and power [38], (2) while it is desirable to achieve the minimum possible settling time, this should be done without imposing unreasonable requirements on the actuator, (3) extra constraints on the design are usually encountered in practice, such as the allowable locations of the sensor and actuator, which may hinder achieving theoretically optimal conditions, and (4) since models are difficult to construct and validate, certain robustness is needed in the control design. Clearly, the role of an actuator and how it interacts with the system dynamics must be understood before these goals can be accomplished.

Models of combustion instability have been suggested in Chapter 2 and [4, 29, 38]. However, effort to model the impact of the actuator on the system dynamics has been limited. In most cases, a simple relation is assumed to exist between the action of an actuator and the system response. As an example, when a speaker is employed, it is often assumed that its primary function is to introduce a pressure signal which counters the existing unstable pressure field (anti-sound). However, the subtle interactions between the actuator signal and the flame will be shown here to lead to different results depending on the structure of the

control algorithm and its implementation into the system design, i.e. the locations of sensors and actuators, etc. We will also study the impact of an oscillating fuel stream.

Here, we present a finite dimensional instability model with different input actions from two different actuator categories, namely, (1) flow sources (e.g., speakers), and (2) heat sources (e.g., fuel injectors). Specifically, in Sec. 3.1.1, the impact of a speaker on the combustion dynamics is derived, followed by a typical model of the inherent dynamics of a speaker. Similarly, in Sec. 3.1.2, both injector's effect on the overall dynamics as well as its inherent dynamics are presented. The analysis of the impact of the former is performed in Sec. 3.3, while for the latter in Sec. 3.4 using a proportional and a phase-lead controller. In both these sections, a dynamic analysis as well as an energy analysis are performed.

3.1 Modeling

3.1.1 Speaker

A commonly used actuator to control pressure oscillations in combustion systems is a loudspeaker. The ease of its implementation as an actuator is one of the predominant reasons for its ubiquity as an actuator in many of the investigations of active control of thermally-driven acoustic instability. In this section we examine the basic role of the loudspeaker by modeling its effect as a source in an acoustic field. The starting point is the conservation equations applied on a deformable control volume. The dynamic effect of the loudspeaker, which is either flush-mounted on the combustor wall or end-mounted, on the acoustic field is shown to be a source of flow, momentum, and energy. Two aspects of modeling will be discussed. First, the contribution of the speaker to the combustion model will be identified in Sec. 3.1.1, and then, the dynamics of the speaker itself will be derived.

Contributions of a Loudspeaker to the Combustion Dynamics

As in [4], the flow is one dimensional with negligible transport processes, combustion occurs within a flame zone localized at $x = x_f$, gases in the reactant and product side are perfect,

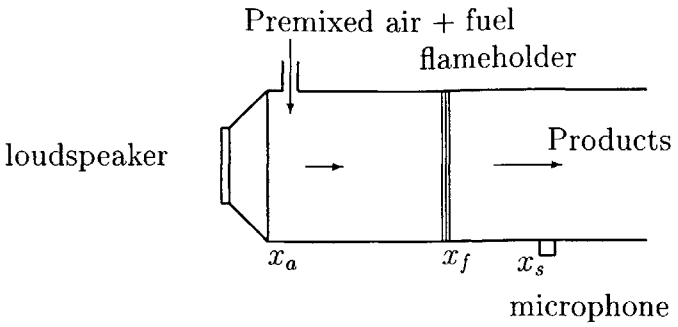

Figure 3-1: Schematic of the combustor with an end-mounted loudspeaker.

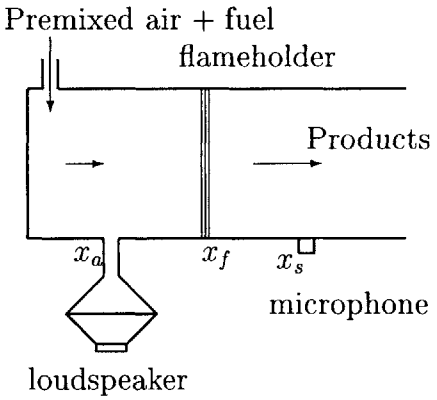

Figure 3-2: Schematic of the combustor with side-mounted loudspeaker.

and unsteady components of the flow variables are small variations about the mean flow. Whether a loudspeaker is end-mounted (see Figure 4-2), or flush-mounted on the wall of a duct, (see Figure 3-2), its diaphragm motion can be modeled as a piston. In the former case, the motion is parallel to the flow, while in the latter, it is in the direction normal to the flow. We assume that the width of the loudspeaker, Δx, is relatively small compared to the smallest wavelength of the relevant acoustic modes, and that the diaphragm motion, in the side-mounted case, is small compared to the diameter of the combustor (see Figure 3-3). The contributions of the diaphragm motion can be represented in the mass, momentum, and energy equations as follows:

$$\frac{\partial \rho}{\partial t} + \rho \frac{\partial u}{\partial x} + u \frac{\partial \rho}{\partial x} = \frac{\rho v_c A_s}{w \Delta x (D_o - y)}, \tag{3.1}$$

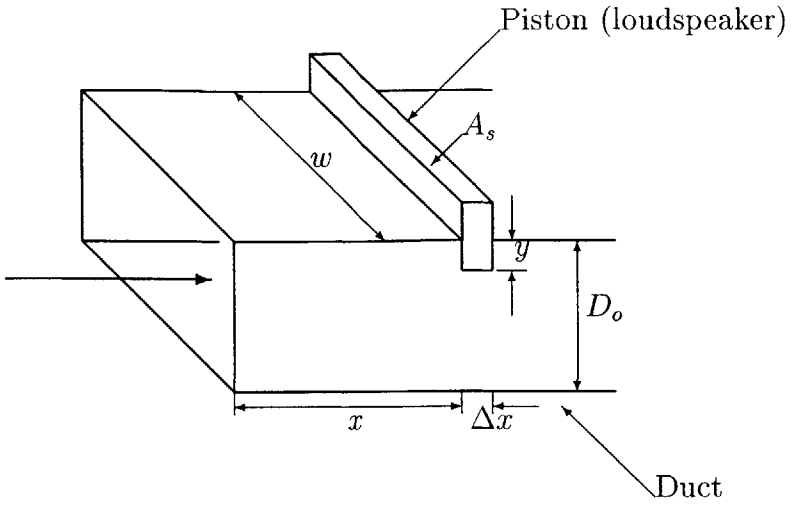

Figure 3-3: Schematic diagram of the combustor with a side-mounted loudspeaker to incorporate the contribution of the loudspeaker modeled as a movable piston of cross-sectional area A_s to the conservation equations in 1-D flow dynamics.

$$\frac{\partial(\rho u)}{\partial t} + u\frac{\partial(\rho u^2)}{\partial x} + \frac{\partial p}{\partial x} = \frac{\rho v_c A_s u}{w\Delta x(D_o - y)}, \tag{3.2}$$

$$\rho\frac{\partial e}{\partial t} + \rho u\frac{\partial e}{\partial x} + p\frac{\partial u}{\partial x} = \frac{\rho v_c A_s}{w\Delta x(D_o - y)}\left[\frac{p}{\rho} + \frac{v_c^2}{2}\right], \tag{3.3}$$

where v_c, y, and A_s are the speaker's diaphragm velocity, displacement, and cross-sectional area, respectively. ρ, p, u, and e denote the density, pressure, velocity and specific internal energy of the fluid, respectively. The duct has a width w and a height D_o.

Our assumptions regarding the loudspeaker imply that Δx, y/D_o and $v_c^2/(p/\rho)$ are small. In the presence of a heat source due to a flame at $x = x_f$, neglecting the effect of mean heat addition and mean flow, the conservation equations of the perturbations can be obtained from as follows [4]:

$$\left(\frac{\partial^2 p'}{\partial t^2} - \bar{c}^2\frac{\partial^2 p'}{\partial x^2}\right) = (\gamma - 1)\left(\frac{\partial q_f'}{\partial t}\delta(x - x_f)\right) + \gamma\bar{p}\alpha_r\frac{\partial v_c}{\partial t}\delta(x - x_a), \tag{3.4}$$

$$\frac{\partial p'}{\partial t} + \gamma\bar{p}\frac{\partial u'}{\partial x} = (\gamma - 1)q_f'\delta(x - x_f) + \gamma\bar{p}\alpha_r v_c\delta(x - x_a), \tag{3.5}$$

where $\alpha_r = A_s/A$, A is the area of cross-section of the combustor, γ is the specific heat ratio, x_a is the speaker's location, $\bar{c}$ is the mean speed of sound, q_f' is the unsteady heat-release

rate per unit area, and $\delta(\cdot)$ is the Dirac delta function. If the loudspeaker is end-mounted, the same analysis can be applied, setting $x_a = 0$, and $\alpha_r \sim 1$.

In Equations (3.4) and (3.5), we assume that the heat-release source is concentrated at the flame holder, x_f. We note also that the loudspeaker, at x_a, is an acoustic source. The boundary effects, which can be considered as additional virtual sources, are introduced implicitly by imposing a spatial distribution of the pressure since its specific shape depends on the boundary conditions.

A Finite Dimensional Feedback Model

Using the Galerkin expansion as in Chapter 2, Eqs. (3.4) and (3.5), after some manipulations, can be written for a single actuator as

$$\overline{p}\sum_{i=1}^{n}\psi_i(x)\ddot{\eta}_i - \overline{c}^2\overline{p}\sum_{i=1}^{n}\psi_i(x)\eta_i(t) = (\gamma-1)\frac{\partial q'_f}{\partial t}\delta(x-x_f) + \gamma\overline{p}\alpha_r\frac{\partial v_c\delta(x-x_a)}{\partial t}, \quad (3.6)$$

$$u'_f(t) = \frac{1}{\gamma k^2}\sum_{i=1}^{n}\dot{\eta}_i(t)\frac{d\psi_i}{dx}(x_f) + \theta a_0 q'_f(t) + \alpha_r v_c \mathcal{H}(x_f - x_a), \quad (3.7)$$

where θ is a parameter that reflects the contribution of the velocity behind and ahead of the flame to u'_f [4]. The loudspeaker and the heat release act as sources at x_a and x_f, respectively, to the acoustic pressure and velocity as shown in Eqs. (3.6) and (3.7). The effect of boundary conditions is implicitly introduced the mode shapes $\psi_i(x)$.

Dynamics of the speaker

The dynamics of a speaker can be accurately represented by a second-order ODE [65]. Its dominant dynamics are caused by the electro-magnetic and mechanical components which can be simplified, when the input is the current, as

$$F_m = B_e l I, \quad (3.8)$$

$$m_s\frac{d^2x}{dt^2} + b_s\frac{dx}{dt} + k_s x = F_m, \quad (3.9)$$

where i is the current, F_m is the magnetic force, x denotes the motion of the armature (connected to the speakers diaphragm) in the direction of the magnetic force, B_e, and l denote, the magnetic flux density, and the length of the armature which moves orthogonal to the magnetic field, respectively. m_s, b_s, and k_s represent the effective mass, damping, and the stiffness of the armature/diaphragm system. In general, the electric time constant is much smaller than the mechanical time constant, and a voltage input will result in similar dynamics. Therefore, the speaker can be represented as [65]:

$$\dot{v}_c + 2\zeta_s\omega_s v_c + \omega_s^2 \int v_c dt \;=\; k_l I, \tag{3.10}$$

where v_c is the velocity of the diaphragm, $\omega_l = \sqrt{k_s/m_s}$ is the natural frequency of the loudspeaker diaphragm, and ζ_s is an equivalent damping ratio, $k_l = B_e l$ is a speaker gain. The speaker parameters were found by performing a system ID on a 0.2 W speaker that was used in experimental active control on an MIT combustor rig [5]. These were found to be: with $k_s = 1404$, its natural frequency, $\omega_s = \sqrt{k_s/m_s} = 1822\ rad/s$, and and its damping ratio $\zeta_s = 0.1$.

3.1.2 Fuel Injector

In this section, we study the contribution of the injector on the combustion dynamics, and we present a generic model of the dynamics of a typical proportional and on-off injector. The contribution of the secondary injector is identical to the effect of perturbations of ϕ' from the fuel main source presented in Chapter 2. The dynamics of the injector itself are presented in the next section.

Contribution of a Fuel Injector to the Combustor Dynamics

The contribution of the injector to the dynamics can be viewed as an additional perturbation in the combustor dynamics in Eq. (2.41). In this case the latter can be represented as

$$\ddot{\eta}_i + 2\zeta_i\omega_i\,\dot{\eta}_i + \omega_i^2\eta_i \;=\; e_1 u' + e_2 \int_{t-\tau_f}^{t} u'(\tau)d\tau + e_3\phi'\} + d_1\,\dot{\phi}', \tag{3.11}$$

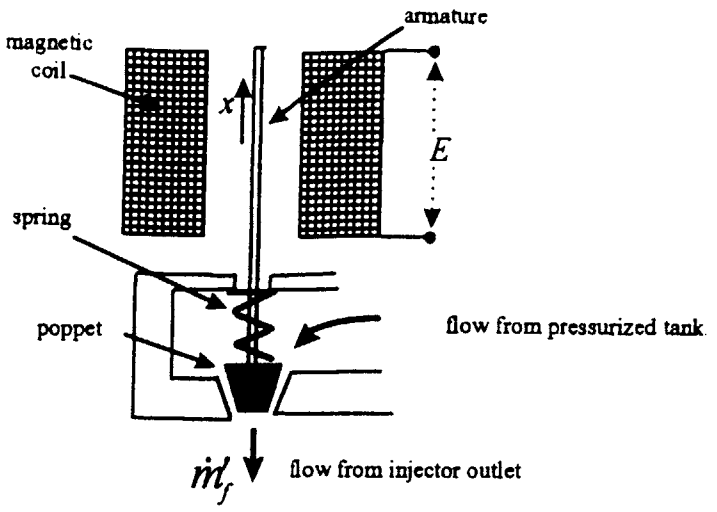

Figure 3-4: A schematic of a typical injector.

where the overall perturbation in the equivalence ratio at the flame, ϕ' is defined as

$$\phi' = \phi'_s(t - \tau_s) + \phi'_c(t - \tau_c), \tag{3.12}$$

ϕ'_c is the controlled injector contribution, and $\tau_c = L_c/\overline{u}$ is the convective delay caused by injecting at a distance L_c upstream the burning zone.

Fuel Injector Dynamics

A Proportional Injector

The pulsating fuel injector delivers oscillations in the mass-flow rate in response to a voltage input. The injector system consists of an electro-mechanical part and a fluidic part, where in the former, the input voltage generates an electro-magnetic field that causes a poppet to move against a spring (as seen in Fig. 3-4). The motion of the poppet controls the aperture of the injector allowing fluid to flow.

The electro-mechanical part relates the voltage E to the poppet position x through the

electrical, electro-magnetic, and mechanical components, which can be modeled as

$$E = iR_e + L_e\frac{di}{dt} + V, \tag{3.13}$$

$$V = B_e l\frac{dx}{dt}, \tag{3.14}$$

$$F_m = B_e l i, \tag{3.15}$$

$$m\frac{d^2x}{dt^2} + b\frac{dx}{dt} + kx = F_m, \tag{3.16}$$

where i is the current, F_m is the magnetic force, x denotes the motion of the armature in the direction of the magnetic force, R_e, L_e, B_e, and l denote, the resistance of the solenoid coil, the inductance of the coil, the magnetic flux density, and the length of the armature which moves orthogonal to the magnetic field, respectively. m, b, and k represent the effective mass, damping, and the stiffness of the armature/poppet system.

The fluidic part can be modeled using the unsteady Bernoulli equation, and the conservation of mass across the injector assuming incompressible flow. The unsteady velocity, v, can be obtained from the former applied between the inlet to the valve which is connected to a pressurized tank (where the flow velocity is ≈ 0, and $p = p_o$), and the outlet to the combustor where $p = p_c$, and $\Delta p = p_o - p_c$, as

$$\rho L_i\frac{dv}{dt} + \frac{1}{2}\rho v^2 = \Delta p, \tag{3.17}$$

In case small perturbations in p_c affect the velocity out of the injector, the unsteady velocity out of the valve, v, is linearized as

$$\tau_{fluid}\frac{dv'}{dt} + v' \cong \frac{-p_c'}{\sqrt{2\Delta\overline{p}\rho}}, \tag{3.18}$$

where $\tau_{fluid} = L_i/\sqrt{2\Delta\overline{p}/\rho}$ is the fluidic time constant, and L_i is the distance between the tank and the valve's outlet. τ_{fluid} is negligible for conditions where $L_i << 1m$, $\Delta\overline{p}$ is large (which is expected), and ρ is small ($O(1kg/m^3)$ for most gaseous fuels)[1].

[1]In the case of liquid fuels, the time constant can be comparable to the acoustics time constant due to large ρ, $O(1000kg/m^3)$.

The mass flow rate, defined as $\dot{m}_f = \rho v A$, is perturbed, assuming oscillations in v (caused by the dynamics in Eq. (3.18)) and A (caused by the motion of the poppet x), as

$$\dot{m}'_f = \rho \overline{A} v' + \rho \overline{v} A', \tag{3.19}$$

where we assume $A' = k_o x$, and $k_o > 0$. Equations (3.18) and (3.19) describe the fluid dynamics due to perturbations in p'_c and/or x. In most practical cases, $\Delta\overline{p}$ is large to guarantee choked conditions in the injector's discharge, thus, the first term in the RHS of Eq. (3.19) can be neglected. Using $\overline{v} = \sqrt{\frac{2\Delta\overline{p}}{\rho}}$ from Eq. (3.17), we simplify Eq. (3.19) as

$$\dot{m}'_f \cong k_o \rho \sqrt{\frac{2\Delta p}{\rho}} x. \tag{3.20}$$

Equations (3.13)-(3.16) and (3.20) determine the input-output relation between the fuel-injector input E and the output $\dot{m}'_f$ which is expressed in the Laplace domain as:

$$\frac{\dot{m}'_f(s)}{E(s)} = \frac{k_v}{(\tau_e s + 1)(ms^2 + bs + k) + B_e^2 l^2 / R_e s}, \tag{3.21}$$

where $k_v = B_e l k_o \rho \sqrt{\frac{2\Delta\overline{p}}{\rho}} / R_e$.

In most solenoid systems, the armature electric time constant, $\tau_e = L_e/R_e$, is negligible compared to the acoustics time constant [71]. In these valves, the stiffness of the spring, k, is large, for a fast closing of the valve, when the voltage is turned *off*. Also, the mass, m, of the armature is very small in many of the typical injectors to minimize inertia forces [71]. The damping term, b, contains the overall damping including stiction and friction, and typically is large. Thus, the mechanical system can be simplified as a first-order system; a damper-spring system [58]. The mechanical time constant usually limits the bandwidth of typical injectors to approximately 100 Hz. (Note that other effects, such as impact dynamics are not included here, since we expect them to be of higher frequencies than the combustor dynamics). Thus, Eq. (3.21) is simplified as

$$\frac{\dot{m}'_f(s)}{E(s)} = \frac{k_v \tau_m}{\tau_m s + 1}, \tag{3.22}$$

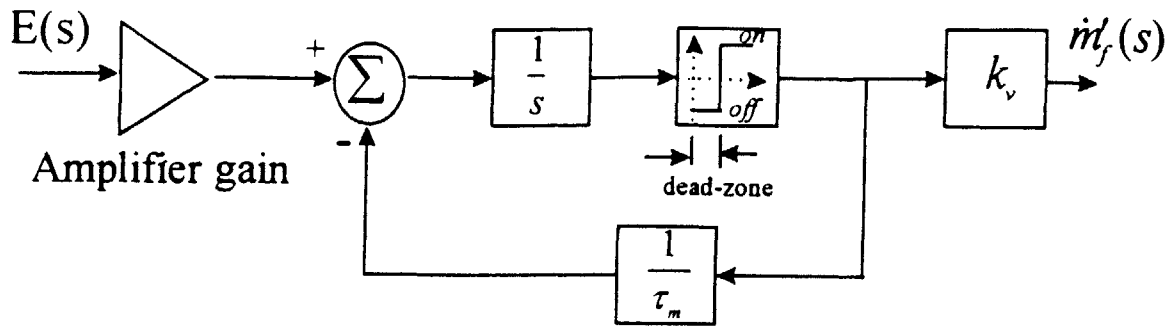

Figure 3-5: Block diagram of a typical two-position injector.

where $\tau_m = (b + B_e^2 l^2 / R_e)/k$.[2]

A Two-Position (on-off) Fuel injector

Some fuel injectors currently used for combustion control [62, 102, 53] operate only between two positions, *on* and *off*. Unlike the proportional injectors discussed above, the physical stops play a more prominent role in the dynamics. However, one can still model two-position injectors in the same manner as above by including the effect of the physical stops as a saturation block together with Eq. (3.22) as shown in Fig. 3-5. A two position injector is set *on*, after the voltage input overcomes a certain threshold, thus creating a dead-zone in the control input (see figure) which will be discussed further when control is implemented in Chapter 4.

An additional point to note is the distinction between the injector dynamics during transition from closing and opening. Typically, the injector is over-driven by a high voltage in the opening mode to ensure fast opening. The opening time constant is different than the closing one. This effect can also be included in the injector model, as seen in Fig. 3-5, by

[2]For more advanced proportional injectors, internal feedback loops exist (using for example a position transducer for the armature) to guarantee accurate metering, and increase its bandwidth, e.g., a Moog DDV proportional valve has a bandwidth of 450 Hz [36].

assuming that τ_m varies between two values τ_{m_1} and τ_{m_2} depending on whether the injector is transitioning from *off* to *on* or *on* to *off*. Note that $\tau_{m_1} = \tau_m$ (as defined before) and $\tau_{m_2} = b/k$. We refer the reader to [11] for more details regarding this model when validated against two different injectors: Parker models (9-130-905) and (9-633-900).[3]

3.1.3 Actuated Combustion Instability Model

A finite dimensional model that includes both means of actuation: speaker [27] and fuel injector [38] has been developed. Two mechanisms of combustion instabilities are reported in practical systems, the first is due to coupling of the heat release with the acoustics through flame surface area perturbations [25, 4] and due to coupling with oscillations in the equivalence ratio [29]. We present the former mechanism of instability in the analysis in this section for its analytical simplicity when propagation effects due to τ_f (as in Chapter 2) are weak (hence their dynamics omitted). Analysis of the case when natural equivalence ratio fluctuations are present is very similar and is omitted here to avoid repetition.[4] The finite dimensional model can be represented in this final form which will be used in the analysis carried out in the next sections:

$$\ddot{\eta}_i + \omega_i^2 \eta_i = \widetilde{b}_i \, \dot{q}'_f + \widetilde{b}_{c_i} \, \dot{v}_c, \tag{3.23}$$

$$\dot{q}'_f + b_f q'_f = \omega_f \widetilde{g}_f \left(\frac{u'_f}{\overline{u}_f} + \frac{\phi'_f}{\overline{\phi}_f} + \frac{\dot{\phi}'_f}{\overline{\omega}_f \overline{\phi}_f}\right), \tag{3.24}$$

$$u'_f = \Sigma_{i=1}^n \widetilde{c}_i \, \dot{\eta}_i + \alpha_r v_c, \tag{3.25}$$

$$p'(x,t) = \overline{p} \Sigma_{i=1}^n c_{c_i}(x) \eta_i(t), \tag{3.26}$$

where $\widetilde{b}_i = \gamma a_o \psi_i(x_f)/E$, $\widetilde{c}_i = \frac{1}{\gamma k_i^2} \frac{d\psi_i(x_f)}{dx}$, $\widetilde{b}_{c_i} = \gamma \alpha_r \psi_i(x_a)/E$, $c_{c_i} = \psi_i(x_s)$, $\omega_f = 4S_u/d_p$, $b_f = \omega_f(1 - \theta a_o \widetilde{g}_f)$, $a_o = (\gamma - 1)/\gamma \overline{p}$, $E = \int_0^L \psi_i \psi_i^T dx$, and $\widetilde{g}_f = n_f \rho \Delta h_r \overline{u}_f \overline{\phi}_f \, (d_p/D)^2$. Note that here we are modeling a premixed-organ-pipe-type combustor of diameter D and length

[3] It should be noted that when inertia forces in the armature are important, a second-order fuel-injector model, with high damping, is more appropriate. The experimental measurements in [53] for a General Valve Series 9 model show similar dynamics.

[4] While equivalence ratio fluctuations instability is governed by an inherent convective delay which reflects the time the perturbations travel from the mixing section to the burning section [29, 40], the end effect of the instability is the same in which p' and q' become in phase, as will be discussed in Sec. 3.2.1. An in depth analysis of actuation in mixture-inhomogeneity-driven instability is carried out in [29, 40].

L with a perforated disk (with n_f holes of diameter d_p) acting as a flame holder [4]. γ, S_u and Δh_r are the specific ratio, the burning velocity and the enthalpy of reaction of the reactants, respectively. v_c and $\dot{v}_c$ are the velocity and acceleration of a typical flow source (e.g. a speaker), respectively, ϕ_f and u_f are the equivalence ratio and the velocity at the flame (out of a perforation), p is the pressure, $\overline{(.)}$ and $(.)'$ are the mean and perturbation of a variable. x_f, x_s, and x_a are the flame, the sensor (e.g., a microphone), and the flow source actuator (e.g., a speaker) locations measured from the upstream end, respectively. α_r is the ratio of the speaker membrane surface area to that of the duct cross section area. $\theta \in (0,1)$ is a parameter expressing the effect of u'_f ahead and behind the flame on its dynamics [4]. k_i and E are the wave number and the energy in the mode, respectively.

3.2 Role of Actuation

3.2.1 Energy vs. Dynamics Analysis

In this section, we present two insightful directions, namely the energy and dynamic analyses, for analyzing combustion instability in organ-pipe combustors which typically model situations of combustion in gas turbines and possibly afterburners in applications that encompass power generation and propulsion.

We start by carrying out an energy balance of the combustor. We should note that the acoustic field (hosted by the combustor tube) is the primary energy storage mechanism in the combustor. Increasing or decreasing the storage (or internal) energy of this field can be achieved by exerting work or heating the field. Since, in our case, the flame is considered a localized heat source, only a small control volume in the acoustic field is heated, the small volume expands and in turn exerts work on the field.

The acoustic energy density, e', in a one-dimensional acoustic field can be derived from the unforced conservation equations as (see [23], for more details)

$$e' = \frac{\bar{\rho} u'^2}{2} + \frac{p'^2}{2\overline{\rho c^2}}, \tag{3.27}$$

where ρ, u, and p are the density, velocity, and pressure in the field, respectively, $(.)'$ and $\overline{(.)}$ are the perturbed and mean values of the parameters, respectively, and $\bar{c}$ is the mean speed of sound. The first term in the RHS is the kinetic acoustic energy and the second is the potential acoustic energy. It is clear that any system that would sustain waves (also, as in many vibration processes) should have these two components of energy, and the periodic conversion from one form to the other sustains the oscillatory behavior.

The momentum and energy conservation equations for small perturbations in a combustor tube hosting a localized heat-release zone, as seen in Fig. 2-1, for zero mean velocity,$\overline{u}$, and for no spatial change in the mean density, $\overline{\rho}$, and pressure, $\overline{p}$, can be written as

$$\overline{\rho}\frac{\partial u'}{\partial t} + \frac{\partial p'}{\partial x} = 0, \tag{3.28}$$

$$\frac{\partial p'}{\partial t} + \gamma\overline{p}\frac{du'}{dx} = (\gamma - 1)q'. \tag{3.29}$$

By performing the operation $u'\times$(Eq. (3.28))$+\frac{p'}{\gamma\overline{p}}\times$(Eq. (3.29)), and using Eq. (3.27), we get

$$\frac{\partial e'}{\partial t} + u'\frac{\partial p'}{\partial x} + p'\frac{\partial u'}{\partial x} = \frac{\gamma - 1}{\overline{\rho c}^2}p'q'. \tag{3.30}$$

Integrating Eq. (3.30) spatially, over the length of the combustor, L, we get

$$\frac{\partial}{\partial t}\int_0^L e'Adx = \frac{\gamma - 1}{\overline{\rho c}^2}\int_0^L p'q'dx - \Delta_L(E'A) - \Phi > 0, \tag{3.31}$$

where $E' = p'u'$, is the acoustic energy flux, Φ is the rate of energy dissipation. x, t are the distance and time, respectively, Δ_L signifies the difference over L, and A is cross-section area of the combustor. Equation (3.31) represents the Rayleigh criterion [81] which, for conditions satisfied by systems analyzed in this work, embodies the main energy transfers in a continuous combustion system. The conclusion drawn from this condition is that a combustion system becomes unstable when $\angle(p' - q') \leq 90°$, as the magnitude of the first term in the RHS is large enough to overcome both the dissipation and the energy flux terms (which are typically small in this class of combustors).

In the case of a concentrated heat release zone, one may consider the boundaries between this zone and the acoustic field as virtual pistons which oscillate in phase with the oscillation of the heat deposition rate into the gas trapped between them. The work done by the oscillating pistons will add energy to the acoustic field. Viewed as such, the first term on the RHS of Eq. (3.31) can be written as a (pdV) work exchange between the small volume, V,within which heat is deposited and the acoustic field. The mass in this control volume undergoes a change in density which follows the heat release rate and leads to the expansion/contraction of the volume, against the fluctuating pressure at its boundaries. The effect of the flame on the acoustic field is therefore analogous to that of a flow source (e.g. speaker) which (as will be shown in Sec. 3.3.2) acts like a monopole [65], and the energy exchange between the flame and the acoustic field can be regarded as "work exchange".

An equivalent, more revealing but less general statement can be obtained by expressing the pressure perturbation as a Galerkin expansion in time and space, $p'/\overline{p} = \Sigma\eta_i(t)\psi_i(x)$, and using the acoustic modes in the absence of heat addition which satisfy the boundary conditions to express the spatial dependence. Assuming that one mode, whose amplitude is η, can be used to capture the dynamics adequately[5], and substituting in the equations governing the perturbation [4], the system response can be described by the following oscillator equation:

$$\ddot{\eta} + \omega^2\eta \;=\; \widetilde{b}\dot{q}', \tag{3.32}$$

where ω is the mode frequency, $\widetilde{b}$ is a constant which depends on the flame location. In Eq. (3.32), it is assumed that the heat release zone is compact, concentrated at a distance from the inlet of the combustor, and that dissipation is negligible. The oscillator equation is closed by expressing q' in terms of η and $\dot{\eta}$ (note that $\dot{\eta}$ is proportional to the velocity perturbation). We can assume, without loss of generality that $q' = q'(\dot{\eta})$ and for convenience write the above as

$$\ddot{\eta} + G(\dot{\eta})\,\dot{\eta} + \omega^2\eta \;=\; 0. \tag{3.33}$$

[5]Without external actuation, this assumption is valid. In case of external actuation, it may be necessary to use more than one mode [4].

This equation shows that a combustion system becomes an unstable oscillator, i.e., possesses "negative damping", when $G(\dot{\eta}) < 0$. For small amplitudes, one can expand G and retain only the constant term to obtain the condition of the linear instability. One can show that this is equivalent to the Rayleigh criterion. As the perturbation grows, and making the reasonable assumption that combustion dynamics become nonlinear before acoustic dynamics, Eq. (3.33) can still be used to approximate the nonlinear behavior and the conditions and mechanisms responsible for establishing limit cycles. In this case, the dependence of G on $\dot{\eta}$, which is the only source of nonlinearity, must be retained. A thorough analysis of nonlinearities in the combustion process is presented in Chapter 5.

3.3 The Role of a Speaker

3.3.1 Dynamic Analysis

Using a single mode to describe the acoustic dynamics, namely the unstable mode[6] we investigate how the loudspeaker impacts the combustor dynamics. For a single mode, Eqs.(3.23)-(3.25) are combined as follows:

$$\ddot{\eta}_1 - \tilde{b}_1\omega_f\tilde{g}_f\tilde{c}_1\,\dot{\eta}_1 + \omega_1^2\eta_1 \;=\; \tilde{b}_1\omega_f\tilde{g}_{f_1}\alpha_r v_c + \tilde{b}_{c_1}\,\dot{v}_c, \tag{3.34}$$

where $\tilde{g}_{f_1} = \tilde{g}_f/\overline{u}_f$. We neglect the second term on the LHS of Eq.(3.24), since the flame characteristic frequency is often smaller than the acoustic frequency by an order of magnitude [25] (bulk modes may be exceptions to this rule, and are treated in [29]). Equations (3.23) and (3.34) show that the speaker affects the combustor dynamics through two parallel paths, a direct path through the pressure generated by its diaphragm acceleration, $\dot{v}_c$, and an indirect path through an additional component of unsteady heat release generated by its diaphragm velocity, v_c. If these two paths are managed, using an intelligent controller, so that they generate, collaboratively, "positive damping" that counters the "negative damping" induced

[6]Under certain circumstances combustor control may require more than one mode for accurate modeling [4], for the sake of analytical tractability and to gain insight, we focus on cases where a single mode is sufficient.

by the unsteady heat release, the combustor can be stabilized. To achieve this, both v_c and $\dot{v}_c$ must have components which are proportional to $\dot{\eta}_1$.

For the dynamics of the speaker as shown in Eq. repsp9, we assume that $\omega_s < \omega_1$ which allows us to approximate the loudspeaker dynamics as

$$\dot{v}_c \cong k_l I. \tag{3.35}$$

The input current into the actuator is determined by a controller according to a measurement of p', u'_f or q'_f which is obtained via a sensor placed at a certain location in the combustor. In the following, we examine the impact of two different control algorithms.

A Proportional Controller:

The measured signal is chosen to be p' which is proportional to η_1, and we need either or both the source terms in the oscillator Eq. (3.34) to be proportional to $\dot{\eta}_1$. The simplest controller that can stabilize the system is a proportional controller, i.e., $I = k_p \bar{p} c_{c_1} \eta_1$. We compute $\dot{v}_c = k_l k_p \bar{p} c_{c_1} \eta_1$ and $v_c = k_l k_p \bar{p} c_{c_1} \dot{\eta}_1 / \omega_1^2$, where the approximate relation, $\eta_1 \cong -\ddot{\eta}_1/\omega_1^2$ is used to get the later. The oscillator equation becomes

$$\ddot{\eta}_1 - \tilde{b}_1 \omega_f \tilde{g}_{f_1} \left(\tilde{c}_1 - \alpha_r \frac{k_l k_p \bar{p} c_{c_1}}{\omega_1^2} \right) \dot{\eta}_1 + \left(\omega_1^2 - \tilde{b}_{c_1} k_l k_p \bar{p} c_{c_1} \right) \eta_1 = 0. \tag{3.36}$$

Equation (3.36) shows that only the indirect path adds damping to the system. A stable oscillator must satisfy

$$\tilde{b}_1 \omega_f \tilde{g}_{f_1} \left(\tilde{c}_1 - \alpha_r \frac{k_l k_p \bar{p} c_{c_1}}{\omega_1^2} \right) < 0. \tag{3.37}$$

The proportional controller has two free parameters: the sensor location which determines c_{c_1}, and the gain k_p, both of which have selectable signs. Interestingly, the actuator location does not contribute to the damping, since it affects only the direct path. Thus, the controller has enough degrees of freedom to satisfy the inequality. Although the proportional controller is able to add enough damping to achieve stability, it requires high gain since it takes advantage of a single channel only. Moreover, it changes the frequency of the oscillation

substantially; part of the input energy is not utilized to suppress the instability. A large change in the frequency is expected, since $\widetilde{b}_{c_1} k_l k_p \overline{p} c_{c_1} > (\widetilde{b}_{c_1} \widetilde{c}_1 / \alpha_r)\omega_1^2$, and $(\widetilde{b}_{c_1} \widetilde{c}_1 / \alpha_r) \approx O(1)$. Thus, a fraction of the input energy is "wasted" and will be quantified in Sec. 3.3.2.

The analysis shows some surprising results. While one traditionally considers the role of an acoustic actuator as a means of imposing a pressure signal which is out of phase with the existing signal, i.e., an anti-sound mechanism, our results here show that this is not always the case. In the case analyzed above, the only mechanism by which the actuator can impact the system is by affecting the heat source, through the extra velocity signal which is managed by the controller for stability.

A Phase-Lead Controller:

To overcome the drawbacks in the proportional controller, one should design a controller such that both source terms in Eq.(8) contribute directly to $\dot{\eta}_1$. This can be achieved using a phase-lead compensator whose dynamics are governed by:

$$\dot{I} + p_c I = k_c \overline{p} c_{c_1} (\dot{\eta}_1 + z_c \eta_1), \tag{3.38}$$

where p_c, z_c, and k_c are the compensator parameters: pole, zero, and gain, respectively. The phase-lead compensator adds a positive phase that can counter the effect of the negative phase by the heat release dynamics, achieved via $p_c > z_c$ [71]. There are two choices for the compensator pole: $p_c > \omega_1$ and $p_c < \omega_1$. We discuss the first one only. In this case,

$$I \cong \frac{k_c \overline{p} c_{c_1}}{p_c} \left[\left(1 - \frac{z_c}{p_c} \right) \dot{\eta}_1 - \frac{\ddot{\eta}_1}{p_c} + z_c \eta_1 \right]. \tag{3.39}$$

Combining Eqs.(3.35) and (3.39), we write:

$$\dot{v}_c \cong \frac{k_o \overline{p} c_{c_1}}{p_c} \left[\omega_1 \left(\frac{z_c}{\omega_1} + \frac{\omega_1}{p_c} \right) \eta_1 + \left(1 - \frac{z_c}{p_c} \right) \dot{\eta}_1 \right], \tag{3.40}$$

which is integrated to

$$v_c \cong \frac{k_o \overline{p} c_{c_1}}{p_c} \left[\left(1 - \frac{z_c}{p_c} \right) \eta_1 - \frac{1}{\omega_1} \left(\frac{z_c}{\omega_1} + \frac{\omega_1}{p_c} \right) \dot{\eta}_1 \right], \tag{3.41}$$

where $k_o = k_l k_c$. Substituting in Eq. (3.34), we obtain:

$$\ddot{\eta}_1 + \left\{ -\widetilde{b}_1 \omega_f \widetilde{g}_{f_1} \widetilde{c}_1 + \frac{k_o \overline{p} c_{c_1}}{p_c} \left[\frac{\widetilde{b}_1 \omega_f \widetilde{g}_{f_1} \alpha_r}{\omega_1} \left(\frac{z_c}{\omega_1} + \frac{\omega_1}{p_c} \right) - \widetilde{b}_{c_1} \left(1 - \frac{z_c}{p_c} \right) \right] \right\} \dot{\eta}_1 + \left\{ \omega_1^2 - \frac{k_o \overline{p} c_{c_1}}{p_c} \left[\widetilde{b}_{c_1} \omega_1 \left(\frac{z_c}{\omega_1} + \frac{\omega_1}{p_c} \right) - \widetilde{b}_1 \omega_f \widetilde{g}_{f_1} \alpha_r \left(1 - \frac{z_c}{p_c} \right) \right] \right\} \eta_1 = 0 \qquad (3.42)$$

The damping terms due to direct and indirect channels (the third and second term in the bracket multiplied by $\dot{\eta}_1$, respectively) show that the condition for the direct path to lead to positive damping is $\widetilde{b}_{c_1} k_o c_{c_1} < 0$, and for the indirect path is $\widetilde{b}_1 k_o c_{c_1} > 0$. Recall that $\widetilde{b}_{c_1}$, $\widetilde{b}_1$, and c_{c_1} depend on the locations of the actuator, flame, and sensor, respectively, while k_o is the gain. The phase-lead controller has enough degrees of freedom to satisfy both inequalities at the same time, since we can choose $sign(k_o c_{c_1}) = sign(\widetilde{b}_1)$, and $sign(\widetilde{b}_{c_1}) = -sign(k_o c_{c_1})$.

For the sake of examining the two effects, let k_o/p_c =const. In this case, the indirect damping decreases with p_c, while the direct damping increases. If the actuator is located close to a pressure node, where $\widetilde{b}_{c_1} = 0$, the indirect damping becomes dominant. The optimization of damping from both channels is not well defined in the absence of actuator constraints, e.g., its location. For instance, when the actuator is close to a pressure node, then $z_c \approx \omega_1$ maximizes damping. However, if we assume that k_o/p_c =const. and $z_c = 0$, maximum total damping is achieved when $p_c \approx \omega_1$. If the actuator is located at a pressure anti-node, maximum damping is achieved when the contribution from the direct and indirect paths are of the same order of magnitude. Similar results are obtained for $p_c < \omega_1$.

Thus, by properly selecting the controller parameters, one can impose damping through both channels and hence minimize the required input energy for a given settling time.

Optimization

Here, we define optimization as minimizing the maximum input power. Using $| \dot{\eta}_1 | \approx \omega_1 |\eta_1|$, we find, for $p_c > \omega_1$, that:

$$|I| \cong \frac{k_c \overline{p} c_{c_1} \omega_1}{p_c} \sqrt{\left(\frac{z_c}{\omega_1} + \frac{\omega_1}{p_c} \right)^2 + \left(1 - \frac{z_c}{p_c} \right)^2} |\eta_1| = P_d |\eta_1| \qquad (3.43)$$

subject to

$$\frac{k_o \overline{p} c_{c_1}}{p_c}\left[\frac{\widetilde{b}_1 \omega_f \widetilde{g}_{f_1} \alpha_r}{\omega_1}\left(\frac{z_c}{\omega_1}+\frac{\omega_1}{p_c}\right)-\widetilde{b}_{c_1}\left(1-\frac{z_c}{p_c}\right)\right]=\text{const.} \tag{3.44}$$

The constraints come from the fact that we need to minimize the input power for a certain settling time, and hence the damping coefficient must be held constant. Let $\frac{k_c}{p_c} = w_1$, $\frac{z_c}{\omega_1}+\frac{\omega_1}{p_c} = w_2$, $1-\frac{z_c}{p_c} = w_3$, $\overline{p} c_{c_1}\omega_1 = g_1$, $k_l \overline{p} c_{c_1}\widetilde{b}_1 \omega_f \widetilde{g}_{f_1}\alpha_r/\omega_1 = g_2$ and $k_l \overline{p} c_{c_1}\widetilde{b}_{c_1} = -g_3$. The minimization problem is written as:

$$P_{d_{min}} = \min\left\{w_1 g_1 \sqrt{w_2^2+w_3^2}\right\}, \tag{3.45}$$

subject to

$$w_1(g_2 w_2 + g_3 w_3) = c_d, \tag{3.46}$$

leading to:

$$P_{d_{min}} = \frac{c_d g_1}{g_3}\min\left[\sqrt{\left(\frac{w_2}{w_3}\right)^2+1}\times\left(\frac{g_2 w_2}{g_3 w_3}+1\right)^{-1}\right]. \tag{3.47}$$

Equation (3.47) shows that the function to be minimized is reduced to a function in a single variable: (w_2/w_3). The minimum power is reached at

$$(w_2/w_3)_{min} = g_2/g_3, \tag{3.48}$$

and the minimum maximum amplitude of the input current is:

$$|I|_{min-max} \cong \frac{c_d g_1}{\sqrt{g_2^2+g_3^2}}|\eta_1|_{max}. \tag{3.49}$$

It is worth noting that the optimal ratio in Eq. (3.48) leads to no change in the natural frequency of the oscillator in Eq.(3.42). Moreover, the problem of maximizing the damping while keeping the input power constant leads to the same result as in Eq. (3.48). Similar results are obtained for $p_c < \omega_1$.

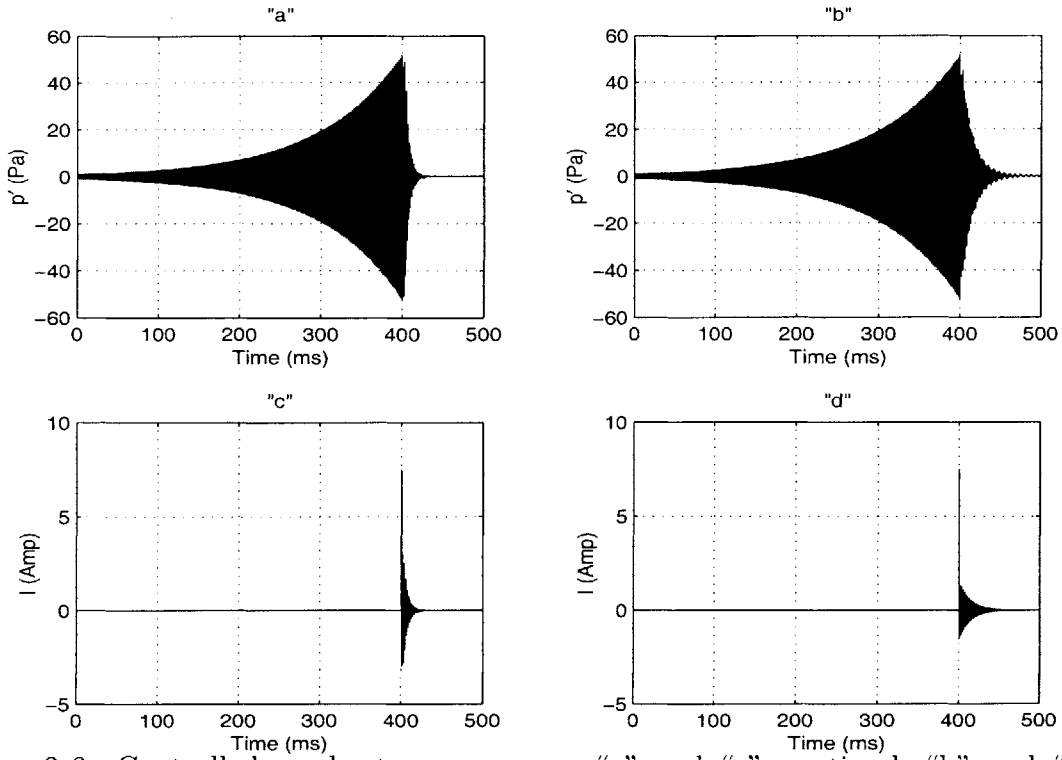

Figure 3-6: Controlled combustor responses. "a" and "c": optimal, "b" and "d": non-optimal

To illustrate the optimization results, we test two controllers, an optimal and a non-optimal, with a combustor setup similar to Ref. [4]. The combustor is 4 cm in diameter and 50 cm long with closed upstream end and open downstream end. The flame is anchored on a perforated disc with 80 holes (each 1.5 mm in diameter), at x_f=32.5 cm. Assuming a perfect gas with $\gamma = 1.4$, $\overline{p}$ =1 atm, and $\Delta h_r = 2.15\times10^6$J/kg, which corresponds to $\overline{\phi} = 0.7$, $S_u = 0.3$ m/s. Effects of the mean flow and mean heat addition are neglected. However, we include two acoustic modes (quarter and three quarter modes), the low frequency dynamics of the heat release, and the speaker dynamics (as in Eq. (3.10), with $k_l = 1404$, $\omega_l = 1822$, and $\zeta = 0.1$) in the combustor model. Since the optimization is based on one mode, we choose the sensor and actuator locations such that the coupling between modes is weak [4], namely we set x_s=1 cm and x_a=15 cm. Using the optimization analysis, we obtain $k_c = -0.1437$, $z_c = 2018.9$, and $p_c = 9173.2$. On the other hand, the second controller which is designed considering the phase needed for stability has $k_c = -0.1437$, $z_c = 100$, and $p_c = 15000$. We choose the gain of the latter to be equal to that of the optimal controller to ensure equal maximum input current. The pressure responses of the two controllers are shown in Figs. 3-6-a and 3-6-b (control is switched *on* at 400 ms). The control effort in terms of the speaker input current is given in Figs. 3-6-c and 3-6-d. One can see that for the same maximum input current, the optimal controller reduces the pressure to 5% of its

initial value in 17 ms, while the non-optimal one needs 41.6 ms, which is more than twice that of the optimal controller.

3.3.2 Energy Analysis

In Sec. 3.3.1, we based the stability analysis on the properties of the oscillator. Here, we pursue a different analysis for the purpose of explaining the origin of the "dissipation". The primary energy storage mechanism in the combustor is the acoustic field. Increasing the stored (or internal) energy of this field can be achieved by doing positive work by "external" sources which include the flame and the actuator. Work from the flame has been explained in Sec. 3.2.1 as done on the field by expansion/contraction of a small volume surrounding it against negative/positive unsteady pressure. When actuation from a speaker is incorporated and dissipation is neglected, the time integral of Eq. (3.31) leads to

$$\begin{aligned}\Delta_\tau\left(\int_0^L e'dx\right) &= \frac{\gamma-1}{\overline{\rho c}^2}\int_0^\tau\int_0^L p'q'dxdt \\ &\quad -\alpha_r\int_0^\tau\int_0^L p'\delta(x-x_a)\vec{v}_b.\hat{n}dxdt-\Delta_L\left(\int_0^\tau E'dt\right),\end{aligned} \tag{3.50}$$

where Δ_τ and Δ_L denote the change over time and over length, respectively, and we denote $\vec{v}_b = -v_c$, since the direction of the velocity from the speaker membrane is opposite to the unit normal to the control surface, $\hat{n}$, (note that the acoustic field is regarded here as the control volume). The RHS terms are the work per unit cross-section area of the combustor done by the heat source, in this case the flame, the speaker, and the net acoustic energy convected across the boundaries, respectively. The loudspeaker which is a flow source exerts work on the acoustic field similar to a monopole source [65].

Rewriting Eq. (3.50) as $\Delta_\tau\left(\int_0^L e'dx\right) = W_f + W_d$, substituting for the heat release dynamics by Eqs. (3.24) and (3.25), neglecting b_f with respect to the acoustics frequencies (as in Sec. 3.3.1), assuming the presence of one mode only, and carrying out the integration over L, we have

$$W_f = W_q + W_i, \tag{3.51}$$

$$W_q = \frac{\gamma-1}{\gamma}\omega_f \tilde{g}_{f_1} c_{c_f} \tilde{c}_1 \int_0^\tau \eta_1^2 dt, \tag{3.52}$$

$$W_i = \frac{\gamma-1}{\gamma}\omega_f \tilde{g}_{f_1} c_{c_f} \alpha_r \int_0^\tau \eta_1 \left(\int_0^\tau v_b dT\right) dt, \tag{3.53}$$

$$\text{and } W_d = \alpha_r \bar{p} c_{c_a} \int_0^\tau \eta_1 v_b dt, \tag{3.54}$$

where Eqs. (3.52)-(3.54) denote the work exchange between the flame and the acoustic field, the actuator and the flame, and the actuator and the acoustic field directly, respectively. W_f is composed of the total work exchange with the flame. Without actuation, only W_q exists and work is done on the acoustic field. W_i results because the speaker does work on the flame (through Eqs. (3.24) and (3.25)) and hence indirectly affects the acoustic field. This is negative work on the field which counteracts W_q. W_d is work done by the field on the speaker.

Without active control,$W_d = W_i = 0$ and for an unstable combustor, $\Delta_\tau \left(\int_0^L e' dx\right) > 0$, and hence $W_f = W_q > 0$, while q_f' and p' are in phase. When active control is applied, the condition for stability, $\Delta_\tau \left(\int_0^L e' dx\right) < 0$, leads to $W_i + W_d < -W_q$.

For the proportional controller considered in Sec. 3.3.1, and for the conditions obtained by the damping analysis (Eq. (3.37)), we find that

$$W_i = -\frac{\gamma-1}{\gamma}\omega_f \tilde{g}_{f_1} \frac{\alpha_r k_l k_p \bar{p} c_{c_1} c_{c_f}}{\omega_1^2} \int_0^\tau \eta_1^2 dt < 0, \tag{3.55}$$

$$\text{and } W_d = \frac{\alpha_r k_l k_p \bar{p}^2 c_{c_1} c_{c_a}}{2\omega_1^2} \left[\eta_1^2(0) - \eta_1^2(\tau)\right] > 0. \tag{3.56}$$

Thus, as shown before in the damping analysis, stabilization comes only from the indirect path while the direct path adds energy to the acoustic field. Moreover, since $W_i < -W_q$, $W_f < 0$, and q_f' and p' are out of phase. Actuation adds energy to the field from the direct channel, W_d, while it modifies the flame oscillations such that the work is done by the field on the flame ($W_f < 0$), and is so much larger than W_d that the overall effect is stabilizing.

The ratio of the useful work done by the loudspeaker, which stabilizes the combustor, and that wasted in the process, i.e., consumed in altering ω_1 as discussed in Sec. 3.3.1, is

$$\left|\frac{W_i}{W_d}\right| = 2\frac{\gamma-1}{\gamma}\frac{\omega_f \tilde{g}_{f_1}}{\bar{p}} \left|\frac{c_{c_f}}{c_{c_a}}\right| \left|\frac{\int_0^\tau \eta_1^2 dt}{[\eta_1^2(0) - \eta_1^2(\tau)]}\right|, \tag{3.57}$$

$$\text{where } \left|\frac{\int_0^\tau \eta_1^2 dt}{[\eta_1^2(0) - \eta_1^2(\tau)]}\right| \cong \frac{1/\omega_1}{\alpha/\omega_1} = \frac{1}{\alpha}, \tag{3.58}$$

and α is the decay rate. This leads to $|W_i/W_d| \approx O(1)$. Thus, the useful work is of the same order as that wasted in changing the potential energy of the acoustic field. This ratio stays the same if q'_f is chosen as the feedback signal since $q'_f \propto \eta_1$. When $u'_f(\propto \dot{\eta}_1)$ is fed back, W_d becomes dominant.

When the phase-lead controller is used, for $p_c > \omega_1$ and maintaining the same stable conditions obtained from the damping analysis (Sec. 3.3.1), the work done per unit area is:

$$W_i \cong -\frac{\gamma-1}{\gamma}\omega_f \tilde{g}_{f_1} \frac{\alpha_r k_o \overline{p} c_{c_1} c_{c_f}}{p_c \omega_1}\left(\frac{z_c}{\omega_1} + \frac{\omega_1}{p_c}\right)\int_0^\tau \eta_1^2 dt < 0, \tag{3.59}$$

$$\text{and } W_d \cong \frac{\alpha_r k_o \overline{p}^2 c_{c_1} c_{c_a}}{p_c}\left(1 - \frac{z_c}{p_c}\right)\int_0^\tau \eta_1^2 dt < 0. \tag{3.60}$$

Both work exchanges are done by the acoustic field on the actuator and the flame, i.e., the imposed action represents an energy sink for the acoustic field. Note that Eq. (3.60) is negative due to the choice of $sign(k_o c_{c_1}) = -sign(c_{c_a}) = sign(c_{c_f})$, agreeing with the stability conditions discussed in Sec. 3.3.1. Similar conclusions can be reached for the case with $p_c < \omega_1$.

Thus, both the indirect and direct actuation paths participate in decreasing the acoustic energy in the combustor. However, while the former mechanism changes the phase between q'_f and p' from a destabilizing to a stabilizing one, the latter appears as work done by the field on the actuator.

Figures 3-7 and 3-8 are a graphical representation of the results for a combustor similar to that in Sec. 3.3.1 except for x_f, x_a, and x_s, which are 24cm, 12.3cm, and 25cm, respectively. The controller parameters are $k_c = 250$, $z_c = 100$, and $p_c = 1000$ and make the direct and indirect work of the same order. Figure 3-7 shows the different energies for conditions when the indirect path is *forced* to zero. The latter can be weak if the flame is robust to fluctuations in the acoustic field. As shown in Fig. 3-7-d, the combustor is driven to stability when the control is *on* at 40ms, and the acoustic energy is reduced to zero. W_f (equivalent to the Rayleigh index) remains > 0 (Fig. 3-7-c), i.e., p' and q'_f remain in phase, whereas

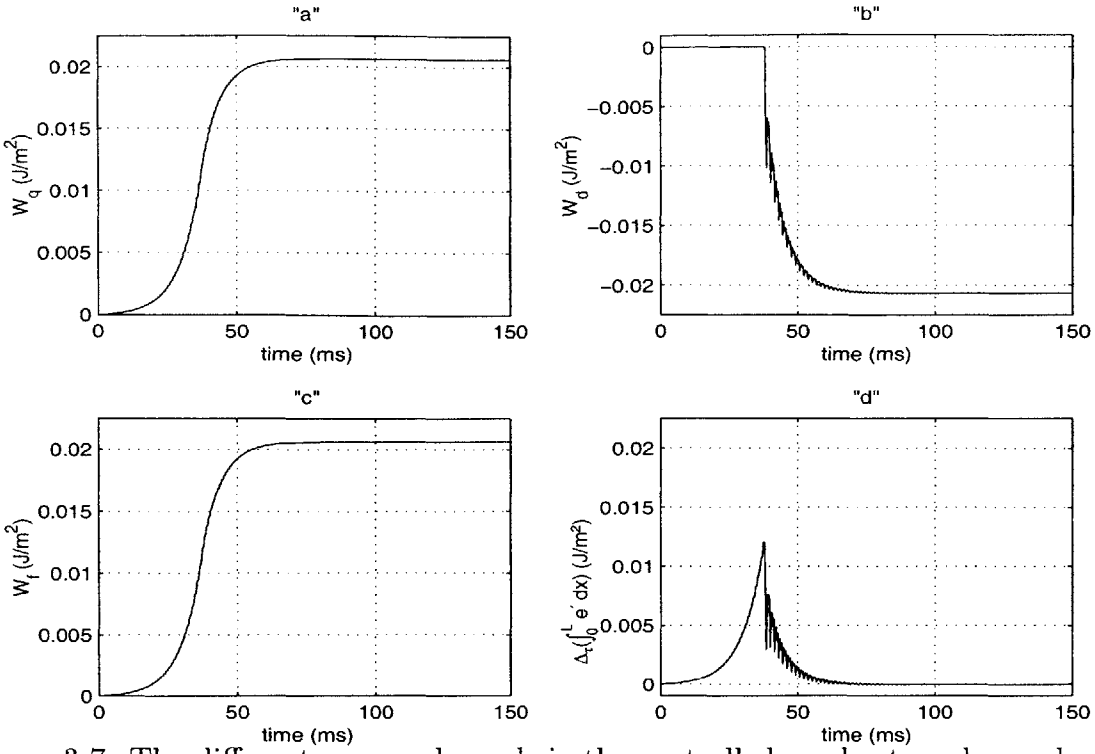

Figure 3-7: The different energy channels in the controlled combustor when only the direct effect is active, and the indirect effect is *forced* to zero

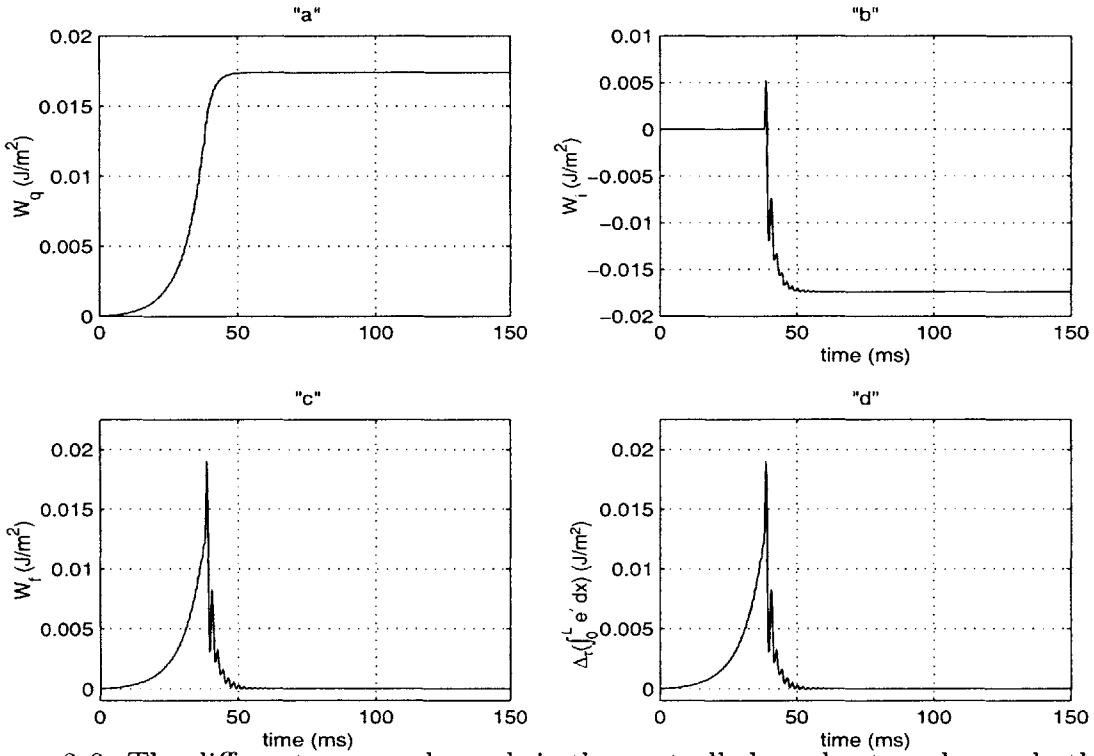

Figure 3-8: The different energy channels in the controlled combustor when only the indirect effect is active, and the direct effect is *forced* to zero

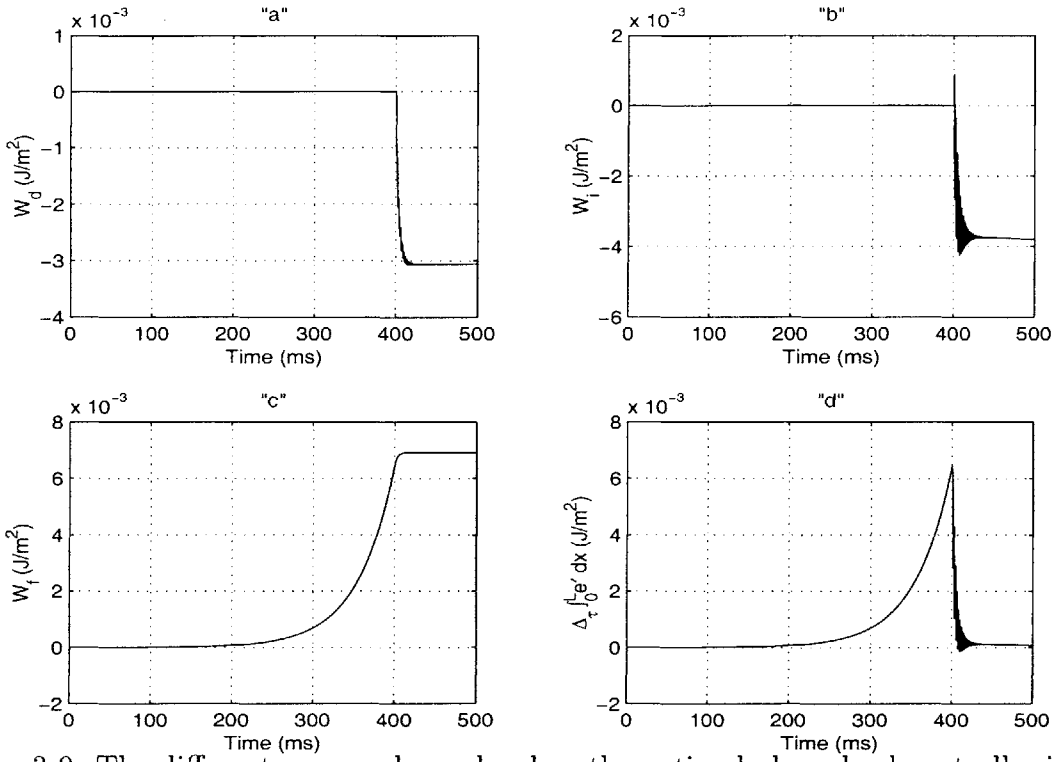

Figure 3-9: The different energy channels when the optimal phase-lead controller is used, as in Sec. 4.1.3

the energy sink stems completely from W_d (Fig. 3-7-b), i.e., the speaker extracts energy from the acoustic field by letting the field do work on it. In Fig. 3-8, when the direct path is *forced* to zero, which can happen if the speaker is placed at a pressure node, $W_i < 0$ as shown in Fig. 3-8-b, i.e., p' and q'_f become out of phase, and W_f decreases as in Fig. 3-8-c. In this case also, the field does work on the speaker.

Using the optimal phase-lead controller designed in Sec. 3.3.1, we illustrate in Fig. 3-9 the different work exchanges. Note that W_d (Fig. 3-9-a) is dominant and contributes more to stabilization than W_i (Fig. 3-9-b). Thus, for this optimal controller, $W_f > 0$ (Fig. 3-9-c), i.e., p' and q'_f remain in phase. Figure 3-9-d shows that the combustor has been stabilized, and the acoustic energy is driven to zero.

The simulation illustrates that the different work exchanges affecting the acoustic energy maintain the same signs as predicted in the one-mode analysis, even in the presence of two modes and with no simplification in the heat release dynamics model (Eqs. (3.23)-(3.26)).

3.4 The Role of a Fuel Injector

In the case where an oscillating fuel stream (operated by a solenoid valve) is used for actuation, as in [55, 101, 15], we choose to inject the secondary fuel either at the burning zone, or upstream the flame where it mixes with the incoming mixture of reactants creating an unsteady equivalence ratio component, ϕ', which is superimposed to the steady equivalence ratio, $\overline{\phi}$. The injection of a secondary fuel is done at a distance upstream the flame to guarantee good mixing, i.e., the time of mixing is smaller than the convective time between injection and the flame. This introduces a convective time lag, τ_c, in ϕ' and the controlled equivalence ratio at the flame can be expressed as $\phi'_f(t) = \phi'(t - \tau_c)$, where $\tau_c = L_c/\overline{u}$, where L_c is the distance between the injector and the flame front, and $\overline{u}$ is the mean velocity of the reactants. τ_c is greater than the acoustic time of the system, τ, ($\tau_c/\tau = kL_c/2\pi\overline{M}$, where k is the wave number and $\overline{M}$ is the Mach number), and conventional control techniques will fail to stabilize the system [71]. Several studies have proposed control solutions for systems with large delays [43, 68]. In this section, for the purpose of this analysis, we will only be concerned with the effect of the resultant equivalence ratio at the flame, ϕ'_f. This can be physically realized in practical combustors by injecting at the burning zone, thus minimizing transport lag. Mixing, on the other hand, should be enhanced to avoid forming a diffusion flame which can be totally uncoupled with the primary premixed flame, and thus ineffective in controlling the system [40]. The control design for compensating for the time delay in combustion systems is discussed in details in Chapter 4[38, 40].

3.4.1 Dynamic Analysis

Equations (3.23)-(3.25) are combined to get the oscillator equation:

$$\ddot{\eta}_1 - \tilde{b}_1\omega_f\tilde{g}_{f_2}\tilde{c}_1\,\dot{\eta}_1 + \omega_1^2\eta_1 \;=\; \tilde{b}_1\omega_f\tilde{g}_{f_2}(\phi'_f + \dot{\phi}'_f\,/\omega_f), \tag{3.61}$$

where $\tilde{g}_{f_2} = \tilde{g}_f/\overline{\phi}_f$. Here, we notice that the combustion system, implicitly through the heat release dynamics in Eq. (3.24), reacts to equivalence ratio perturbations, and the rate of these perturbations [29, 38] as shown in the first and second terms in the RHS of Eq. (3.61),

respectively. It is obvious that if ϕ'_f is modulated in such a way to create positive damping that would counteract the destabilizing damping caused by the heat release, stability can be reached. For the purpose of this paper, the dynamics of the injector will be disregarded for simplicity, and are studied in [38]. Here, we make the assumption that the bandwidth of the injector is much higher than the acoustic frequencies, therefore, we assume $\phi'_f \cong k_i I$. Using a pressure transducer as sensor, consistent with the analysis done with the speaker in Sec. 3.3, the signal fed to the controller is proportional to η_1.

A Proportional Controller:

Proportional control is the simplest structure that can be used to stabilize the combustor. Similar to Sec. 3.3.1, the equivalence ratio at the burning zone can be computed as $\phi'_f = k_i k_p \overline{p} c_{c_1} \eta_1$, with a rate of change $\dot{\phi}'_f = k_i k_p \overline{p} c_{c_1} \dot{\eta}_1$, and hence the oscillator becomes

$$\ddot{\eta}_1 - \widetilde{b}_1 \omega_f \widetilde{g}_{f_2} \left(\widetilde{c}_1 - \frac{k_i k_p \overline{p} c_{c_1}}{\omega_f} \right) \dot{\eta}_1 + \left(\omega_1^2 - \widetilde{b}_1 \omega_f \widetilde{g}_{f_2} k_i k_p \overline{p} c_{c_1} \right) \eta_1 = 0, \tag{3.62}$$

which shows that only the $\dot{\phi}'_f$ adds damping to the system, whereas the ϕ'_f channel contributes only in changing the frequency of at which the system oscillates. The condition for stability is

$$\widetilde{b}_1 \omega_f \widetilde{g}_{f_2} \left(\widetilde{c}_1 - \frac{k_i k_p \overline{p} c_{c_1}}{\omega_f} \right) < 0. \tag{3.63}$$

The proportional controller has enough degrees of freedom to stabilize the system in the form of the sensor's location, c_{c_1}, and the gain, k_p, both of which have selectable signs. Here, we note that unlike the speaker in Sec. 3.3.1, the "wasted" effort is much less, and can be estimated using Eqs. (3.62) and (3.63) as $\widetilde{b}_1 \omega_f \widetilde{g}_{f_2} k_i k_p \overline{p} c_{c_1} > \omega_1$ which is less than ω_1^2 by $O(\omega_1)$. In section 3.4.2, this "wasted" energy will be estimated as a fraction of the "useful" energy.

A Phase-Lead Controller:

For the case when $p_c > \omega_1$, a phase-lead controller can be approximated as in Eq. (3.39), and ϕ'_f will replace $\dot{v}_c$ in Eq. (3.40), with $k_o = k_i k_c$, and its rate can be computed as

$$\dot{\phi'}_f \cong \frac{k_o \overline{p} c_{c_1}}{p_c} \left[\omega_1^2 \left(1 - \frac{z_c}{p_c} \right) \eta_1 + \omega_1 \left(\frac{z_c}{\omega_1} + \frac{\omega_1}{p_c} \right) \dot{\eta}_1 \right], \tag{3.64}$$

resulting in

$$\begin{aligned} \ddot{\eta}_1 \; + \; & \left\{ -\tilde{b}_1 \omega_f \tilde{g}_{f_2} \tilde{c}_1 - \tilde{b}_1 \omega_f \tilde{g}_{f_2} \frac{k_o \overline{p} c_{c_1}}{p_c} \left[\omega_1 \left(\frac{z_c}{\omega_1} + \frac{\omega_1}{p_c} \right) + \left(1 - \frac{z_c}{p_c} \right) \right] \right\} \dot{\eta}_1 \\ + \; & \left\{ \omega_1^2 - \tilde{b}_1 \omega_f \tilde{g}_{f_2} \frac{k_o \overline{p} c_{c_1}}{p_c} \left[\omega_1 \left(\frac{z_c}{\omega_1} + \frac{\omega_1}{p_c} \right) - \omega_1^2 \left(1 - \frac{z_c}{p_c} \right) \right] \right\} \eta_1 = 0. \end{aligned} \tag{3.65}$$

We note that both channels contribute to "positive" damping when the condition for stability $\tilde{b}_1 k_o c_{c_1} < 0$, and hence $sign(k_o c_{c_1}) = -sign(\tilde{b}_1)$, is satisfied.

As in the case of the proportional controller, we note also that there is some energy wasted in changing the frequency of the oscillator, and this can be estimated following arguments similar to 3.3.1 for the speaker. In order to force the injector to target all the effort towards adding damping without any waste in changing the potential energy of the system, i.e., ω_1, an optimal approach similar to Sec. 3.3.1 can be carried out. As discussed before, the optimization will lead to zero change in the natural frequency.

Moreover, in Sec. 3.4.2, we will quantify both analytically and graphically the contribution of $\dot{\phi'}_f$ and ϕ'_f to positive damping.

3.4.2 Energy Analysis

The energy balance with an injector assuming no dissipation is identical to Eq.(3.50) without the second term in the RHS (which is due to the speaker). One can see that the only means for stabilizing the combustor using a secondary fuel injector is to alter the phase between q'_f and p', similar to the indirect actuation in the speaker (Sec. 3.3.2). Because of the linearity of the problem, one can identify easily the work contributed by actuation, W_{inj}, and by the

acoustic field, W_q, to the total work, W_f, and we write

$$W_f = W_q + W_{inj}, \tag{3.66}$$

$$W_{inj} = W_\phi + W_{\dot{\phi}}, \tag{3.67}$$

$$W_\phi = \frac{\gamma-1}{\gamma}\omega_f \tilde{g}_{f_2} c_{c_f} \int_0^\tau \eta_1 \left(\int_0^\tau \phi'_f dT \right) dt, \tag{3.68}$$

$$\text{and } W_{\dot{\phi}} = \frac{\gamma-1}{\gamma}\omega_f \tilde{g}_{f_2} c_{c_f} \int_0^\tau \frac{\phi'_f}{\omega_f} \eta_1 dt, \tag{3.69}$$

As discussed in Sec. 3.4.1, the injector has two contributions one from the equivalence ratio and the other from its rate of change, they are denoted here as W_ϕ, and $W_{\dot{\phi}}$, respectively. $W_q > 0$ (and is defined in Eq. (3.52)), when no active control is implemented, the energy in the combustor grows according to Eq. (3.50). Thus, the condition for stability, is to induce an additive negative work by altering ϕ'_f in order to satisfy $W_{inj} < -W_q$.

As discussed before in Sec. 3.4.1, when using a proportional controller with same stable conditions as in Sec. 3.4.1, only the $\dot{\phi}_f$ is contributing to stability, and this can be illustrated also in terms of the work done per unit area where:

$$W_{\dot{\phi}} \cong \frac{\gamma-1}{\gamma}\omega_f \tilde{g}_{f_2} k_i k_p \bar{p} c_{c_1} \int_0^\tau \eta_1^2 dt < 0, \tag{3.70}$$

$$\text{and } W_\phi \cong \frac{\gamma-1}{\gamma}\frac{\omega_f \tilde{g}_{f_2} k_i k_p \bar{p} c_{c_1}}{2\omega_1^2}[\eta_1^2(0) - \eta_1^2(\tau)] > 0. \tag{3.71}$$

The ratio of useful work, targeted towards dissipative energy, to the work wasted in changing the potential energy of the system can be estimated by considering Eqs. (3.70) and (3.71), with (3.58), as

$$\left| \frac{W_{\dot{\phi}}}{W_\phi} \right| \cong \frac{2\omega_1^2}{\omega_f}\frac{1}{\alpha} \cong O\left(\frac{\omega_1}{\omega_f}\right) > 1. \tag{3.72}$$

In this case, unlike the speaker (Sec. 3.3.2), the useful work of the injector is larger than the wasted one, supporting the results in the dynamic analysis in Sec. 3.4.1.

The phase-lead controller, as discussed in Sec. 3.4.1, has sufficient degrees of freedom to

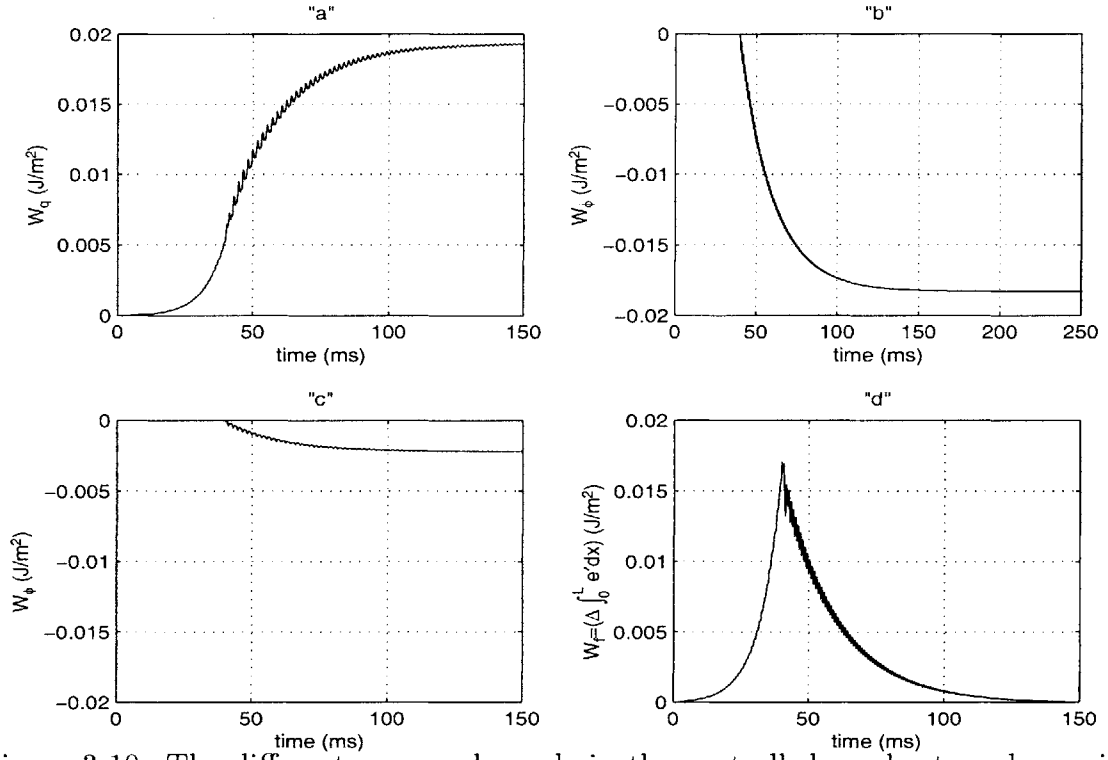

Figure 3-10: The different energy channels in the controlled combustor when using a fuel injector.

accomplish stability, and one can show that

$$W_{\dot{\phi}} \cong \frac{\gamma-1}{\gamma}\omega_f \tilde{g}_{f_2} \frac{k_o \overline{p} c_{c_1} c_{c_f}}{p_c \omega_f} \left(\frac{z_c}{\omega_1} + \frac{\omega_1}{p_c}\right) \int_0^\tau \eta_1^2 dt < 0, \tag{3.73}$$

$$\text{and } W_\phi \cong \frac{\gamma-1}{\gamma}\omega_f \tilde{g}_{f_2} \frac{k_o \overline{p}^2 c_{c_1}}{p_c} \left(1 - \frac{z_c}{p_c}\right) \int_0^\tau \eta_1^2 dt < 0. \tag{3.74}$$

Although both $W_{\dot{\phi}}$ and W_ϕ contribute in stabilizing the combustor, the former effect is larger than the latter, and this can be quantified as

$$\left|\frac{W_{\dot{\phi}}}{W_\phi}\right| = \frac{\left(\frac{z_c}{\omega_1} + \frac{\omega_1}{p_c}\right)}{\left(1 - \frac{z_c}{p_c}\right)} \frac{\omega_1}{\omega_f} \sim O(10). \tag{3.75}$$

Figure 3-10 is a graphical representation of the analytical results. The phase-lead parameters are $k_c = 2000$, $z_c = 100$ and $p_c = 1000$. Both channels, $W_{\dot{\phi}}$ (in Fig. 3-10-b) and W_ϕ (in Fig. 3-10-c), suppress the instability by doing work on the heat release such that the phase between q'_f and p' is modified to ¡90°, similar to the indirect effect in a speaker, as discussed in Sec. 3.3.2. It is worth noting, from Fig. 3-10 b and c, that $W_{\dot{\phi}}/W_\phi \sim O(10)$ as estimated by Eq. (3.75).

Chapter 4

Control

In this chapter, both actuators presented in Chapter 3 will be used with model-based control. First, in Sec. 4.1, a speaker is used, and model-based control is implemented in simulation as well as experimentally on an MIT test-rig. We show that an LQG/LTR controller is appropriate when speakers are used and when instabilities are caused by flame area fluctuations through phase-lag instability, i.e., without pure time delays. Second, in Sec. 4.2, and injector is implemented through simulations for two different combustors: a typical organ-pipe combustor which replicates some of the dominant dynamics in real combustors and is built at MIT (similar to [48, 34]) and a dump combustor similar to the one used by UTRC [15]. We show that LQG/LTR controller is appropriate when the system is devoid of convective or propagation time delays. When the latter exist, two categories of controllers are presented that take into account the delays. (i) In Sec. 4.2.1, we propose a group of controllers that is able to stabilize a combustor that exhibits a bulk-mode instability, while (ii) in Sec. 4.2.2 we present a Posi-Cast control that is capable of stabilizing a combustor with multiple longitudinal modes.

Moreover, the impact of fuel injectors characteristics including bandwidth, authority (pulsed-fuel flow rate), and whether it applies a proportional or a two-position (on-off) injection are discussed.

4.1 Control Using a Speaker

In this section, instability due to area fluctuations driven by a phase-lag mechanism ($\gamma_1 < 0$, and $\tau_f \sim 0$ in Eq. (2.42)) is considered as it applies to a combustor rig at MIT similar to those used in [77, 34]. In general, a host of control methods can be applied to stabilize the combustor whether the actuator is side-mounted or end-mounted. The dominant features of the combustor that should be kept in mind while carrying out the control design are (i) the order of the system including the speaker dynamics is $2n + 3$, where n is the number of acoustic modes, (ii) the system has two complex unstable poles, (iii) the system can have unstable zeros for a number of actuator-sensor locations even when they are collocated [4], (iv) the different modes of the system are coupled [4], (v) all states are not accessible, (vi) the system is controllable and observable for a number of actuator-sensor positions, (vii) the actuator output is constrained to lie within specified bounds and (viii) nonlinearities are present whose effect is a stabilizing one leading to a limit-cycle behavior.

The gain and phase characteristics of the combustor can vary significantly over a wide range of frequencies [4]. Therefore, considerable care must be taken to design a dynamic compensator which takes into account the frequency characteristics of the open-loop transfer function. In particular, the phase and gain variations of such a compensator must be shaped appropriately so that destabilizing effects are avoided [27]. When two modes are present, because the underlying system is of order seven, a first-order phase-lead controller is inadequate for many actuator-sensor locations due to insufficient degrees of freedom in the controller parameterization [4]. Below, we propose a control design of the requisite complexity, motivated by an optimization point of view. This is followed by simulations and experimental results of an organ-pipe combustor rig.

4.1.1 LQG/LTR control

The idea behind the Linear-Quadratic-Gaussian Regulator with Loop-Transfer Recover (LQG/LTR) is to design a stabilizing control input for a finite-dimensional linear system which simultaneously optimizes a quadratic cost function in the system states and control inputs. The

resulting control design has been thoroughly analyzed for two decades for its robustness and performance and has been applied successfully in a range of applications, especially in aircraft and process control. Next, we summarize the outline of such a design, and refer the reader to [12, 91, 1] for further details.

The LQG/LTR control procedure consists of a combined estimator-state feedback design, with the former assuming a fictitious Gaussian noise and a quadratic cost in the estimation error and the latter based on a quadratic cost in the system response as well as the control effort. The controller has the form:

$$\begin{aligned} \dot{\hat{x}} &= A\hat{x} + Bu + H\left(y - C\hat{x}\right) \\ u &= -K\hat{x} \end{aligned}$$

where the estimator gain H and the state feedback gain K are to be designed. The matrices A, B, and C are from the plant state space model. An optimal control strategy proposed in [91] leads to a natural specification of K and H. K can be determined using a cost function

$$J = \int_0^\infty \left(y^T Q y + u^T R u\right) dt \qquad Q = I,\ R = \rho_c I \tag{4.1}$$

so that ρ_c is a scaling factor that determines the trade-off between fast transients and magnitude of the control input. H can be determined by posing the problem as the design of a Kalman filter which ensures that $\hat{x}$ converges to x as efficiently as possible, by introducing a fictitious input noise with a variance I and an output noise with a variance $R_f = \mu I$. One can use the Matlab control toolkit to compute K and H efficiently, by fine-tuning ρ_c and μ.

The resulting control strategy is of the form

$$u = G_{lqr}(s)y$$

where

$$G_{lqr}(s) = -K\left(sI - A + BK + H\right)^{-1} H \tag{4.2}$$

The order of $G_{lqr}(s)$ is the same as that of the combustor model. The parameters of $G_{lqr}(s)$ are determined by J, which requires that the pressure response decays as quickly as possible with a small control effort. The relative weighting between the speed of response and control effort is determined by ρ_c. By increasing ρ_c, we penalize the control effort more which indirectly accommodates the effect of control saturation.

Since it is the total energy J in the system that is being minimized, the resulting LQG/LTR can generate satisfactory performance over the whole range of frequencies encompassing the acoustics, the heat release and the actuator dynamics. This is because the cost function J is equivalent to [1]

$$J = \int_0^\infty \left(\hat{y}(j\omega)^2 + \rho_c \hat{i}(j\omega)^2\right) d\omega$$

where $\hat{y}$ and $\hat{i}$ are the Fourier transforms of y and i respectively. This shows that the LQG/LTR is such that the closed-loop system exhibit suppressed oscillations not only at the unstable frequency but over the entire range of frequencies captured by the system model. It is this property of this optimal control methodology that provides an edge over the empirical control designs discussed in [27]. We elaborate briefly on this comparison through a numerical and experimental example in the coming sections.

4.1.2 Numerical vs. Experimental Results of the Controlled MIT Combustor

Experimental Set-up Description and Modeling

A bench-top combustor rig was constructed to evaluate the model-based approach to control design (See Figures 4-1 and 4-2 for the set-up and its schematic). The test rig consists of an air supply through a low-noise blower, a settling chamber, a rotameter for adjusting and measuring the air flow rate, a fuel (propane) supply through a pressure regulator, a rotameter for adjusting and measuring the fuel flow rate, and a nozzle for enhancing mixing between fuel and air. The combustion chamber is a 5-cm diameter, 47-cm long tube closed at upstream end and open at downstream end. The flame was anchored on a perforated disc with 80

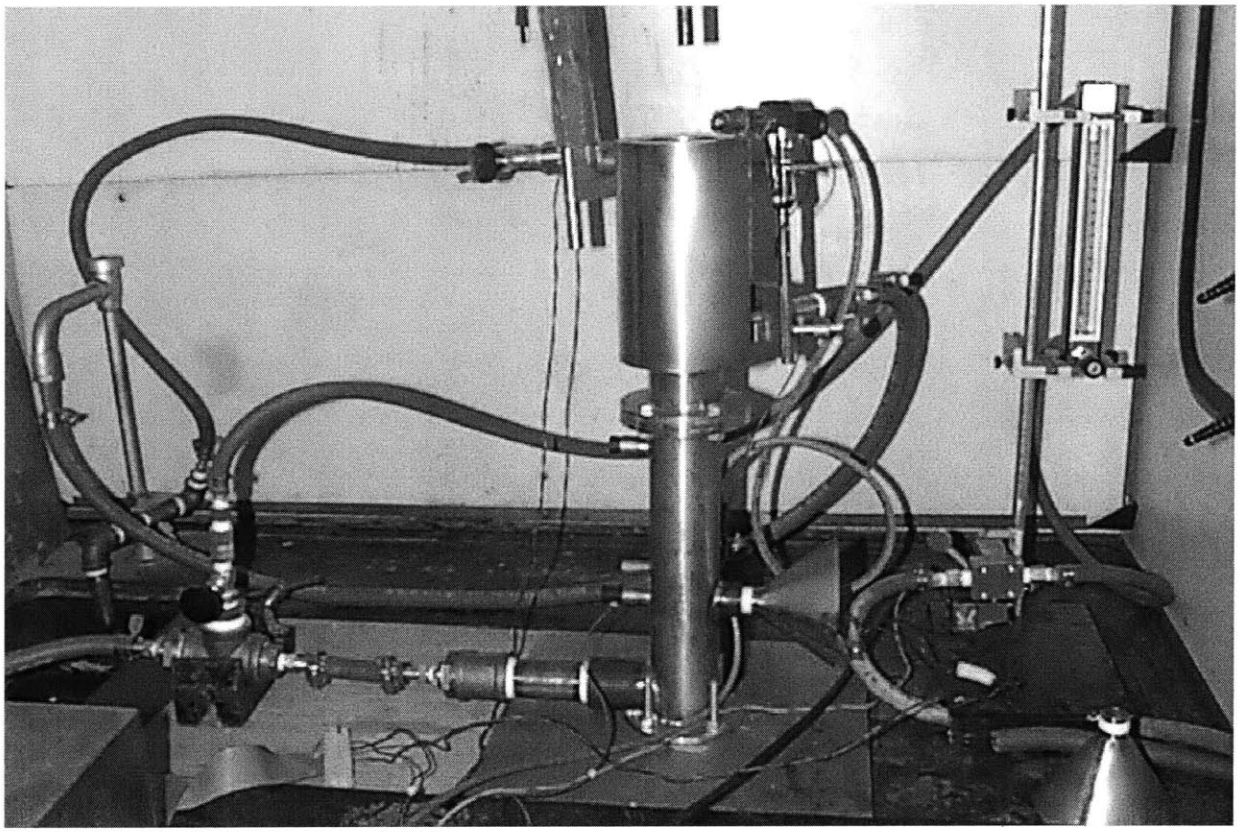

Figure 4-1: The Bench-top combustor rig.

holes (concentrated in a concentric 2-cm diameter circle area) fixed 26 cm from upstream end with several ports included for mounting actuators and sensors. Pressure is measured using a calibrated capacitance microphone, and a 0.2 W Radio Shack loudspeaker is used as an actuator. Due to design limitations, we restricted our experimental investigations to the case when the loudspeaker was side-mounted. Measurements on the test rig were recorded using a Keithley MetraByte DAS-1801AO data acquisition and control board, with a maximum sampling frequency of 300 kHz. The board was hosted in a Pentium PC. The sensors are connected to the board through appropriate signal conditioning circuits. Most experiments were conducted with an equivalence ratio between 0.69 and 0.74 and an air flow rate of 333 mL/s (0.38 g/s), which corresponded to an unstable operating condition without control (Equivalence ratios of less than 0.69 corresponded to a stable operating point). The flow rate was varied between 267 mL/s and 400 mL/s and the power of the combustor was rated at 1 kW, approximately. A sampling rate of 10 kHz was found to be more than sufficient to prevent aliasing. The unstable frequency of the combustion process was found to be 470 Hz.

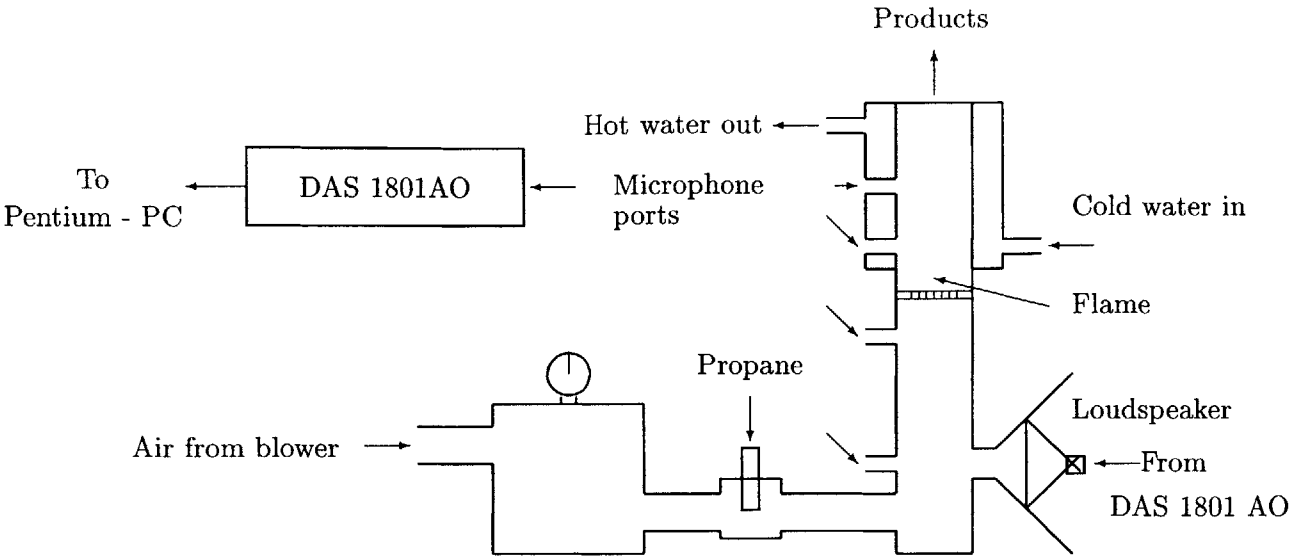

Figure 4-2: Schematic of the combustor test rig, data-acquisition, and control.

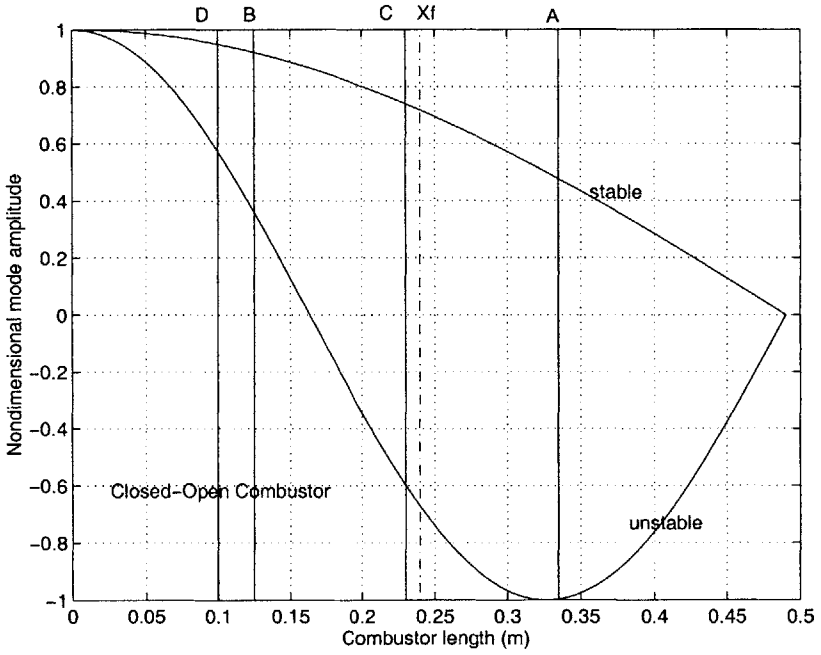

Figure 4-3: Mode shapes for closed-open combustor boundary conditions and actuator-sensor-flame locations.

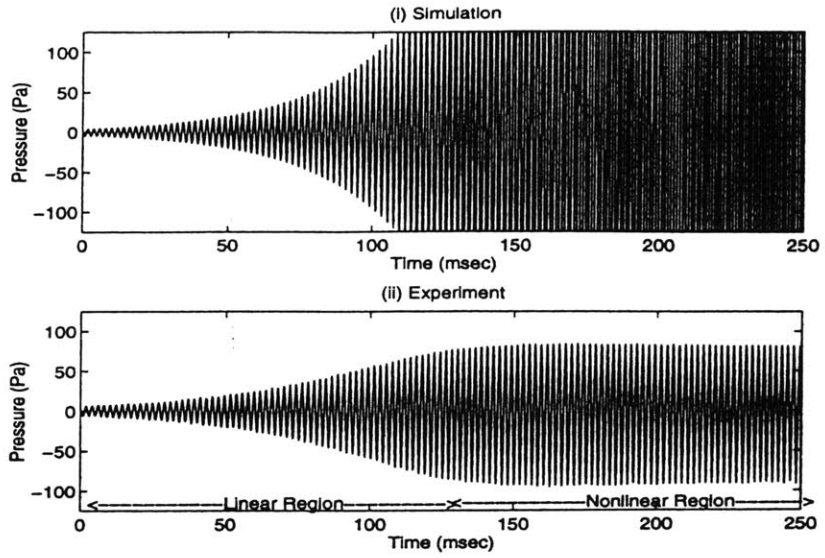

Figure 4-4: Pressure oscillations for uncontrolled combustor (i) Simulation results using the two mode model and (ii) Experimental results.

Using the information from the bench-top combustor rig, the combustor model was simulated as in Eqs. (2.9) (without ϕ'-fluctuations and for $\tau_f \approx 0$) and (2.30) with the following parameters: $L = 0.62m$ [1], $\gamma = 1.4$, $\bar{p} = 1atm$, $\bar{c} = 347m/s$, $\bar{M} = 3.612 \times 10^{-4}$, $\rho_u = 1.163kg/m^3$, $\Delta q_r = 2.26 \times 10^6 J/kg$ (for $\phi = 0.74$), $S_u = 0.3m/s$, $\theta = 0.5$, $d_p = 1.5 \times 10^{-3}m$, $D = 0.05m$, and $n_f = 80$. The choice of these values follows directly from the geometry and fuel properties. A closed-open boundary condition was chosen due to the structure of the flow conditions. The effect of mean heat, as mentioned earlier, contributed to a reduction in the effective length, $L_e = 0.535$m. A damping ratio $\zeta = .0033$ was added at all frequencies to account for passive damping in the system, the effects of which were not included in the model. The choice of ζ was therefore arbitrary, and was selected so as to match the experimental growth rates over as wide a range of equivalence ratios as possible. The corresponding mode shapes, k_i, were computed as shown in Figure 4-3 and ω_i to be 162 Hz and 488 Hz for $i = 1, 2$. Denoting $W_{\mathrm{A/B}}(s)$ as a transfer function with the actuator at B

[1] L corresponds to the acoustic length, which was determined by locating the pressure null in the combustor. It was found that the length of the air/fuel feed tube as well as an end-correction at the downstream end contributed to this acoustic length.

and sensor at A, the resulting plant transfer functions are of the form

$$W_{D/D}(s) = 2.15 \times 10^5 \frac{(s+440)(s^2-83s+7.70\times10^6)}{(s+14.9)(s^2+407s+1.03\times10^6)(s^2-63s+9.41\times10^6)},$$
$$W_{C/D}(s) = 8.38 \times 10^4 \frac{(s+589)(s^2-26s+1.47\times10^7)}{(s+14.9)(s^2+407s+1.03\times10^6)(s^2-63s+9.41\times10^6)},$$

assuming that only the first two modes are present (see Figure 4-3 for locations of C and D). We note that in this closed-open case, $W_{D/D}$ has unstable zeros even though the actuator-sensor pair is collocated. The performance of the uncontrolled combustor for both the simulation and the experiment is shown in Figure 4-4, which shows that over the first 70 milliseconds the simulation and experimental growth rates match closely. Beyond this point, the pressure level continues to grow in the linear model, as expected, while nonlinearities begin to dominate in the experimental combustor and a limit cycle is reached.

The efficacy of the active control designs were evaluated using a loudspeaker as an actuator and a microphone as a sensor. To determine the loudspeaker dynamics, using a function generator and a photo sensor for measuring the displacement of the loudspeaker diaphragm, a frequency analysis was carried out. This analysis was used to determine the transfer function relating the voltage into the loudspeaker to the acceleration of the loudspeaker diaphragm. A 0.2W loudspeaker used in experimental investigations was modeled as

$$G_l(s) = \frac{35.5s^2}{s^2+364s+3.320\times10^6} \tag{4.3}$$

The natural frequency of the loudspeaker, which was at 290 Hz, is of the order of the first acoustic mode, indicating the necessity of including the actuator dynamics in the control design process. To complete the model of the experimental system, a sensor gain of $45.3 Pa/Volt$ was included in the simulation.

For the 0.2W loudspeaker that we used, the housing dynamics was not important. This was due to the location of the loudspeaker in the funnel which was used to mount the speaker to the side of the combustor. Since the loudspeaker diameter was only slightly larger than the hole leading to the combustor, the size of the cavity between the speaker and combustor was small, preventing housing dynamics from having an effect.

In addition to the combustion dynamics, loudspeaker dynamics, and sensor gain, the power limitations of the instrumentation were considered when designing a controller. The data acquisition board was limited to an output of ± 10 volts, from which we computed the maximum diaphragm acceleration that our experimental system could provide with the 0.2 W loudspeaker at the unstable frequency, which was $600 m/s^2$. This limitation on the maximum control effort was taken into account when designing the controllers, the details of which are described below.

Results

For the system model given by $W_{\mathrm{D/D}}(s)G_l(s)$, the two design parameters μ and ρ_c were chosen so that the maximum loudspeaker acceleration was close to $600 m/s^2$, and were given by $\mu = 0.01$, and $\rho_c = 0.1$. The resulting LQG/LTR controller (after a stable pole-zero cancellation) is:

$$G_{\mathrm{D/D}}(s) = \frac{5.05 \times 10^3 (s - 2071)(s^2 - 418s + 5.06 \times 10^6)(s^2 + 459s + 1.54 \times 10^6)}{(s^2 + 1378s + 6.06 \times 10^6)(s^2 + 766s + 1.05 \times 10^7)(s^2 + 750s + 7.37 \times 10^5)} \tag{4.4}$$

For the second configuration given by $W_{\mathrm{C/D}}(s)G_l(s)$, the controller is:

$$G_{\mathrm{C/D}}(s) = \frac{5.05 \times 10^3 (s - 2071)(s^2 - 418s + 5.06 \times 10^6)(s^2 + 459s + 1.54 \times 10^6)}{(s^2 + 1378s + 6.06 \times 10^6)(s^2 + 766s + 1.05 \times 10^7)(s^2 + 750s + 7.37 \times 10^5)} \tag{4.5}$$

The resulting performance obtained from the benchtop rig using the above controllers with the actuator-sensor pair at D/D and C/D are shown in Figure 4-5 which resulted in a settling time of 59 *msec* and 47 *msec*, respectively. These matched the simulation results of the controlled combustor using (4.4) and (4.5) shown in Figure 4-6. The improvement in the performance at C/D is possibly due to the fact that the sensor is closer to the anti-node when placed at C and therefore results in a larger system gain. We also observed that the LQG/LTR control designs based on the unstable mode alone failed to stabilize the oscillations, indicating that for the configuration in the experiment, the inclusion of the system dynamics at all frequencies lower than the unstable value at around 500 Hz is necessary.

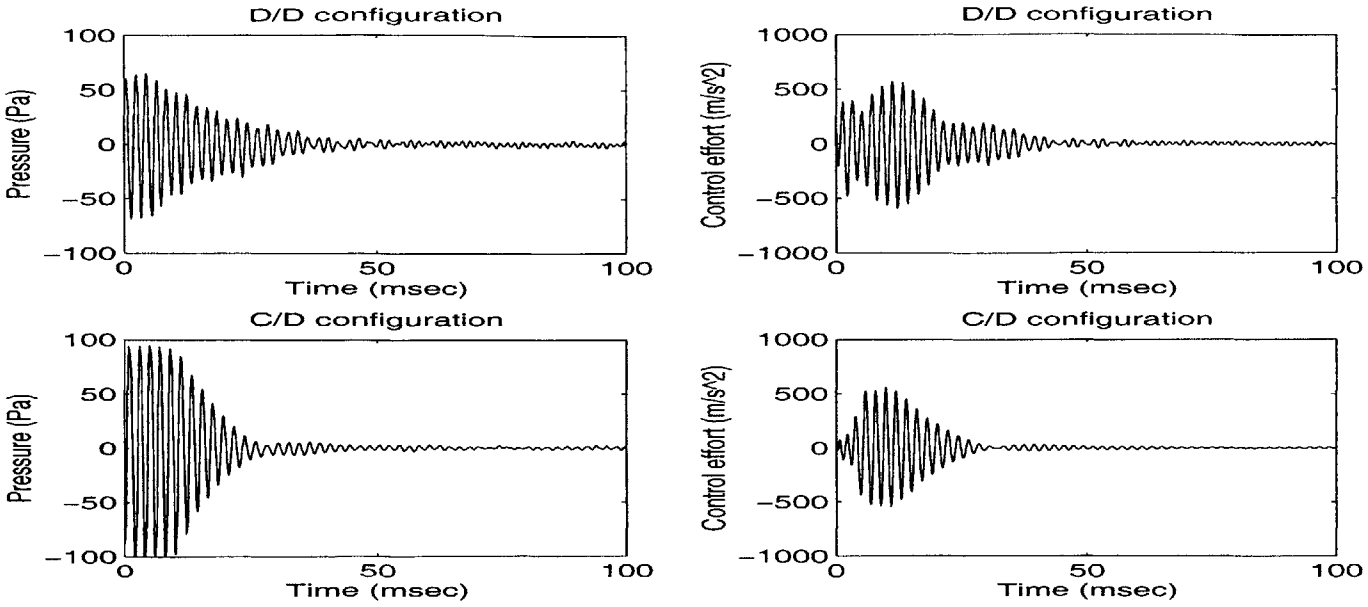

Figure 4-5: Pressure response and control input for a side-mounted loudspeaker with D/D and C/D configurations, and LQG control: Experimental results for $\phi = 0.7$.

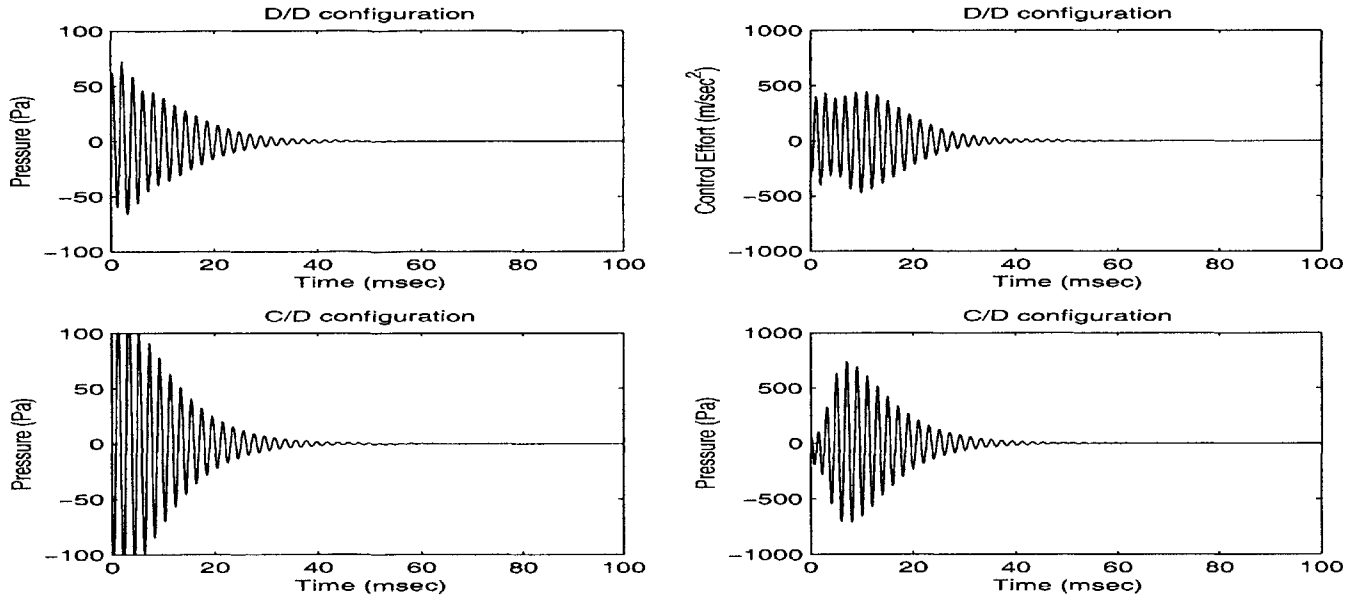

Figure 4-6: Pressure response and control input for a side-mounted loudspeaker with D/D and C/D configurations, and LQG control: Simulation results for $\phi = 0.7$.

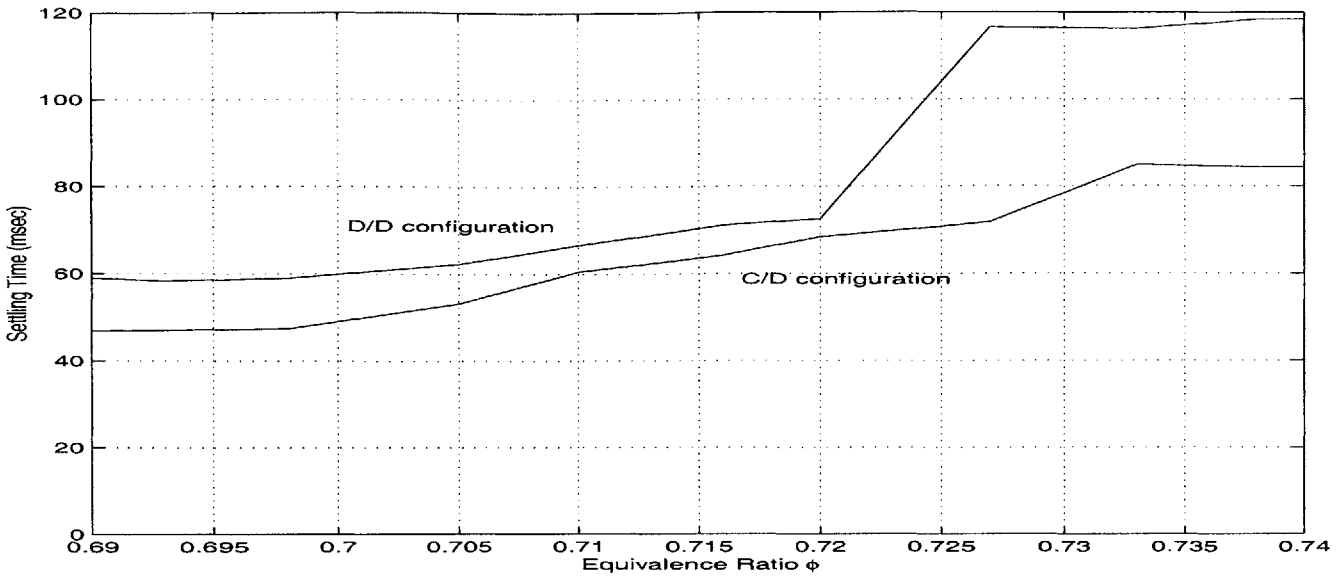

Figure 4-7: 5%-settling time achieved using the LQG controller as a function of the equivalence ratio for the D/D and C/D configurations, respectively.

The performance of the LQG controller was tested for flow rates between 267 mL/s and 400 mL/s and equivalence ratios between 0.69 and 0.74 and in all cases, the thermoacoustic instability was successfully suppressed with no secondary peaks. Changes in the flow rate while maintaining the same equivalence ratio did not affect the ability of the controller to stabilize the thermoacoustic instability, in contrast to Ref. [34]. As ϕ increased, the settling time increased (see Fig. 4-7) which may be due to the fact that the pressure levels and therefore the required control effort increase with ϕ whereas the loudspeaker has limited control authority (see the control effort in Figure 4-5). If μ and ρ_c were chosen in the control design such that the control effort required was significantly larger than that which could be achieved by the experimental system, the simulations indicated a fast settling time, but the experimental controller was not be able to achieve the same performance due to loudspeaker saturation and the actual settling time was much larger.

Using the LQG controller, we were able to suppress the pressure level from 250 Pa (at A) to an ambient noise level of 1.5 Pa, which corresponds to a reduction of 45 dB. The residual noise is mostly due to the blower which accounts for the small amplitude of the pressure oscillations in steady-state. A power spectrum of the combustor with and without control is shown in Figure 4-8 along with the power spectrum of the system with no combustion for

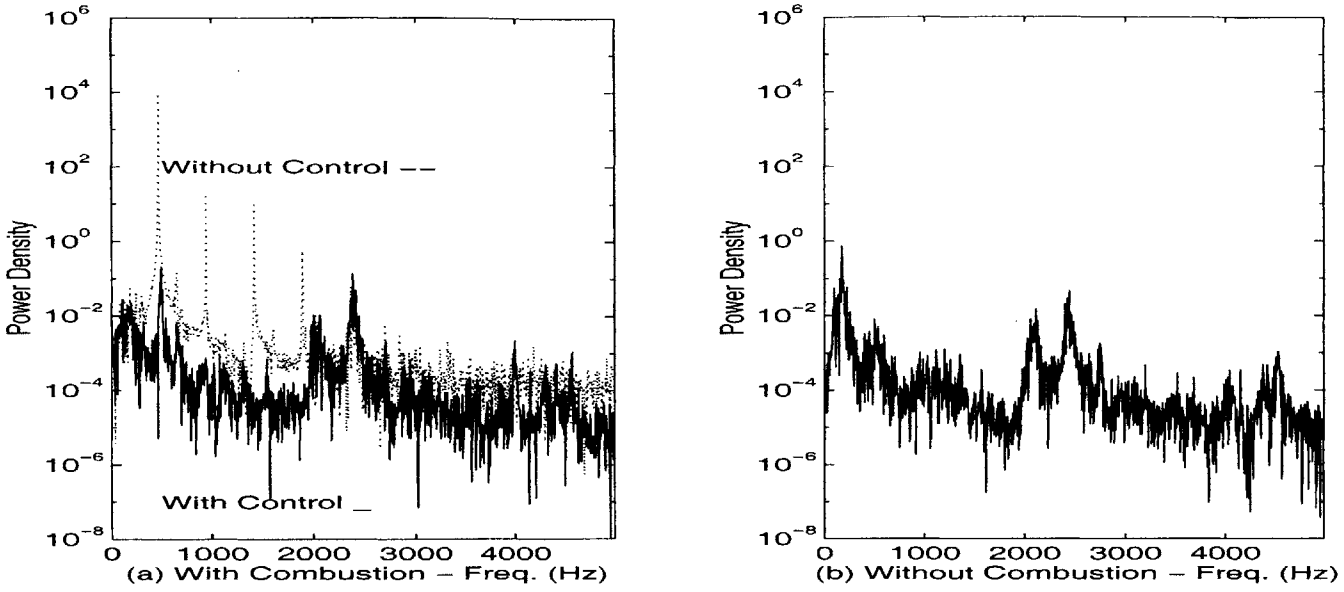

Figure 4-8: Power spectrum of the pressure response (a) with and without control and (b) with blower noise without combustion.

reference. The figure demonstrates that no secondary peaks were observed since the LQG-LTR controller provides appropriate phase compensation at all the modeled frequencies unlike phase-shift control designs based on the behavior at the unstable frequency alone [28, 41]. When an empirically designed phase-shift controller was implemented following an "anti-sound" approach as in [34], although the combustor was stabilized, the controller excited two peaks, at 200 Hz and 700 Hz, approximately, which did not exist in the open-loop response as seen in the experimental and the simulated power spectra, shown in Figs 4-9 and 4-10, respectively. An in depth analysis of the origin of these peaks is presented in Ref. [27], and will be omitted here.

We evaluated the performance robustness of the LQG design by perturbing many of the parameters in the model. We found that a 20% change in L destabilized the closed-loop system, while the controller was successful in stabilizing the combustor in the presence of 20% perturbations in ϕ, S_u, θ, and ϵ. In the latter case, robustness was evaluated by perturbing S_u, θ, and ϵ in the model and by changing ϕ on-line in the experiment by varying the fuel flow rate. The controller provided a robust performance over all values of $\phi \in [0.55, 0.74]$ even though the uncontrolled model and the experiment differed in the stability behavior for $\phi < 0.69$. This could be attributed to the fact that the former set of parameters does

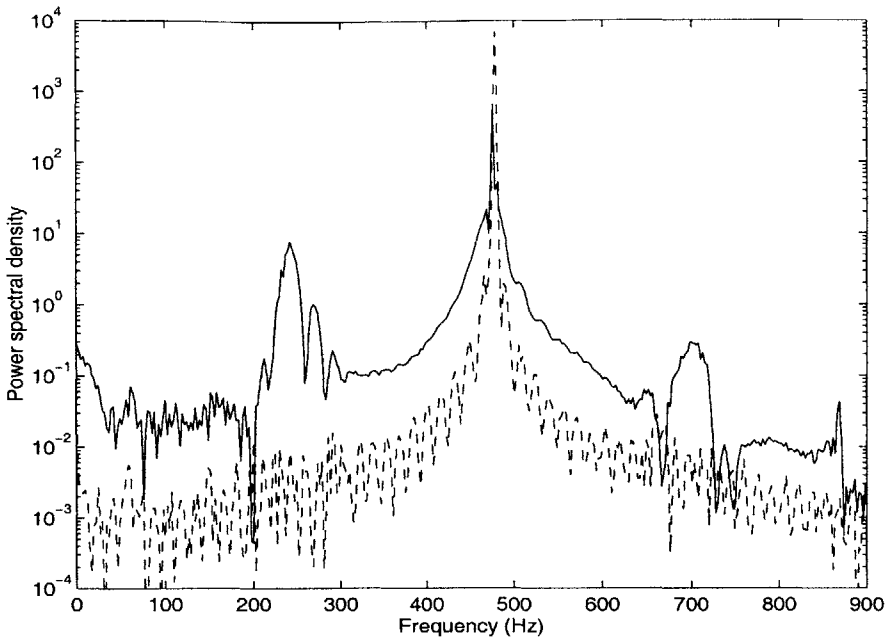

Figure 4-9: Power spectrum for the controlled pressure response "-" compared with the uncontrolled pressure "- -", experimental results

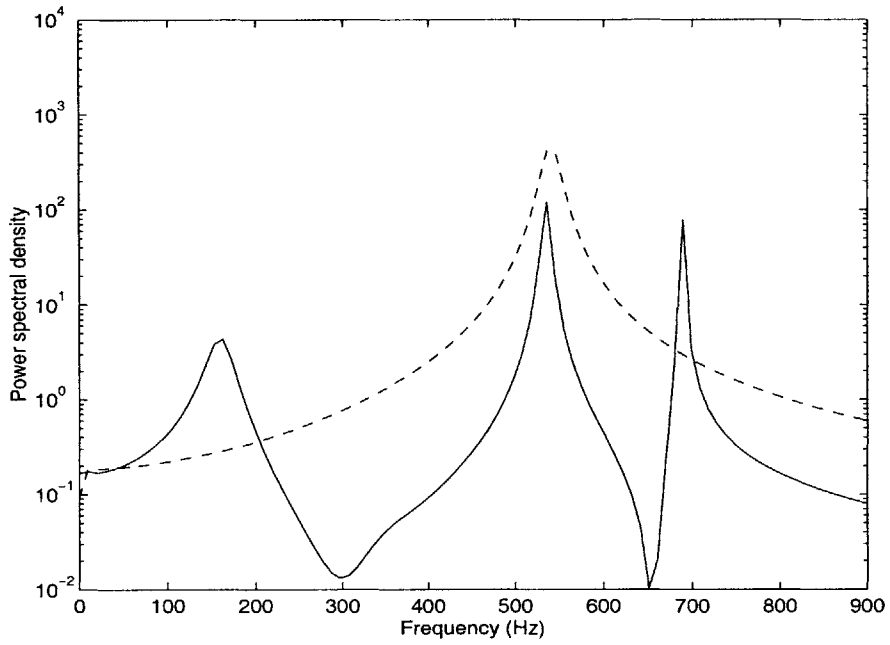

Figure 4-10: Power spectrum for the controlled pressure response "-" compared with the uncontrolled pressure "- -", simulation results

not affect the behavior of the model at the unstable frequency whereas changes in L directly affect the system poles and zeros, thereby changing the gain and phase at the unstable frequency. An adaptive self-tuning controller has been developed and has shown to succeed in stabilizing the combustor with perturbation in some of the parameters up to 40 % [3].

4.2 Control Using a Secondary Fuel Injector

In this section, two situations in actual combustors are handled and active control using fuel injection is implemented on both. The first is for a combustor hosting a bulk mode instability which is caused by ϕ'-fluctuations as discussed in Sec. 2.4. Control strategies are proposed for this situation and are compared with controlled data from a sector-rig combustor of an engine used at UTRC [15] (see Sec. 4.2.1). The second is for a combustor hosting multiple longitudinal modes which resembles the situation in an experimental rig at MIT [5], and instability is due to flame area fluctuations as seen in Sec. 2.4. The latter is presented in Sec. 4.2.2. For both cases, injection at and upstream the flame is investigated.

4.2.1 Bulk-Mode Instability Control: A Single Mode Approach

We consider here a combustor which hosts a bulk-mode instability as in [15]. Instability is generated by the equivalence ratio perturbation as discussed in Chapter 2. Thus, fuel injectors become natural choices of actuation. In this section, we propose a number of strategies for incorporating controlled actuation to suppress the instability. In all cases, the control designs are based entirely on the structure of the model. We investigate the impact of the location of a secondary injector with respect to the main fuel supply and the burning zone, and how it affects the control algorithm, its robustness, the control input, and the settling time.

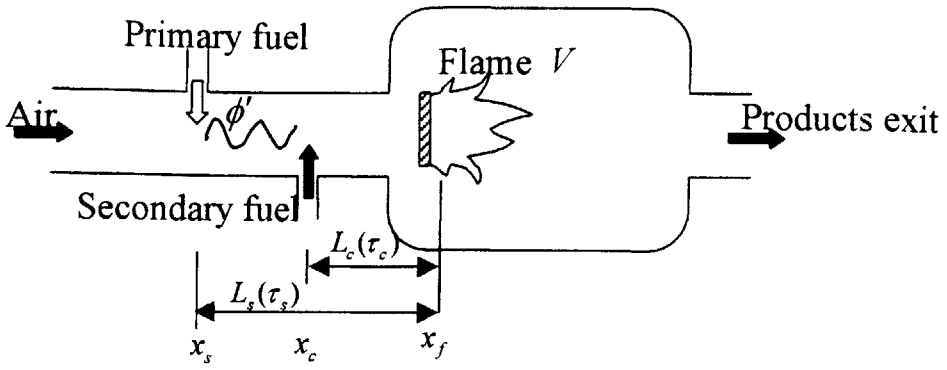

Figure 4-11: Schematic diagram of the combustor with different time delays.

Actuated Combustion Model

The combustor model with actuation for this situation can be derived as

$$\mathcal{L}_\omega(p) - \Gamma p(t-\tau_s) \;=\; \Gamma_c\, \dot{\phi}_c\,(t-\tau_c), \tag{4.6}$$

where $\mathcal{L}_\omega = \frac{d^2}{dt^2} + 2\zeta\omega\frac{d}{dt} + \omega^2$ is wave operator used to simplify the forthcoming analysis, ϕ_c is the effect of the secondary injector on the equivalence ratio, $\Gamma_c = \frac{(\gamma-1)A_i\bar{\beta}\Lambda_\phi}{V\bar{S}_u}$, and τ_c represents yet another delay from the moment the secondary fuel is injected at x_c (see Fig. 4-11), upstream the burning zone, and when it burns at x_f, $\tau_c \approx \frac{L_c}{\bar{u}}$, where $L_c = x_c - x_f$.[2]

In the controlled simulations presented herein, we will omit including the injector dynamics for simplicity. We assume that the injector bandwidth is higher that the unstable acoustics frequency which is 200 Hz. Injectors of higher bandwidth exist, e.g., a Moog DDV proportional injector has a bandwidth of 450 Hz [87].

[2] τ_c also includes burning delay due to evaporation and mixing if liquid fuel is injected close to the burning zone.

Active Control by Injection at the Fuel Supply ($\tau_c = \tau_s$)

We choose to inject the secondary "control" fuel at x_s either using a secondary injector or superimposing an additional control signal onto the main fuel injector, thus guaranteeing that $\tau_c = \tau_s$. The active control principle here is to cancel perturbations in ϕ and rely on the passive damping of the combustor to enhance stability. An integral control signal

$$\phi_c \;=\; -K_c \int p dt, \tag{4.7}$$

where the controller gain is chosen to be $K_c = \frac{\Gamma}{\Gamma_c}$, can accomplish the task. This is a very simple controller to implement and since it utilizes secondary fuel injection at the fuel supply good mixing is guaranteed before the burning zone. However, for stability, the controller requires an accurate knowledge of Γ and Γ_c. In case of uncertainties, $K_c = \frac{\Gamma+\Delta_k}{\Gamma_c}$, the oscillator model becomes $\mathcal{L}_\omega(p) + \Delta_k p(t-\tau_s) = 0$. In this case, stability is achieved when the following conditions are satisfied [70, 67]:

$$\text{for } \zeta < 0.707, |\Delta_k| < 2\zeta\omega^2\sqrt{1-\zeta}, \;\text{ and for } \zeta > 0.707, \; |\Delta_k| < \omega^2. \tag{4.8}$$

Normally, Δ_k is small so as to satisfy both conditions. Also, "passive" damping is small, hence, the first condition guarantees robustness.

For the combustor in [15], assuming that $\zeta = 0.05$, the control law in Eq. (4.7) is used to stabilize that combustor. Figure 4-12 illustrates the response of pressure and the required ϕ_c. While stability is guaranteed, the settling time depends strongly on ζ. The control strategy used here is similar to the one applied to the experiment in [15] in that the secondary fuel was injected at the source of the primary fuel. In the experiment, an extra delay, $0 \leq \tau_{c_2} \leq 5\ ms$, was introduced in the feedback loop to study its impact on stability. It was noted that the pressure was suppressed below the uncontrolled value for $0 \leq \tau_{c_2} \leq 1.2$, and $4 \leq \tau_{c_2} \leq 5$, as shown in Fig. 4-13. To explain these observations, we develop the model further by introducing this extra control delay in the feedback loop. In this case,

$$\mathcal{L}_\omega(p) - \Gamma p(t-\tau_s) \;=\; \Gamma\, \dot{\phi}_c\, [t - (\tau_s + \tau_{c_2})]. \tag{4.9}$$

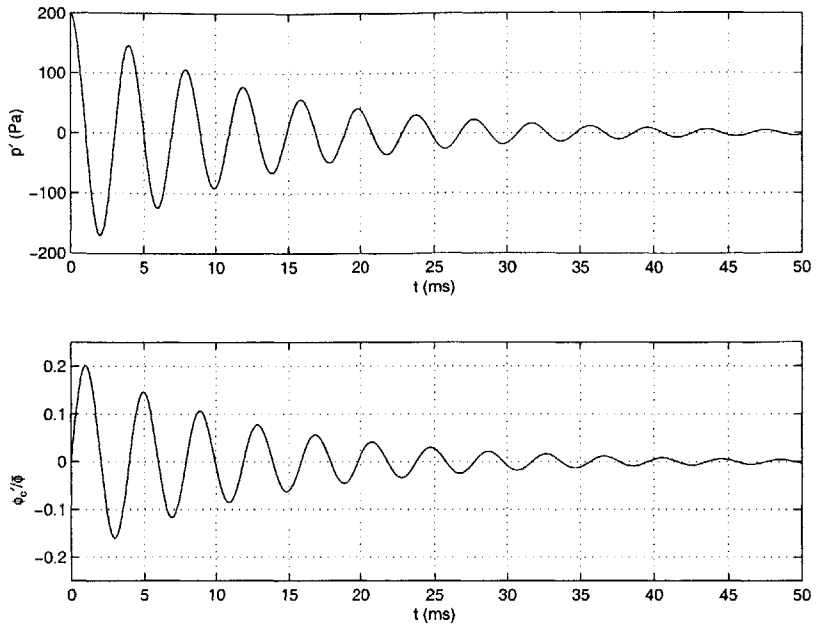

Figure 4-12: Controlled response for controller in Eq. (9), when injecting at the primary fuel supply.

The solution shows that this system is stable when

$$n \leq \tau_c/\tau_{ac} \leq 1.3/\tau_{ac} + n \qquad n = 0, 1, 2, 3..., \tag{4.10}$$

where the unstable acoustics time constant, $\tau_{ac} = 5\ ms$ in this combustor. The result in Eq. (4.10) for the values of τ_c and τ_a in [15] is shown in Fig. 4-13. The regions of stability agree with the experiment (where we have interpreted limit cycles of amplitude lower than -27 dB to be stable).

It should be noted that this control method could fail if strong perturbations in the flame area, which might occur in phase with the pressure thus adding negative damping to the system (see [39]), coexist with the equivalence ratio perturbations. In such case, it is not sufficient for the controller to eliminate the perturbations in ϕ to achieve stability, and the addition of a second component of control that alters the relation between the pressure and the heat release is required for stability. This could prove challenging using the controller since all action introduced by an injector is delayed since it is located away from the flame.

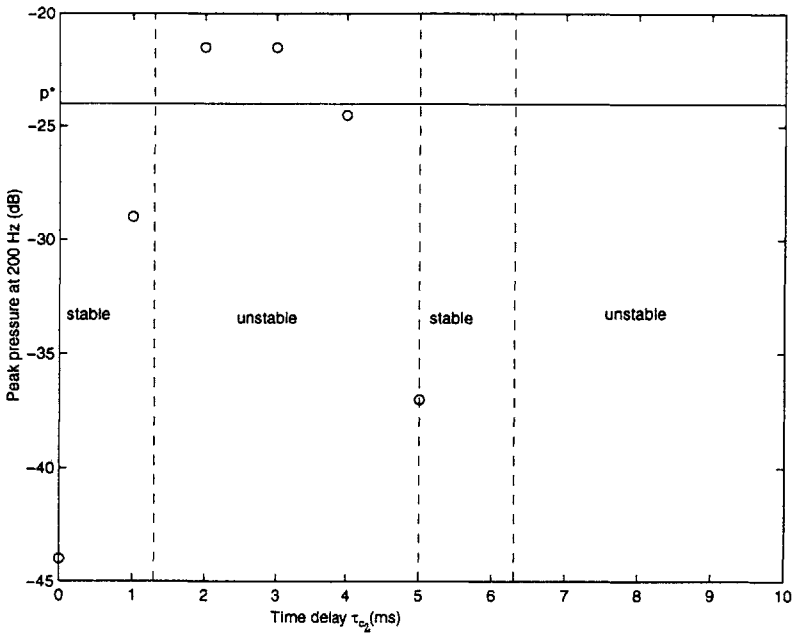

Figure 4-13: Stability map for the controlled combustor as predicted by Eq. (12). ○ are peak pressure amplitudes measured versus changing the control delay, τ_{c_2}, as in Ref. [1], and p^* is the level of the uncontrolled pressure.

Creating an undelayed active damping term in the oscillator is possible by minimizing the delay, i.e injecting on the flame as will be discussed in the next section, or by using more elaborate control techniques, such as the Posi-Cast algorithm, which is also introduced later.

Active Control by Injection on the Flame($\tau_c \approx 0$)

By injecting at x_f (see Fig. 4-11), we eliminate most of τ_c and an externally delayed term is required to cancel out the intrinsic delayed term in the left-hand side of Eq. (4.6). Moreover, since we are injecting at the flame, a non-delayed signal can be used to add positive "damping". In this case, a delayed integral-plus-proportional control is used:

$$\phi_i = -K_p p - K_c \int p(t - \tau_{c_2}) dt, \tag{4.11}$$

with $K_p > 0$, $K_c = \frac{\Gamma + \Delta_k}{\Gamma_i}$, and $\tau_c = \tau_s + \Delta_\tau$ (Δ_τ being the uncertainty in the inherent delay).

In the case of $\Delta_k = \Delta_\tau = 0$, the closed-loop is stable (see Fig. 4-14). Note that K_p is an additional degree of freedom which can compensate for the presence of any negative damping which may enter due to, e.g., perturbations in the flame surface area [39][3]. It also increases the robustness of the controller in case of uncertainties, as discussed next.

In the case when Δ_k is non zero, the extra active damping introduced by K_p guarantees the robustness condition (similar to Eq. (4.28)) in Section 4.2.1. When uncertainty exists in τ_c, the oscillator can be described as $\ddot{p} + \Gamma_i K_p \dot{p} + \omega^2 p + \delta p^* = 0$, where $\delta p^* = \Gamma(p(t - \tau_s - \Delta_\tau) - p(t - \tau_s))$ is a disturbance input. Assuming small uncertainty, $\delta p^* \approx \gamma^* p(t - \tau_s) + \epsilon^*$, γ^* and ϵ^* are constants, and hence similar arguments on robustness can be evaluated as in the previous section.

Another algorithm can be implemented for controlling the combustor using the stability bands discussed in Section 2. For simplicity let us assume that the natural damping, ζ, is negligible. Stability is achieved if a controller is capable of changing the resonant frequency

[3]The words "negative" and "positive" damping are used here to indicate heat-release perturbation which is out-of-phase and in-phase with the pressure oscillation, respectively. We have shown in Chapter 3 that the effect of flame-area perturbation can be modeled as a negative damping term. Controlled heat release can be modulated to produce a positive damping term, as shown next.

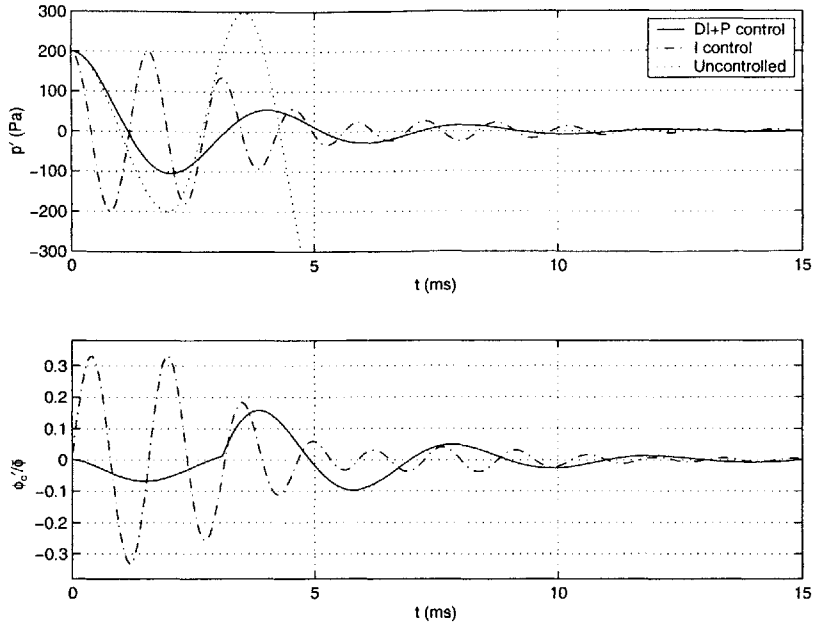

Figure 4-14: Comparison between the delayed integral-plus-proportional control (DI+P), as in Eq. (13), and the integral control (I), as in Eq. (9), when injecting at flame.

such that it falls within a stable band. To affect only the resonant frequency, the same integral control expressed by Eq. (4.7) is used. In this case, the oscillations are governed by $\ddot{p} - \Gamma p(t - \tau_s) + \tilde{\omega}^2 p = 0$, where $\tilde{\omega}^2 = \omega^2 + K_c \Gamma_c$, and the system is stable if

$$0 < \Gamma < \tilde{\omega}^2, \text{ and } \frac{n}{2} < \frac{\sqrt{\tilde{\omega}^2 + \Gamma}\tau_s}{2\pi} < \frac{n+1}{2} \quad \text{for } n = 0, 2, 4, ... \tag{4.12}$$

The smallest K_c (and hence $\tilde{\omega}$) that satisfies Eqs (4.12) is obtained when $n = 2$ with

$$K_c = \frac{(2.5\pi/\tau_n)^2 - (\omega^2 + \Gamma)}{\Gamma_c} \tag{4.13}$$

which satisfies conditions at the middle of a stable band.

The controlled responses for the delayed integral-plus-proportional control, Eq. (4.11), and the integral control, described above, are illustrated in Fig. 4-14. We note that the first controller input is less by 50% for the same settling time. This is important since injecting more fuel at the burning zone increases the chances of creating hot spots, resulting in higher

NO_x emissions. Moreover, the second controller increases the frequency of the system to achieve stability, thus, requiring an injector with a higher bandwidth.

The control techniques analyzed in this section have an advantage over that in the previous section. They are capable of increasing the decay rate while ensuring faster control action, since the delay time is minimized. Injection at the flame has been successful experimentally [55, 101]. An important consideration is to guarantee good mixing at the injection port with the reactants to avoid forming a secondary diffusion flame which can be completely decoupled from main premixed flame, and thus ineffective in suppressing the instability.

Active Control by Injection at an Arbitrary location ($0 < \tau_c \leq \tau_s$)

In some cases, hardware limitations, or concerns about emissions may make it difficult to place an actuator near the primary source or the flame. In this case, we must design a controller for an injector located at an arbitrary position $x_s < x_i \leq x_f$ (see Fig. 4-11). Algorithms similar to those presented before can be implemented. We start with the assumption that ζ is arbitrary and use an integral controller, which cancels the delayed term in the left-hand side of Eq. (4.6), i.e.,

$$\phi_c = -K_c \int p(t - \tau_{c_2}) dt \tag{4.14}$$

with $K_c = \frac{\Gamma}{\Gamma_c}$, and $\tau_{c_2} = \tau_s - \tau_c$. The stability of the controlled combustor depends on $\zeta > 0$ as in Section 4.2.1. Hence, uncertainties in the parameters Γ_i, Γ, τ_s, and τ_c can be accommodated by similar robustness arguments as before. This controller, although similar to the one in Eq. (4.8), produces a faster action on the heat release since the injector is located closer to the burning zone.

When $\zeta \approx 0$, another algorithm that exploits the presence of stability bands can be implemented. This adds another term to Eq. (4.14) so that there are sufficient degrees of freedom to guarantee stability, i.e.,

$$\phi_i = -K_c \int p(t - \tau_{c_2}) dt - K_d \int p dt, \tag{4.15}$$

where $\tau_{c_2} = \tau_s - \tau_c$, and both K_d and τ_c satisfy

$$0 < K_d\tau_c < \omega^2, \text{ and } \frac{n}{2} < \frac{\tau_c}{\tau_a} < \frac{n+1}{2} \quad \text{for } n = 0, 2, 4, ... \tag{4.16}$$

Note that here the controller induces a new delayed term $p(t - \tau_c)$ in the oscillator equation for stability, whereas in the case of the controller Eq. (4.14), it changed the frequency of the closed-loop. Moreover, we have two degrees of freedom, the location of the injector, and the control gain K_d, both can be selected to satisfy stability conditions in Eq. (4.16). The controlled response, using combustor parameters as in [15], is shown in Fig. 4-15 for a delay $\tau_c = 1.5\ ms$ (which lies in the first stable band, i.e., $n = 0$) which represents an injector located half-way between the main fuel source and the burning zone. The control action at the flame is retarded by τ_c due to the position of the injector. The closer it is to the burning zone, the faster it affects the heat-release, since the "dead" time when the flame is insensitive to the controlled fuel injected is shorter. This impacts the control input, i.e., fuel consumption, which has to be larger to result in the same settling time. Hence we expect that for similar control input, the pressure will decay faster if we inject directly on the flame, as in Fig. 4-14. The delayed integral-plus-proportional control as seen in the figure consumes a similar maximum amount of fuel as the integral control discussed here and shown in Fig. 4-15, but the former stabilizes the system much faster.

Posi-Cast Control

The control methods presented so far in Eqs. (4.7), (4.11), (4.14) and (4.15) are simple to implement. However, they require one or more of the following: (i) An estimate of the passive damping, ζ, (ii) Direct injection on the flame to provide active "undelayed" damping terms, (iii) The presence of stability bands in the uncontrolled system. An estimate of ζ may be hard to obtain, and it varies with conditions and a wrong estimate of ζ may be dangerous since it would give incorrect estimates of the stability bands. Injection at the flame [55, 101] carries a penalty because it creates hot spots on the flame, i.e., high NO_x emissions, when premixed combustion is used. In this section, a control design that is capable of bypassing (i)-(iii) is introduced.

Our starting point is Eq. (4.6), assuming for simplicity that $\zeta = 0$. The following control structure is suggested:

$$\phi_i = \phi_1 \quad + \quad \phi_2, \tag{4.17}$$

$$\text{with } \phi_1 = -K_c \int p(t - \tau_{c_2})dt, \quad \text{and} \quad \phi_2 = -K_p p(t + \tau_c), \tag{4.18}$$

where $K_c = \frac{\Gamma}{\Gamma_i}$, $\tau_{c_2} = \tau_s - \tau_c$, and $K_p > 0$. Using this controller stabilizes the combustor because the algorithm cancels the natural delay term and adds active damping. However, its success depends on Eq. (4.18) which requires the controller to predict future outputs at $(t + \tau_c)$. Since ϕ_1 cancels the intrinsic delayed dynamics, the following equation

$$\ddot{p}(t) + \omega^2 p(t) \;=\; \Gamma_c \, \dot{\phi}_2 \, (t - \tau_c) \tag{4.19}$$

can be used to construct ϕ_2 as follows. The same equation can be used to forecast p after a time τ_c given an input ϕ_2. Using this property, the dynamics of ϕ_2 in Eq. (4.18), after some manipulations, can be represented as

$$\ddot{\phi}_2(t) + \omega^2 \phi_2(t) \;=\; -K_p\{\Gamma_c \left[\dot{\phi}_2 \, (t) - \dot{\phi}_2 \, (t - \tau_c)\right] + \ddot{p}(t) + \omega^2 p(t)\}, \tag{4.20}$$

which is realizable, since it relies on current and past knowledge of the dynamics. The latter equation can be implemented in real-time control using a filtered version of the control signal (which is proportional to the equivalence ratio), and the measured pressure, as

$$\phi_2 \;=\; G_{c_1}(s) \left[G_{c_2}(s)\phi_2(t - \tau_c) + p(t)\right], \tag{4.21}$$

where $G_{c_1}(s) = K_p \frac{s^2+\omega^2}{s^2+K_p\Gamma_c s+\omega^2}$ and $G_{c_2} = \frac{\Gamma_c K_p s}{s^2+\omega^2}$ represent filters, and s is the Laplace operator.

The controlled response is shown in Fig. 4-15 for parameters similar to [15] and for a delay of $\tau_s = 1.5\ ms$. While the pressure response is comparable to that of the integral control in Eq. (4.15), the control input is less by 30% for the same settling time.

We should note that for the same maximum control input, $|\phi_c|_{max}$, the settling time, τ^*,

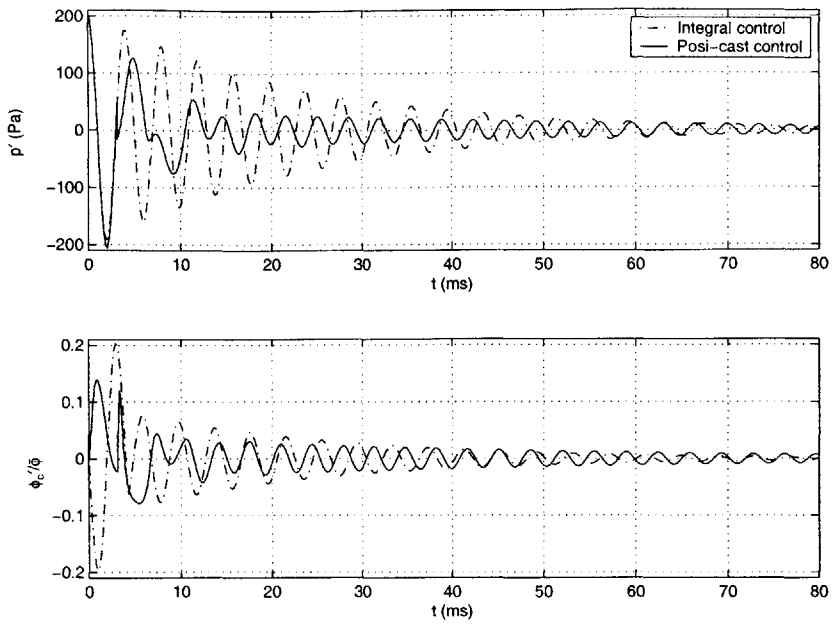

Figure 4-15: Controlled response using control in Eq. (17) and Posi-Cast control, when injecting half-way between the main fuel source and the burning zone.

increases as the location of the injector is moved upstream of the burning zone, i.e., as τ_c increases. This can be extracted from the damping coefficient in the controlled oscillator as

$$\tau^* \sim \frac{const.}{|\phi_c|_{max}} + \tau_c, \tag{4.22}$$

showing that as the injector is located further upstream of the flame, more "dead" time is needed for control authority to reach the burning zone, and hence higher control input is needed to produce the same settling time. The freedom to locate the injector offers flexibility in satisfying a maximum allowable amount of secondary fuel, and a fast settling time, while maintaining admissible levels of NO_x emission.

The method presented in this section relies on the accurate modeling of the combustor, and the control law is based entirely on the dynamic structure of the model. We note that the algorithm is from the same family of a more general technique for compensation of systems with time delay, known as Posi-Cast (positive forecasting), or Smith predictor [90]. This general algorithm is useful when the dynamics of the actuated combustor are of higher order

[68], and is currently used in our effort to stabilize systems exhibiting several longitudinal modes and high-order dynamics in the injector as will be discussed in the next section.

4.2.2 Longitudinal-Modes Instability Control: Multiple Modes Approach

In this section, we investigate model-based control strategies for abating combustion instability using secondary fuel injection. We assume that the pressure signal is the measured output, using a pressure transducer. The transducer dynamics is neglected since it typically has a much higher bandwidth than the combustion dynamics. We examine the control with an injector located at (i) the burning zone or (ii) further upstream. We include the injector dynamics and consider situations where proportional and two-position injector are used, unlike Sec 4.2.1. We assume in particular that the combustion dynamics is determined by several coupled acoustic modes [4]. We also assume that instability is primarily induced by fluctuations in the flame area coupled with the acoustics.

Actuated Combustor

Denoting the contribution of the fuel injector to the equivalence ratio as ϕ_c', we have that $\phi_c' = \frac{m_f'}{\overline{m}_a}/\alpha_o$, where $\overline{m}_a$ and α_o are the mean air mass flow rate, and the stoichiometric fuel to air ratio, respectively. m_f' is the output from the injector as given in Chapter 3, Sec. 3.1.2. We assume that ϕ_c' is uniform radially, and that perturbations are carried intact by the mean flow to the burning zone, after a time delay τ_c, where $\tau_c = L_c/\overline{u}$, L_c is the distance between the injector discharge and the burning zone, and $\overline{u}$ is the mean velocity of the reactants in the combustor.

As shown in Sec. 3.1.2, the impact of ϕ_c' on the combustion dynamics can be taken into account as

$$\ddot{\eta}_i + 2\zeta\omega_i\,\dot{\eta}_i + \omega_i^2\eta \;=\; \frac{\widetilde{b}_i}{A_c}\left[\overline{\kappa}Ru' + d_1\dot{\phi}_c'(t-\tau_c)\right], \tag{4.23}$$

for $i = 1, 2, .., n$, where i denotes the mode number.

Injection at the Burning Zone

Injection at the flame has shown success in several experimental facilities [62, 102, 53], and in a practical full-scale 170 MW gas-turbine combustor [87]. We carry out active control design assuming that the injection is at the flame, using the model in Eq. (4.23) while $\tau_c \approx 0$, together with the injection dynamics described by Eq. (3.22). The input-output model relation between the injector input voltage, E, and the pressure, p', is given by

$$p'(s) = W_p(s)E(s), \qquad W_p(s) = \frac{k_p Z_p(s)}{R_p(s)}, \tag{4.24}$$

where $W_p(s)$ is the transfer function of a finite-dimensional model of the combustor, k_p, $Z_p(s)$ and $R_p(s)$ are the corresponding gain, numerator and denominator, respectively.

An appropriate optimal control for the finite-dimensional system as in Eq. (4.24) is LQG/LTR [91], as explained in Section 4.1.1. This method has been successful in suppressing combustion instability as shown in Sec. 4.1 and in [37]. Its success lies in its ability to generate satisfactory performance over a wide range of frequencies, unlike phase-shift controllers which can destabilize stable dynamics [27]. Experimental validation of the LQG/LTR for combustion control has been demonstrated in [11, 5, 63]. In [5], a similar physically-based model was used with a loudspeaker as an actuator. In [11, 63], a system-ID approach based on subspace and ARMAX methods [52] was used to suppress pressure oscillations in a dump and a swirl-stabilized combustors, respectively, using pulsed injection. In this thesis, we show through simulation studies that, as in [37], LQG/LTR can also be used successfully based on a physical model, using fuel injector as an actuator. For details of the LQG/LTR control design, we refer the reader to [37, 5].

Simulations of the LQG/LTR Controller

A fifth order combustor dynamics model including the first two modes, the flame dynamics, and the injector dynamics is considered. The combustor parameters and conditions are taken as in [37], these cause a three-quarter-mode instability which resonates at 500 Hz approximately, and has unsteady pressure amplitudes of $O(100Pa)$.

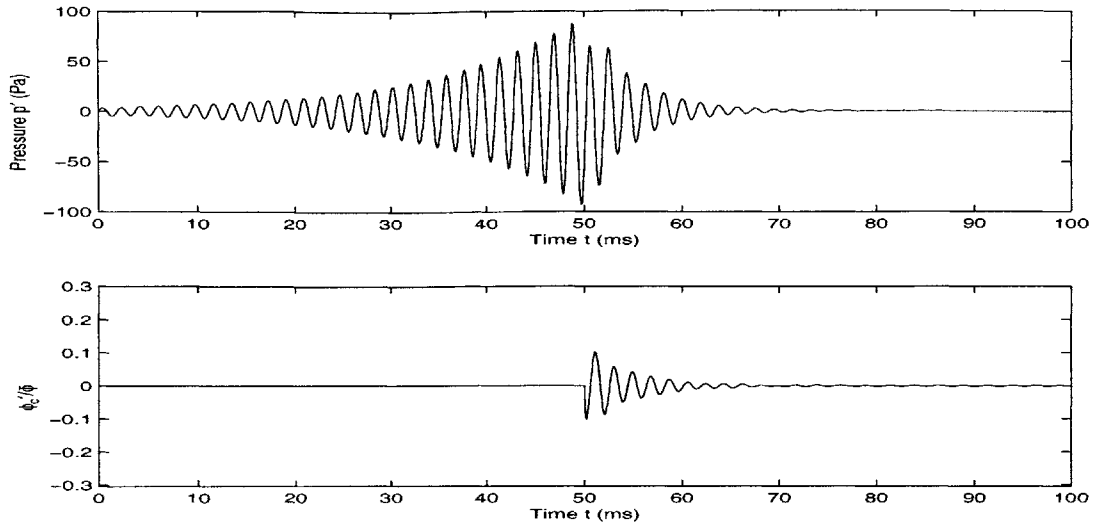

Figure 4-16: Response of the controlled combustor with a proportional injector with a bandwidth of $\approx$ 300 Hz.

We choose first a proportional injector, as in [87], with a bandwidth of 300 Hz which is in the range of available high-speed injectors [36]. Figure 4-16 shows the time response of the pressure and the control input, $\phi_c'/\overline{\phi}$ ($\overline{\phi} = 0.7$). Control is applied at $t = 50ms$. We note that although the bandwidth is lower than the system dynamics, the control with proportional injector is still capable of stabilizing the system, since the dynamics of the injector are taken into consideration in the design of the LQG/LTR. As seen in Eq. (3.22), the injector dynamics are first order, and the gain and phase introduced by the injector depend on its bandwidth. For smaller bandwidths cases, the phase increases while the control authority, i.e., the gain, is dramatically decreased around acoustic frequencies. The controller, however, has enough degrees of freedom to adjust the phase, and increase the voltage amplitude into the injector to produce the required control authority, $\phi_c'/\overline{\phi}$, around the acoustics frequencies thus guaranteeing stability.

While a low bandwidth proportional injector is capable of maintaining the system at vanishingly small pressure perturbations, a two-position injector may not be as effective [102, 53, 63]. Using a 300 Hz bandwidth injector, the LQG/LTR is still capable of stabilizing the system, but the pressure is suppressed to a small but finite amplitude limit cycle as seen in Fig. 4-17. The reason is that the injector has a threshold input voltage value at which it

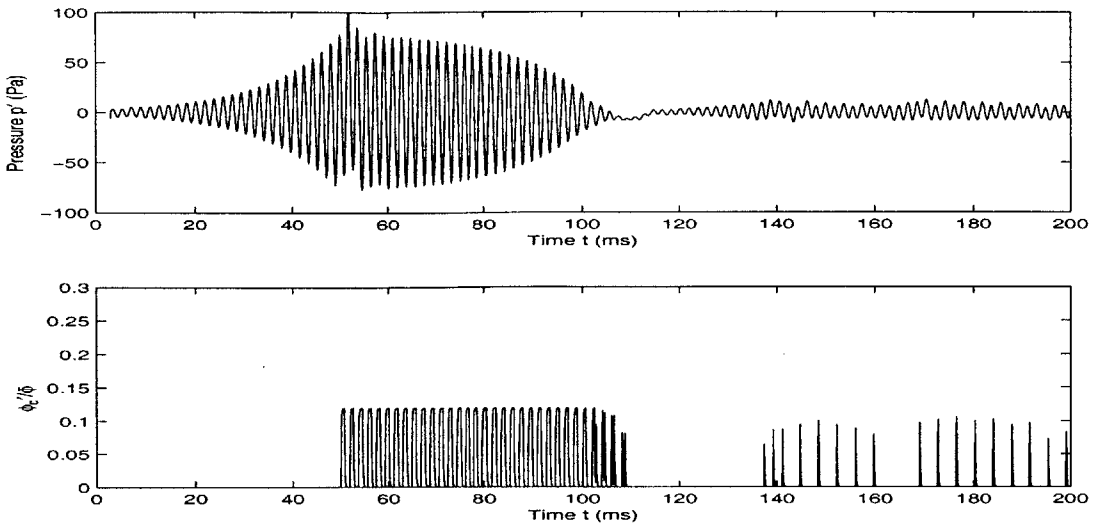

Figure 4-17: Response of the controlled combustor with an on-off injector set to deliver $\frac{\phi_c|_{max}}{\overline{\phi}} \approx 0.125$ and with a bandwidth $\approx$ 300 Hz.

is activated. Thus, following the suppression of the instability, the injector stops pulsing at from $t \approx$105-138ms, as seen in the figure. Disturbances in the combustor force the pressure to grow, until the measured voltage by the microphone reaches the threshold at which the injector starts to fire again. In the case simulated, this occurs at $t > 138ms$. This sequence is repeated indefinitely.

Increasing the control fuel-flow rate, and thus $\phi_c|_{max}$, the combustor is stabilized in a smaller settling time. As seen in Fig. 4-18, when $\phi'_c|_{max}/\overline{\phi}$ is doubled, the settling time diminishes by $\sim$ 80%. Moreover, the rms of the steady-state pressure is smaller. A similar effect has been observed in [102].

We also investigate the effect of bandwidth for a two-position injector. Limiting it to 50 Hz, as seen in Fig. 4-19, the pressure settles to a higher-amplitude limit cycle, and the injector is incapable of tracking the command from the controller; the injector stays open all the time. This shows that injector bandwidth is a serious problem [102, 63]. Different solutions have been proposed that include: (i) Developing faster injectors [36]. (ii) Use of multiple injectors which are fired alternatively to increase the apparent frequency of actuation [102]. A different approach that has shown promise regardless of high-bandwidth injectors is through fuel pulsing at low frequencies (much lower than the acoustics). This is demonstrated

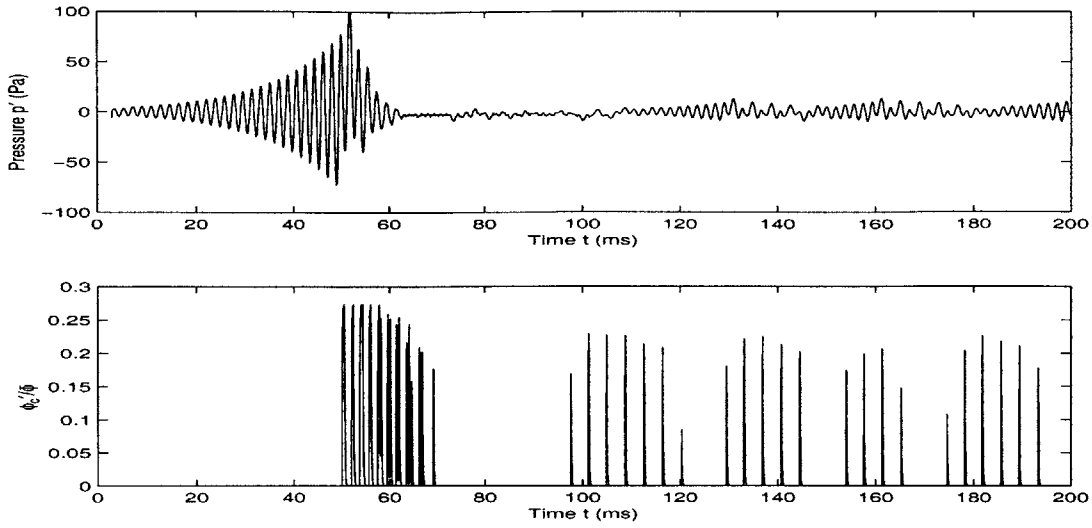

Figure 4-18: Response of the controlled combustor with on-off injector set to deliver $\frac{\phi_c|_{max}}{\bar{\phi}} \approx 0.27$, and with a bandwidth of 300 Hz.

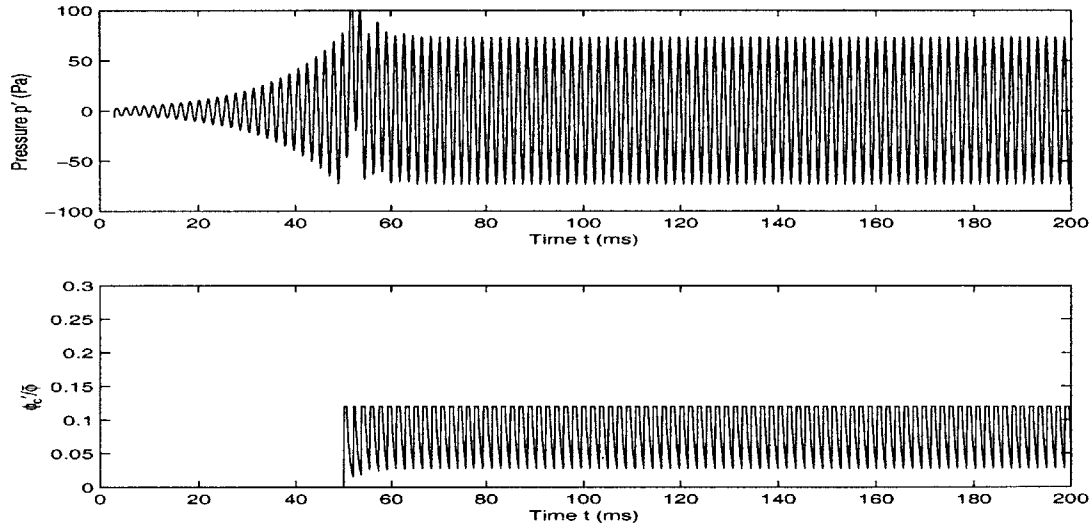

Figure 4-19: Response of the controlled combustor with on-off injector with lower bandwidth $\approx$ 50 Hz (the acoustics unstable frequency is 500 Hz, approximately).

experimentally in [82, 88], and analytically in [78].

Injection Upstream the Burning Zone: Delay in the Control Input

While injecting fuel directly on the flame [87, 62, 102, 53] can avoid actuation delays, it introduces hot spots at the flame surface thus increasing emissions. In addition, if mixing is weak at the injection port, we run the danger of creating a secondary diffusion flame which can be completely decoupled from the main premixed flame, and hence become ineffective in suppressing the instability [4].

In this section, we study the effects of pulsed-fuel injection upstream the burning zone. This has been utilized in [15] where secondary injection was done at the primary fuel source. In [40], we presented a Posi-Cast control capable of working with an injector located at an arbitrary distance upstream the flame. In that case, a bulk mode was unstable. Here, we extend the analysis of the Posi-Cast control, and show that it is capable of stabilizing longitudinal modes as well.

Posi-Cast Control

A powerful approach for controlling systems with known time-delay was originated by Smith [90], known also as Posi-Cast for "positive forecasting" of future states. The idea is to compensate for the delayed output using input values stored over a time window equal to the delay time, i.e. $[t-\tau_c, t]$, and estimate the future output using a model of the combustor. Only stable systems were considered. An extension to include unstable systems was proposed in [54] using finite-time integrals of the delayed input values thereby avoiding unstable pole-zero cancellations which may occur. A frequency-domain pole-placement technique for unstable systems was first proposed in [43] and a similar technique will be presented here.

The model in Eq. (4.24), in the presence of a time delay, τ_c, can be re-written as

$$p'(t) = W_p(s)[E(t-\tau_c)], \qquad W_p(s) = \frac{k_p Z_p(s)}{R_p(s)}. \tag{4.25}$$

[4] This has been noticed in experiments at MIT and at UTRC [14].

Due to the nature of the combustion system, not all states are accessible, only the system input, i.e. the voltage to the injector $E(t)$, and the output, p' in our case are measured. A standard pole-placement controller is required (for more information, see [43, 99]). The presence of the time-delay, τ_c, in the control input, motivates the use of an additional signal in the control input, $E(t)$, denoted as $E_1(t)$ which anticipates the future output using a model of the system [40]. The resulting controller structure is described as

$$\begin{aligned} E(t) &= \frac{c(s)}{\Lambda(s)}E(t-\tau_c) + \frac{d(s)}{\Lambda(s)}p'(t) + E_1(t), \\ E_1(t) &= \frac{n_1(s)}{R_p(s)}E(t) - \frac{n_2(s)}{R_p(s)}E(t-\tau_c), \end{aligned} \tag{4.26}$$

where $\Lambda(s)$ is a chosen stable polynomial of degree $n-1$, $d(s), n_1(s)$ and $n_2(s)$, are polynomials of degree $n-1$ at most, and $c(s)$ is of degree $n-2$ at most. For stability, these must satisfy the relations

$$c(s)R_p(s) + k_p d(s)Z_p(s) = \Lambda(s)n_2(s), \tag{4.27}$$

$$n_1(s) = R_p(s) - R_m(s), \tag{4.28}$$

where $R_m(s)$ is the desired characteristic equation, which is a stable monic polynomial of the same order of $R_p(s)$.

Using the controller structure in Eq. (4.26) with the conditions in Eqs. (4.27) and (4.28), the closed-loop transfer function can be computed as

$$W_{cl}(s) = \frac{k_p e^{-s\tau_c}}{R_m(s)}. \tag{4.29}$$

The control input law, in Eq. (4.26), introduces additional dynamics including non-minimum phase zeros having the same eigen-values of $R_p(s)$. Obviously, these lead to unstable pole-zero cancellations since the combustor model is open-loop unstable (i.e., $R_p(s)$ has unstable eigen values). Unstable pole-zero cancellations are known to cause problems concerning observability and controllability of the plant (see [71] for more details). As a result, a modification in the synthesis of $E_1(t)$ in Eq. (4.26) was suggested by [54]. To avoid

unstable pole-zero cancellations, $E_1(t)$ must be generated as a finite integral of the form

$$E_1(t) = \sum_{i=1}^{n} \left(\int_{-\tau_c}^{0} e^{-\lambda_i \sigma} E(t+\sigma) d\sigma \right), \tag{4.30}$$

where λ_i's are the eigen values of the combustor system, i.e. $R_p(s) = \Pi_{i=1}^{n}(s - \lambda_i)$. Taking the Laplace transform of Eq. (4.30), one can show that

$$\frac{n_1(s)}{R_p(s)} = \sum_{i=1}^{n} \frac{\alpha_i}{s - \lambda_i}, \frac{n_2(s)}{R_p(s)} = \sum_{i=1}^{n} \frac{\beta_i}{s - \lambda_i}, \tag{4.31}$$

where $\beta_i = \alpha_i e^{\lambda_i \tau_c}$. Another condition for the successful use of the finite integral in Eq. (4.30) is that $R_p(s)$ has no repeated roots [43].

The controller described in Eqs. (4.26) and (4.30) is sufficient to stabilize the combustor provided that an accurate description of the plant and the time delay are available. This controller has been shown to provide robustness to uncertainties in the plant including the time delay [54]. Adaptive versions of the same controller have been investigated [72, 68], and have shown to extend the robustness of the controller to parameter uncertainties.

Simulations of the Posi-Cast Controller

The controller in Eqs. (4.26) and (4.30) is implemented for injection at a distance of $\sim 3cm$ upstream the burning zone. τ_c is estimated to be $100ms$, which is about 50 times the time constant of the unstable frequency.

The closed-loop simulation is illustrated in Fig. 4-20. Although control is switched *on* at $t = 50ms$, the pressure keeps increasing for an additional $t = \tau_c = 100ms$ (from $t = 50 - 150ms$), then stalls for another 100 ms (from $t = 150 - 250ms$) before decaying. The reason for the former delay is physical and is due to the time taken for the pulsed-fuel to reach the burning zone. The latter is due to a computational delay in the controller. Specifically, the finite integral in Eq. (4.30) outputs incorrect values for a period of τ_c. This is because the computation of the finite integral relies on a stored window of the past values of the control input of the size of τ_c. When control is switched *on*, the window consists of control inputs proportional to p' which has not yet "felt" the effect of control due to the

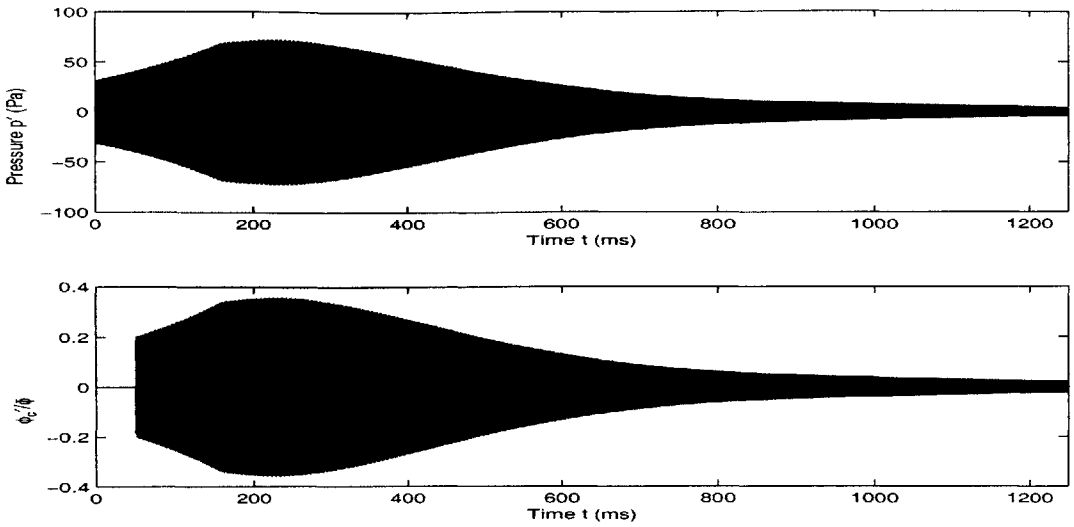

Figure 4-20: Response of the controlled combustor with a time-delay of $100ms$ in the input signal, proportional injector.

physical delay τ_c (the values of p' are still those of the open-loop combustor). It requires therefore $t = 2\tau_c$ to start forming a window of integration with control input corresponding to closed-loop values. This confirms observations in [54].

In Fig. 4-21, a two-position injector is used. The control design is based on the linear model, and its parameters are fine-tuned to handle the nonlinearities. As discussed earlier, the control is switched *on* at $50ms$, and stabilizes the system. The injector stays *on* as long as the voltage signal into the injector is greater than a threshold, as discussed before in Sec. 3.1.2.

It should be noted that when combustion instability is caused by ϕ'_s fluctuations, the characteristic equation will look different than in Eqs. (4.24) and (4.25). $R_p(s)$ will have terms which are delayed, due to the convective delay, τ_s, carried by ϕ'_s. Hence, $R_p(s)$ becomes infinite dimensional. To circumvent this, a Padé approximation [6] is used to get a finite dimensional description of $R_p(s)$, and thus the LQG/LTR and Posi-Cast controllers as described in Secs. 4.2.2 and 4.2.2, respectively, can similarly be used for this case.

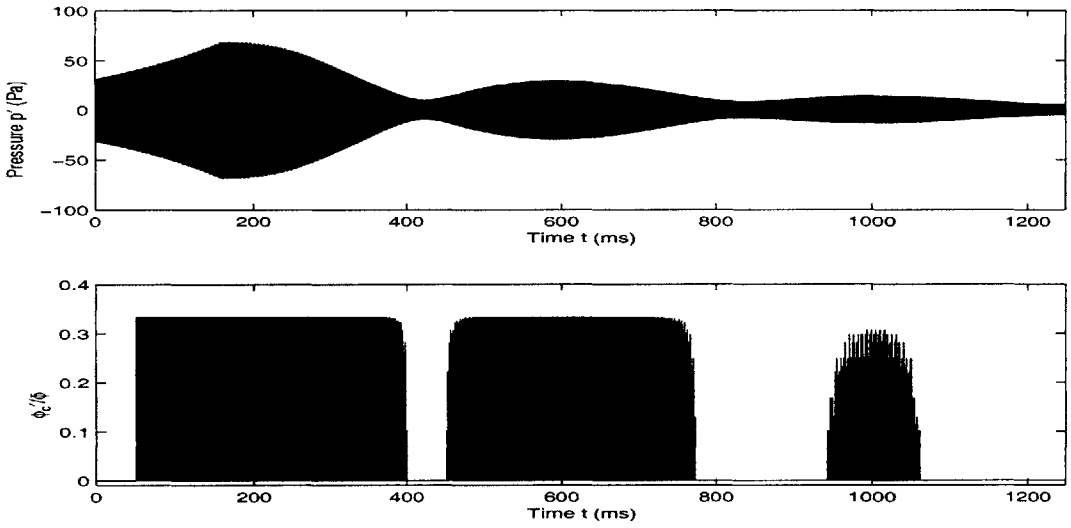

Figure 4-21: Response of the controlled combustor with a time-delay of $100ms$ in the input signal, on-off injector.

Chapter 5

Nonlinearities in the Heat Release Dynamics

The two prongs of combustion instability are the acoustics and the heat release. Either or both can behave nonlinearly. It all depends on the amplitude of oscillations of the pertaining acoustic and heat release parameters. It has been observed that the rate of heat-release fluctuations is closely related to fluctuations in the velocity rather than in the pressure [9]. In addition, the pressure amplitudes in actual low Mach number combustors have been observed to reach a maximum perturbation of 10 % the mean pressure, whereas velocity perturbations can reach 100 % of the mean velocity [9, 76]. In response the heat release perturbations which scale as $\frac{q'}{\overline{q}} \sim \frac{u'}{\overline{u}}$, are also observed to be large. This indicates that the heat-release fluctuations are likely to reach the nonlinear regime before the acoustics.

In this chapter, an extension of the linear models developed in Chapter 2 for combustion instability is presented. This pertains to the inclusion of nonlinear phenomenological mechanisms in the heat release dynamics so that the resulting model is capable of predicting limit cycle behavior that is ubiquitous in combustion instability pressure, velocity and heat release oscillations. An experiment is carried out to capture the onset of the nonlinear effect and its origin. Nonlinear models which exhibit a similar behavior to the experiment are proposed. These can give more insight on the reason linear control is successful in stabilizing the instability, and are a first building block in the pursuit of deriving a physically-based

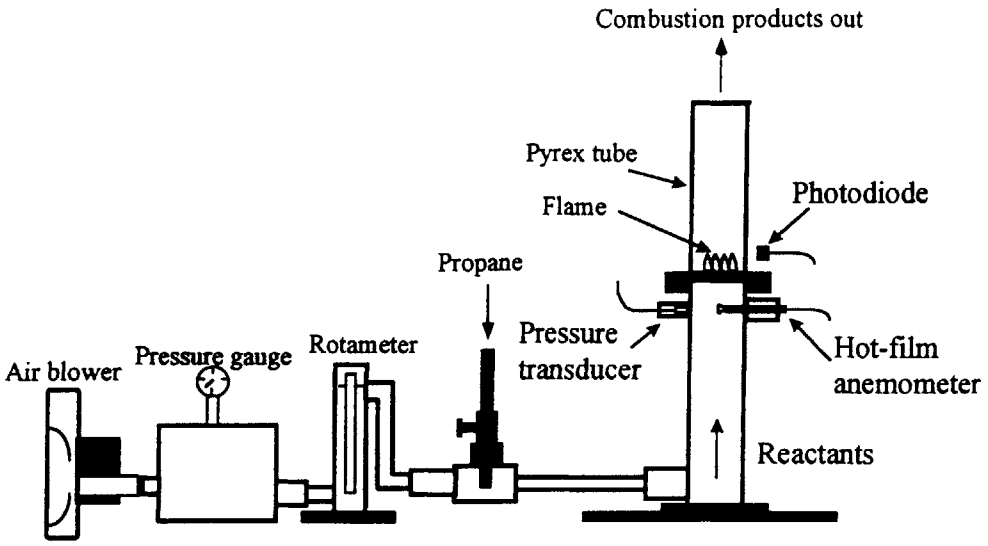

Figure 5-1: Schematic diagram of the combustor with the incorporated sensors.

nonlinear combustion model.

5.1 Experiment

A combustor rig with a power rated at 1 KW approximately is used to study the heat-release dynamics/acoustics interactions. First, we describe the set-up, then analyze the measurements and observations pertinent to nonlinearities in the heat release.

5.1.1 Set-up

The combustor rig is illustrated in Fig. 5-1. It consists of an air supply through a low-noise blower, a settling chamber, a rotameter for adjusting and measuring the air flow rate, a fuel (propane) supply through a pressure regulator and another rotameter. The combustion chamber is a 5 cm diameter, 26 cm long tube which represents the cold section. At the downstream end of this latter, the flame is stabilized on a perforated disc with 80 holes, 1.5

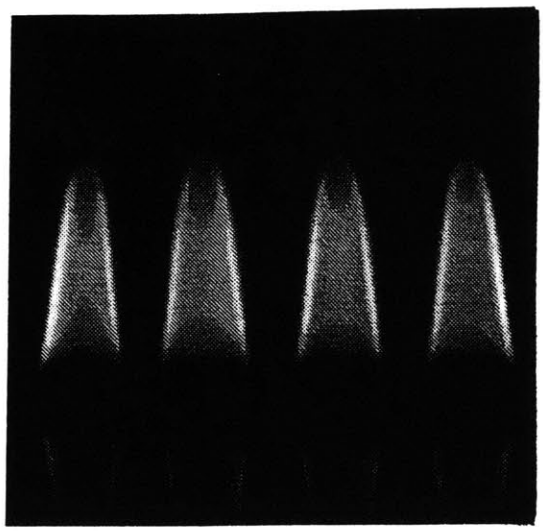

Figure 5-2: Picture of the flamelets anchored to the perforated plate

mm in diameter each, concentrated in a 2 cm diameter circular area. The flame is contained in the hot section which consists of a Pyrex tube 22 cm long to allow visual access to the burning zone. Several ports exist in the cold section for mounting sensors. Measurements on the test rig are recorded using a Keithley MetraByte DAS-1801AO data acquisition board with a maximum sampling frequency of 300 KHz. A software package, ExcelLINX, is used for data processing. The board is hosted in a Pentium PC. The combustor is equipped with several sensors including a Kistler pressure transducer, a TSI hot-film anemometer, and a Hamamatsu photodiode to measure the dynamic pressure, velocity and heat release (through light intensity). The first two are measured from a port which is 1 cm upstream the perforated plate (in the cold section), the latter is pointed at the flame from outside the Pyrex glass at a distance of 0.5 cm approximately. This allowed it to measure an integrated value of the light projected from the side-view area of the burning zone. A picture of the flamelets (forming the burning zone) from the photodiode's view point is shown in Fig. 5-2 (only four are shown for clarity).

Preliminary measurements showed to be noisy, especially for the velocity and the heat

release. This was circumvented by using shielded coaxial cables that were shortened as much as possible to avoid capturing ambient noise. Although the pressure transducer and the photodiode had a much higher bandwidth than the instability frequency, the anemometer had a bandwidth lower than the acoustics. This has been taken into account in processing the velocity measurements.

5.1.2 Results and Observations

The combustor exhibited an instability at 490 Hz, approximately, with steady-state pressure amplitudes of 0.1 % of the atmospheric mean and velocity amplitudes of 30 % the mean velocity which was measured to be 0.16 m/s, approximately, in the cold section. For this condition, the equivalence ratio, ϕ, was 0.7, approximately. The boundary conditions are closed upstream and open in the downstream end, and the unstable frequency corresponded to the three-quarter-wave mode. Our interest was to understand the dynamics that lead to limit cycles through changes in the heat release in response to growing pressure and velocity. To realize an experiment that captures the changes in the dynamics of heat release/acoustics when the system is in transition from small perturbations (linear growth) to sustained oscillations (nonlinear limit cycles), the following procedure is implemented: (i) We set ϕ =0.68, which corresponds to a stable operating for this combustor. (ii) The fuel flow rate is suddenly increased to ϕ =0.7 which corresponds to an unstable operating condition. At that instant, we start recording measurements for the pressure,p', the velocity, u', and the heat release, q', which increase through a transient and finally establish a limit cycle as shown in Fig. 5-3. The data is then filtered around the unstable frequency to remove any possible low frequency dynamics noise (e.g., from the blower or other electrical devices surrounding the rig).

We then analyze the time traces of the measured quantities and extract the amplitude and phase changes during the transient. We noticed a gradual change of phase between $u' - q'$ and $p' - q'$ as shown in Figs. 5-4 and 5-5, respectively. The former shows a phase change of about 50° from time $t = 0$ until reaching the limit cycle. A similar change is noticed in the latter figure, where the phase lag between $p' - q'$ is 20°, approximately, at

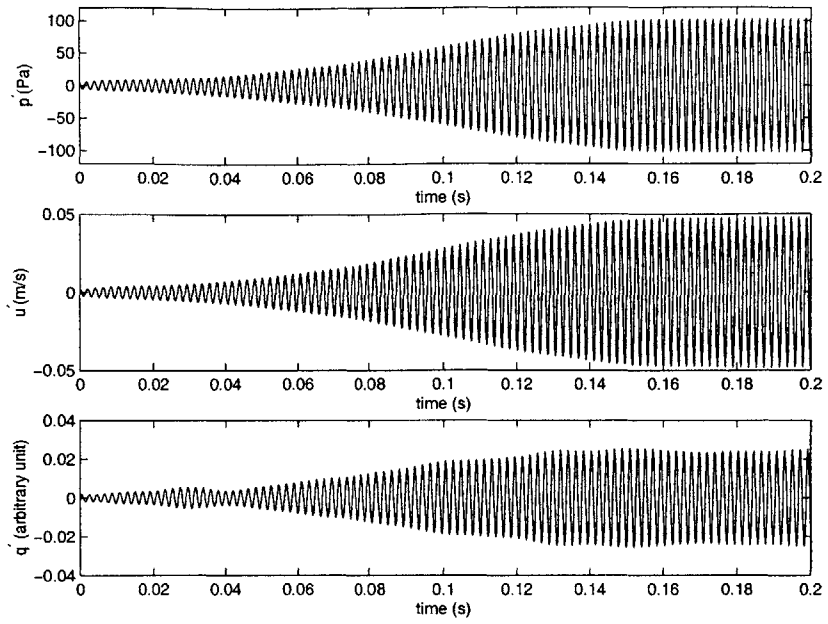

Figure 5-3: The measured responses from the combustor during a transient.

$t = 0$, and the phase lag increases gradually to reach a maximum of 70°, approximately, at the limit cycle. No evidence of saturation in q' was noticed as u' amplitudes increased as shown in Fig. 5-6. Saturation in q' was observed [21, 22, 61, 74], and was considered the primary cause for limit-cycling effect. The flame in these cases has shown to exhibit different dynamics than the one we are studying here. In [21, 22], the flame was stabilized behind a gutter, whereas in [61, 74] the flame was stabilized in a dump. In these, saturation in the heat release can be explained by the fact that the flame hits the walls and this constrains it from growing in response to increased perturbations in u', thus impeding the heat release to increase further. In [21, 22], saturation was blamed on flow reversal. We believe that flow reversal could also cause phase changes but no measurements in the latter references were carried out to support this.

It should be noted that the change in phase follows the predictions of the Rayleigh criterion. The condition under which a combustion system is unstable has been expressed in terms of the celebrated Rayleigh criterion [81] which, for conditions satisfied by systems

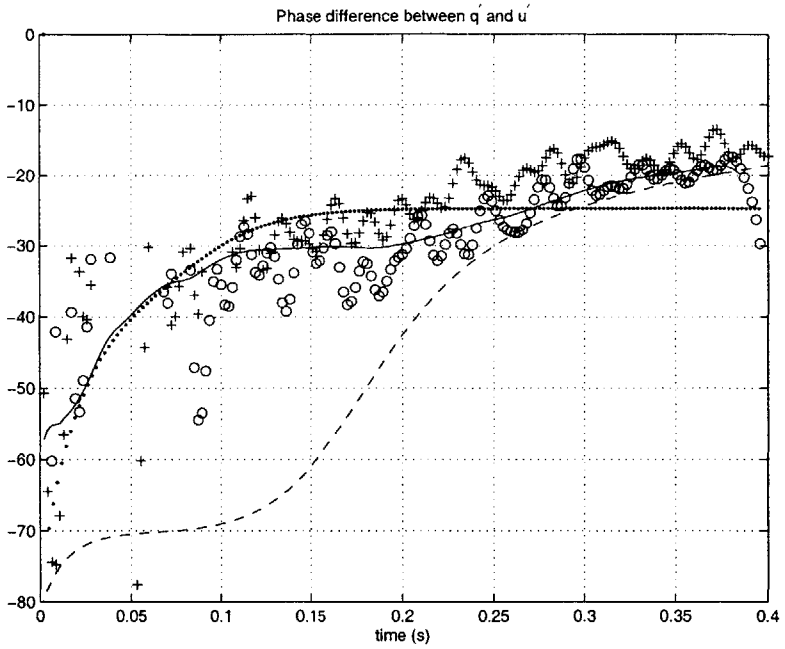

Figure 5-4: The measured phase-change between u' and q' during a transient. "o" and "+" are the experimental measurements for two different transients, "-" is an average curve fit of the experimental data, "- -" and "..." are the results of the reduced-order models in Eqs. (5.13) and (5.14), respectively.

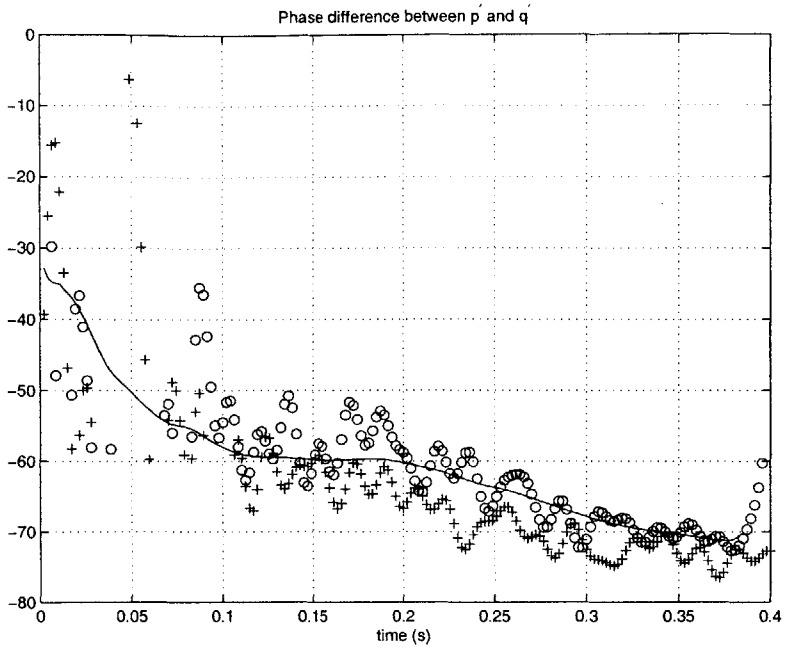

Figure 5-5: The measured phase-change between u' and q' during a transient. "o" and "+" are the experimental measurements for two different transients, and "-" is an average curve fit of the experimental data.

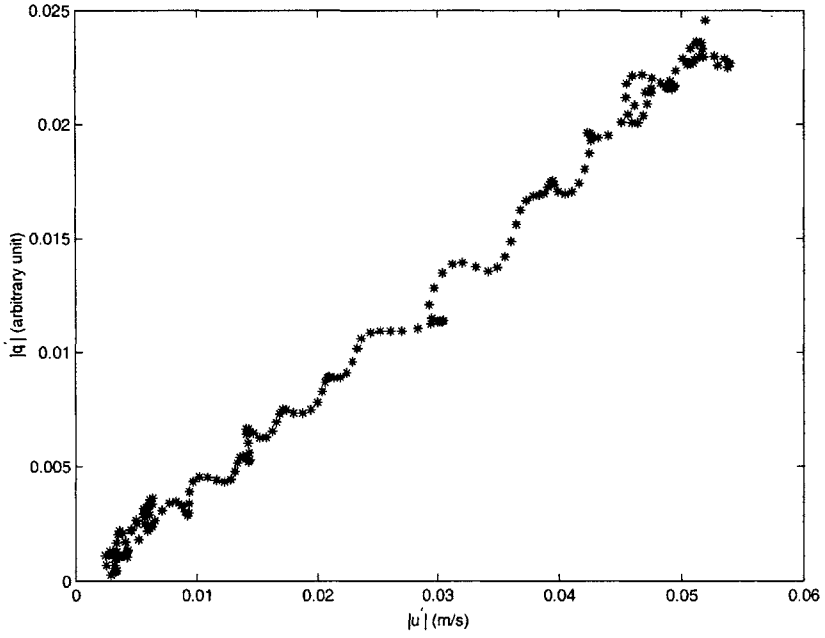

Figure 5-6: The measured change in amplitude of q' in response to an increase in the amplitude of u' during a transient.

analyzed in this work, and neglecting the effect of the mean flow, can be written as follows:

$$\frac{\partial}{\partial t}\int_0^L e'Adx = \frac{\gamma-1}{\overline{\rho c}^2}\int_0^L p'q'dx - \Delta_L(E'A) - \Phi > 0, \tag{5.1}$$

where $e' = \frac{p'^2}{2\overline{\rho c}^2} + \frac{\overline{\rho}v'^2}{2}$, and $E' = p'v'$, are the acoustic energy density and acoustic energy flux, respectively, ρ' is the perturbation in the density of the unburned mixture, A is the cross-sectional area of the combustor, Φ is the perturbation in the rate of energy dissipation, x, t are the distance and time, respectively, and Δ_L signifies the difference over the combustor length L. The conclusion drawn for this mathematical condition is that a combustion system becomes unstable when the heat release increases at a moment of pressure rise, i.e., $\angle(q' - p') \leq 90°$. Equation (5.1) shows that the acoustic energy accumulation depends on the acoustic boundary conditions and the dissipation in the system, and hence the gain in the $(p' - q')$ relationship also plays an important role in determining the characteristics of instability. The phase depends on how q' changes with p' (or u'), i.e., on the combustion dynamics, the location of the heat-release zone, and the boundary conditions.

As noticed in Fig. 5-5, p' and q' are approximately in phase in the first instants of the transient response, and gradually become less in phase until the phase lag reaches 70°, approximately. Ideally, without dissipation[1], the Rayleigh criterion would require the phase lag between $(p' - q')$ to be 90°, which implies that the response will be neither growing nor decaying and would settle at a limit cycle. In the experiment, the phase lag reaches only 70°, this is believed to be caused by the existence of natural damping in the system.

More insight is gained by looking at the evolution of the Rayleigh index, $R_m = p'q'$, shown in Fig. 5-7. Here, we see that larger positive values of R_m exist at earlier times, from $t = 0 - 0.07s$, followed by a continuous drop until it settles to oscillations around the zero mean at later times (from $t = 0.14 - 0.2s$). A similar result was observed in [75].

Next, we derive phenomenological heat-release dynamics models which capture the phase change described above through nonlinear effects.

[1]Dissipation in combustors could arise due to heat losses and viscous effects

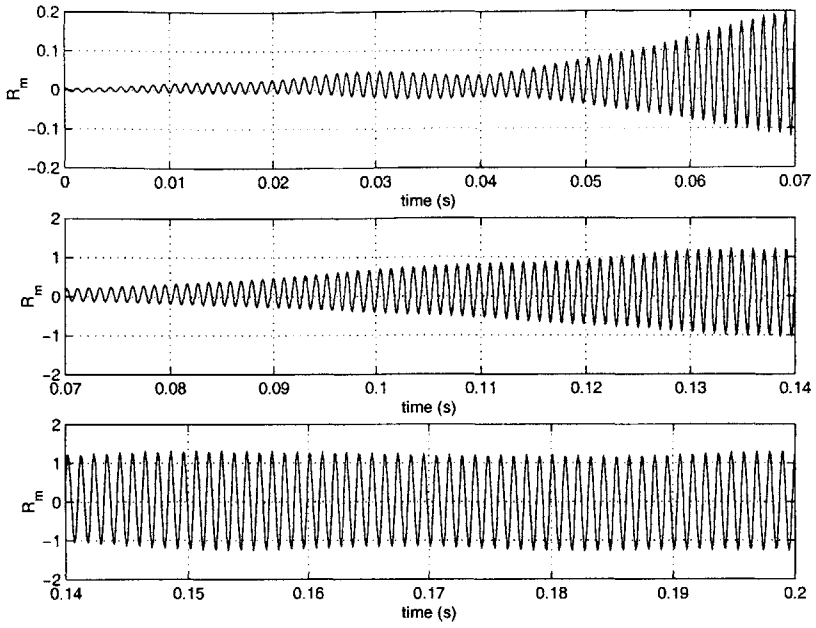

Figure 5-7: The measured Rayleigh index.

5.2 Numerical Simulation of Nonlinear Flame Response

In this section, we now obtain numerical simulations of Eq. (2.1) taking into consideration nonlinearities in the burning velocity, S_u. We consider the conical flame downstream each hole as being axisymmetric and almost independent of other flames, i.e. that the distance between the centerlines of neighboring holes is larger than the hole radius. This has been observed in the experiment as shown in the picture in Fig. 5-2. The velocity field downstream a single hole is taken to resemble that of a jet [86],

$$u = \frac{C_1}{z + z_o} \frac{1}{1 + \xi^2/4}, \tag{5.2}$$

where, C_1, C_2 and z_o are constants. The difference between this velocity and that of a jet stems from the presence of multiple holes, and the overall confinement of the flow downstream the perforated plate. The flow downstream the hole is assumed to be laminar since we are interested in cases for which the Reynolds number is relatively low and thus turbulent phenomena, such as vortex shedding, are neglected. The burning velocity is assumed

to change according to an equation which satisfies the conditions necessary for anchoring. Thus, Su is forced to decrease/increase for small/large values of ξ, reaching its nominal values several flame thickness downstream the perforated plate, and decrease/increase as the absolute value of the velocity increases/decreases. This can be described by the following heuristic relation:

$$S_u = S_u^o \left(1 - e^{-\xi}\right) \left(1 + 10 \frac{u}{u_m} \frac{\xi}{R}\right) \left(1 - \frac{l_m}{R_c}\right), \tag{5.3}$$

where u_m is the mean velocity in the hole, R_c is the flame-base radius, and l_m is the characteristic length of the flame.

The simulation of the flame surface dynamics is performed using a flame surface tracking algorithm in which the convective propagation is implemented by moving a large number of marker particles at the local velocity, while burning propagation is implemented by moving these particles at the local laminar burning velocity in the direction normal to the local flame surface [30]. The last step is complemented by the application of the Huygen's principle, in which the flame propagation due to burning is computed as the maximum of the burning along all possible directions from the local flame, to guarantee that the burning step is computed accurately. This implementation, is guaranteed to remain stable and does not suffer from the problems often encountered in computing the normal, especially where it may not be defined. The results presented next were obtained for $C_1 = 0.0375m2/s$, $C_2 = 70$, $z_o = 0.0115m$, $u_m = 1.6m/s$, the nominal laminar burning velocity $S_u^o = 0.4m/s$, and the hole radius $R = 0.75mm$. The frequency of the simulation is $\omega = 515$ Hz. Figure 5-8 shows different superimposed time frames for the flame area response to (a) small perturbations in the velocity ($u'/u_m \sim 0.01$), and (b) large perturbations (u'/u_m 0.4). In both cases, the flame maintains the conical shape, with most of the profile satisfying the condition $\frac{\partial \xi}{\partial r} > 1$. Only close to the perforated plate, where the flame is "anchored", is where this condition is violated. The point where the transition occurs, $r \sim r^*$, moves towards the centerline as u' increases, i.e., as conditions become more nonlinear. In all cases, the flame oscillations are much stronger closer to the tails where the average velocity is weaker and the relative perturbation is stronger. There, the flame is almost normal to the streamlines and thus more vulnerable to the imposed oscillations. It appears that the onset of the nonlinear flame

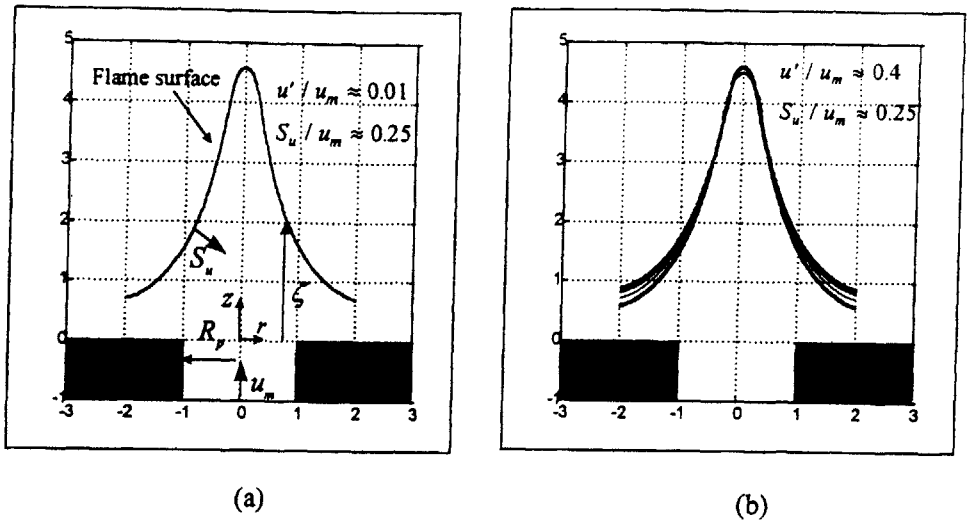

Figure 5-8: Flame surface for (a) small and (b) large u'/u_m.

response is associated with the conditions close to the anchoring point. The shape of the simulated flame in Fig. 5-8 is qualitatively similar to the experimental picture of the flames in our test-rig (Fig. 5-2). It is interesting to notice that the section of the flame for which the slope is high, $r < r^*$, suffers the smallest oscillations. There, the flame response remains "linear", i.e. with weak oscillations, even at higher flow velocity perturbations. This is most likely due to the extra freedom the flame has away from the anchoring zone. As is well known, away from the anchoring zone, the flame surface can change its angle continuously in response to changes in the flow velocity.

The dependence of the phase between the heat release rate on the velocity amplitude is shown in Fig. 5-9. This is the open loop response, i.e. at a fixed u' amplitude. As in the linear analysis, for weak perturbations at high frequency, the heat release rate lags behind the velocity by almost 90°. For the intermediate amplitude, the absolute value of the phase is much smaller, with heat release still lagging behind the velocity. For yet larger amplitudes, the heat release crosses the zero phase, and actually leads the velocity perturbations by a small positive phase.

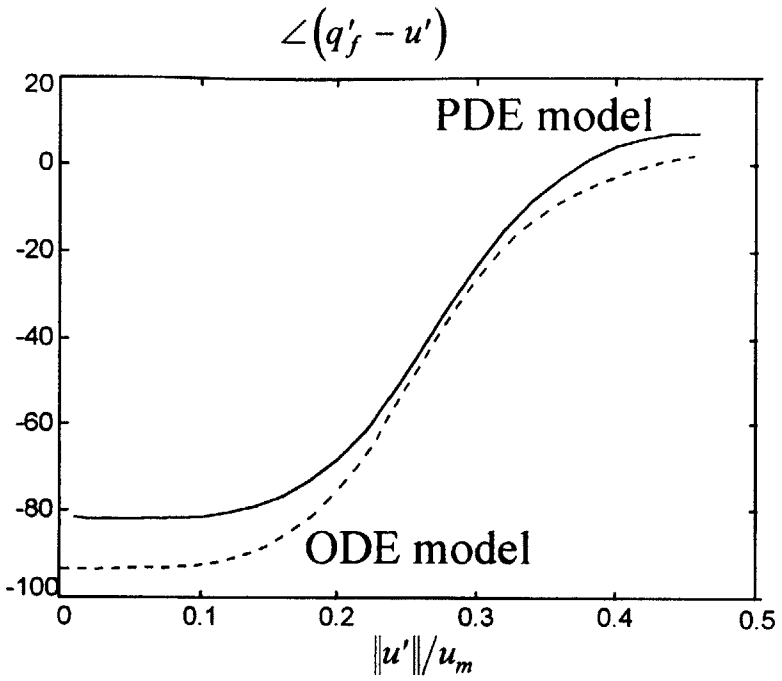

Figure 5-9: Comparison of the heat release-velocity phase as a function of $|u'|/u_m$ for the PDE's solution "-" and the reduced-order model (ODE) with two modes "- -"

The trend of the phase change seen in these results resembles that measured in the experiment in Fig. 5-4. The discrepancy in phase which is about 20° at both the linear and nonlinear limits can be explained by the fact that no dissipation in the form of heat loss for instance was included in the simulation.

5.3 Limit-Cycle Simulations

As mentioned before, if the Rayleigh criterion is satisfied, i.e., the phase between the pressure and the heat release must be $< 90°$, the velocity amplitude grows. The phase between the velocity and pressure depends on the boundary conditions and the position. Since the phase between the heat release and the velocity is determined by the flame dynamics and the frequency, the conditions for instability depend on where the flame is located within the acoustic field. Once the flame is located where the instability conditions are satisfied, small perturbations grow via the linear mechanism and the system is considered as being unstable.

Left without external intervention, it is often observed that the instability reaches a limit cycle in which the amplitude remains constant. There are many mechanisms for achieving limit cycles: a balance between the dissipation, which grows with the growing amplitudes, and the energy fed by the instability, nonlinear acoustics, saturation, or changing phase between the pressure and heat release, through the flame mechanism, leading to a situation in which the Rayleigh index reaches zero or even becomes negative. In the experiment in Sec. 5.1, we noticed that the phase-lag mechanism between p' (or u') and q' may be the primary player in causing limit cycles. In this section, we investigate if this mechanism is sufficient to cause limit cycles regardless of nonlinearities in the acoustics.

5.3.1 Nonlinear Acoustics

We performed a numerical simulation using the full, nonlinear gas dynamics equations coupled with the heat release dynamics model given by Eqs. (2.1) and (2.2). The governing equations for an inviscid, one dimensional, perfect gas flow are utilized [94]. The numerical solution of these equations is performed using the split coefficient matrix [30]. The heat release is concentrated at the flame location x_f and the velocity in Eq. (2.1) is taken as the average value before and after the flame surface. Results are shown in Fig. 5-10 for the heat release rate and the velocity at early and late times. The simulations are obtained for the combustor described in Sec. 5.1 with an estimated enthalpy of reaction of $\Delta h_r = 2.4381106 J/kg$ and with inlet conditions of $p = 1 bar$ and $T = 300°K$.

As expected from the boundary conditions and the flame location, an instability at $\omega = 535$ Hz grows linearly, with the heat release lagging behind the velocity by 90°. However, at latter times, the instability saturates and we reach a limit cycle at which the velocity and heat release are almost in phase. Figure 5-11 illustrates the same message through the Rayleigh index and integral, and agrees with the experimental observations in Fig. 5-7, and in [75].

It should be mentioned that the maximum pressure amplitude of the limit cycle never exceeds 0.5% of the mean, a value consistent with the acoustic approximation. Meanwhile the maximum velocity amplitude reaches a value of 40% of the mean, which is again consistent

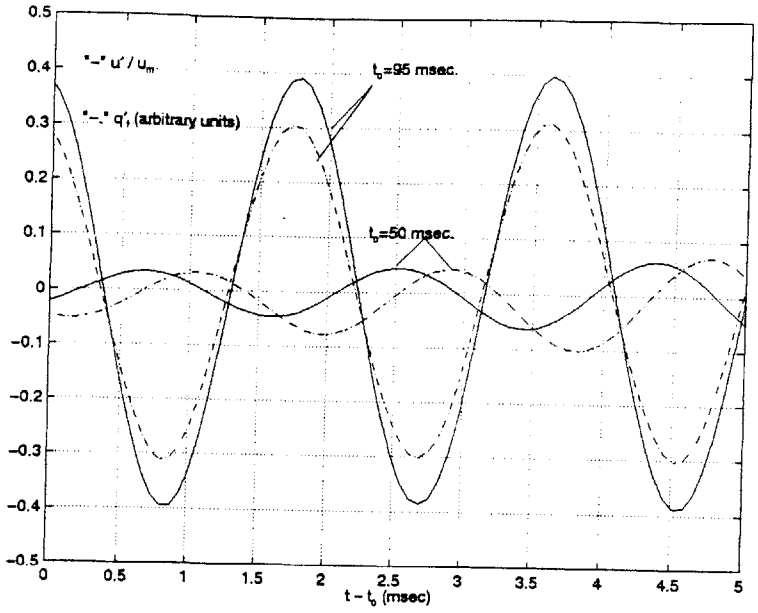

Figure 5-10: Heat release-velocity phase at different times, t_o defines the starting time of each set of curves.

with the low Mach number of the simulations. Similar quantities were measured in the experiment as discussed in Sec 5.1. Moreover, since the acoustic frequency has not changed, the phase between the heat release rate and the velocity must have changed according to the plot shown in Fig. 5-9

We should mention that our model is non dissipative and thus there is no need for a finite energy input to sustain the oscillation. In practice, it is expected that this integral would rise steadily to compensate for the dissipation. These results confirm the early conclusion that reaching a limit cycle is connected to the inherent flame dynamics which causes the phase change as the u' amplitude grows.

5.3.2 Linear Acoustics

Since one of our goals is to determine whether transition to nonlinear behavior and the establishment of a limit cycle is due to the combustion nonlinearity or not, we repeated the simulations presented in Sec. 5.2.1 while using a linear acoustic model for the flow.

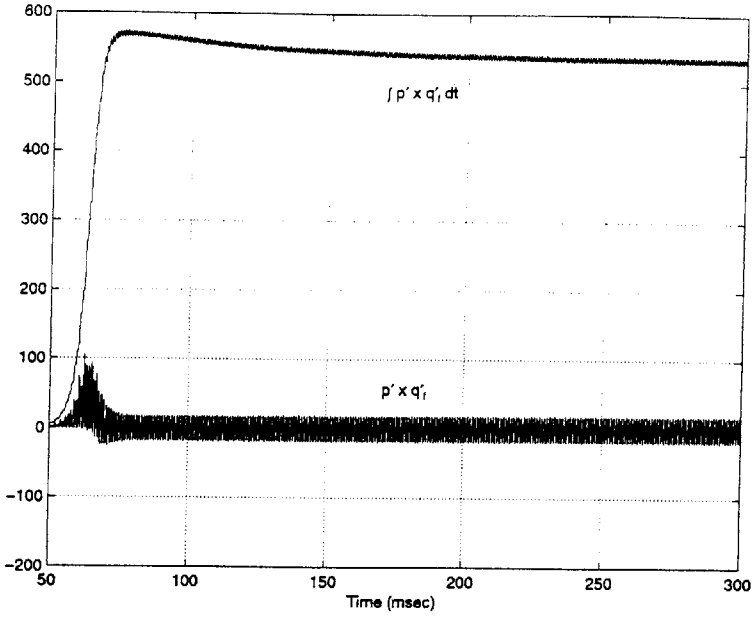

Figure 5-11: Rayleigh index and integral of the simulation in Sec. 5.2.1

For this purpose, the governing equations were linearized around their mean and a finite dimensional model was obtained assuming that the pressure can be represented using the classical Galerkin expansion [4].

The results of these simulations agree with those presented in the previous section, confirming that acoustic nonlinearities do not play a role in determining the nonlinear characteristics of the instability. For example, we show the evolution of the pressure perturbation obtained from the simulations in here and Section 5.2.1 in Fig. 5-12. Note that the limit cycle amplitude is well predicted by the linear acoustics solution. This is because it is governed by the behavior of the phase as a function of the velocity amplitude, shown in Fig. 5-9. The disagreement between the two solutions within the linear range is most likely due to errors in evaluating the time derivative perturbation in the heat release rate (which is not needed in the nonlinear acoustics model).

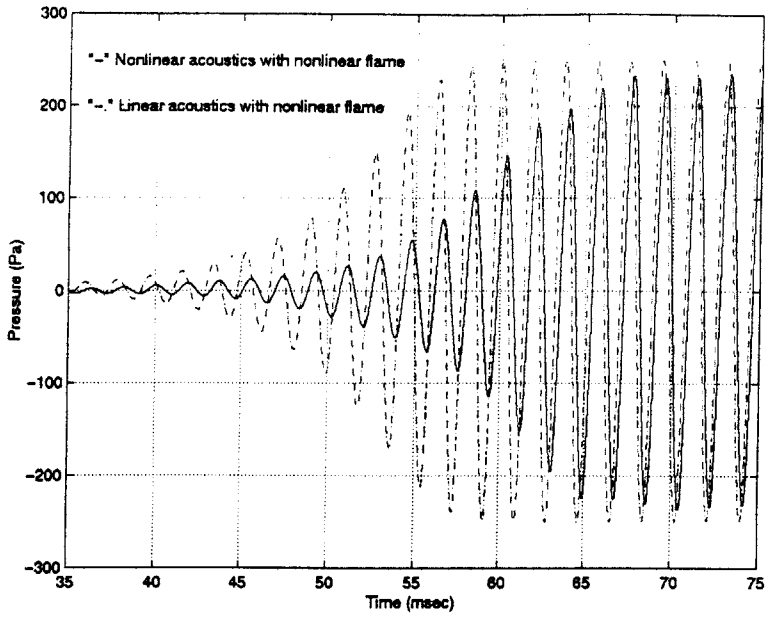

Figure 5-12: Evolution of the pressure with linear and nonlinear flame model.

5.4 Finite-Dimensional Model of the Nonlinear Heat Release Dynamics

Since our goal is to develop reduced-order models for the combustion dynamics that capture the dominant dynamics of the combustor, and can be used to design compensators for suppression of pressure oscillations, we derive a nonlinear finite dimensional model for the heat-release dynamics. Using the Galerkin expansion, we can derive a set of ODE's that describe the evolution of the flame surface as well as the rate of heat release. First we expressed the flame location as [30].

$$\xi(r,t) = \bar{\xi}(r) + R\sum_{j=1}^{m}\eta_{f_j}(t)\psi_{f_j}(r), \tag{5.4}$$

where η_{f_j}, ψ_{f_j} are the j^{th} modal amplitude and basis function for the perturbation in the flame location, respectively. The flame structure under laminar flow conditions suggests the

choice of basis functions as polynomials, i.e.,

$$\psi_{f_j} = \left(\frac{r}{R}\right)^{j-1}, \quad j = 1, 2, ..., m. \tag{5.5}$$

Using both Eqs. (5.4) and (5.5) in Eq.(2.1), and integrating over the entire radius of the flame base, the following set of ODE's, written in vector form, are obtained

$$A\dot{\eta}_f = Bu' - f(\eta_f), \tag{5.6}$$

$$Q'(t) = \overline{r}ho\Delta h_r\{\int_0^R rS_u\sqrt{\left(\frac{d\overline{\xi}}{dr} + R\sum_{j=1}^{m}\eta_{f_j}\frac{d\psi_{f_j}}{dr}\right)^2 + 1}dr - \int_0^R r\overline{S}_u\sqrt{\left(\frac{d\overline{\xi}}{dr}\right)^2 + 1}dr\} \tag{5.7}$$

where

$$A_{i,j} = \int_0^R r\psi_{f_i}(r)\psi_{f_j}(r)dr,$$

$$A_{i,j} = \int_0^R r\psi_{f_i}(r)dr, \quad i = 1, 2, ..., m, \quad j = 1, 2, ..., m,$$

$$f(\eta_f) = \int_0^R r\psi_{f_i}(r)S_u\sqrt{\left(\frac{d\overline{\xi}}{dr} + R\sum_{j=1}^{m}\eta_{f_j}\frac{d\psi_{f_j}}{dr}\right)^2 + 1}dr - \int_0^R r\psi_{f_i}(r)\overline{S}_u\sqrt{\left(\frac{d\overline{\xi}}{dr}\right)^2 + 1}dr$$

Equation (5.6) can be solved for the modal amplitudes, then Eq. (5.7) can be used to evaluate the rate of unsteady heat release. We computed the phase between the unsteady heat release and the velocity as the amplitude of the latter changes, using only two modes for the flame location. Figure 5-9 shows a comparison between the phase obtained from the numerical simulation of the PDE's of the flame kinematics and that of the two modes reduced-order model of the flame. Although we used only two modes in the reduced-order model, it captures well the main features of the infinite-dimensional case.

5.5 Phenomenological Models

A reduced-order model, based on a lumped representation of the flame, has been derived in Chapter 2. This model has shown to be accurate in modeling flames stabilized behind a perforated plate and is used in this section to derive phenomenological nonlinear models

of the heat release. While this approach is not derived directly from rigorous physics, but rather guided by the experimental results in Sec. 5.1, the simplicity of the models are very advantageous when model-based active control is concerned.

We start by considering the lumped-flame model when only perturbations in the velocity exist. Considering a control volume, V, enveloped by the flame base area (i.e., the perforation area), A_p, and its surface area, A_f, the conservation of volume requires:

$$\dot{V} = uA_p - S_u A_f, \tag{5.8}$$

where u is the velocity in the perforation and S_u is the burning velocity. We define $V_f = S_u A_f$, which represents the "burnt" volume, and we assume a geometrical relation between the "accumulated" volume and the area of the flame as $V = \alpha A_f$, thus, Eq. 5.8 is integrated as

$$V_f(t) = \frac{S_u}{\alpha} \int_0^t [u(t)A_p - V_f(t)] d\tau, \tag{5.9}$$

We assume that the term (Su/α) is the main source of nonlinearity in the flame. S_u is function of the flame curvature, flow strain effects, heat losses, while α is function of the anchoring mechanism, the velocity profile and S_u. The dependence of S_u and α on the mentioned parameters and each other is not well known, and hence the term (Su/α) contains also uncertainties. For the class of premixed flames at high Damkohler numbers and moderate turbulence intensity, the heat release, Q, is governed by (as in Chapter 2)

$$Q = \rho_u \Delta h_r S_u A_f, \tag{5.10}$$

where ρ_u is the density, and Δh_r is the enthalpy of reaction per unit mass of the mixture. Since $\overline{Q} = \rho_u \Delta h_r \overline{u} A_p$, the perturbed heat release can be written as

$$Q' = \rho_u \Delta h_r (V_f - A_p \overline{u}). \tag{5.11}$$

The perturbed "burnt" volume is quantified as

$$V_f' = \frac{S_u}{\alpha} V' + \overline{V}_f \left(\frac{S_u/\alpha}{\overline{S}_u/\overline{\alpha}} - 1 \right), \tag{5.12}$$

which is simplified further by neglecting the second term in the RHS. This means that changes in (Su/α) are of the order of the mean. At this point, the reasoning for neglecting this term is not based on any physical ground, as mentioned before, we seek here to capture the phase-change nonlinearity by the simplest nonlinear form possible.

We present here two nonlinear examples for the relation between V_f' and V'. The following equations represent possible forms of nonlinearities that may exist in (S_u/α) and cause phase-lag change between u' and q' (this can be verified using describing function arguments as in [89, 85]:

$$V_f' = a_1(1 - a_2 V'^2 + a_3 V'^4)V' + a_4 V_i'^3, \tag{5.13}$$

and

$$V_f' = b_1 e^{-b2|V'|}V' + b_3\left(e^{-b_4|V_i'|} - b_5 e^{-b_6|V_i'|}\right)V_i', \tag{5.14}$$

where $V_i' = \int_0^t V' d\tau$, and the parameters a_j and b_j where tuned to get similar changes in phase as in the experimental results measured in Fig. 5-4.

The nonlinearities in Eqs. (5.13) and (5.14) together with linear acoustics exhibiting one mode(the unstable three-quarter-wave mode as in [4]) exhibit limit cycles as seen in Fig. 5-13. The frequency of the acoustic mode was $\omega \sim 500$Hz, and a passive damping ratio of 0.05 was taken. For Eq. (5.13) the parameters were taken as: $a_1 = 60$, $a_2 = 0.45/\omega^3$, $a_3 = 6/\omega_5$, $a_4 = 8$, and for Eq. (5.14), $b_1 = 55$, $b_2 = 10^{-6}$, $b_3 = 10^6$, $b_4 = 10^{-4}$, $b_5 = 0.8$, and $b_6 = 2.10^{-3}$. These parameters led to a phase-change nonlinearity for both models in Eqs. (5.13) and (5.14), and the change in phase during a transient is superimposed on the experimental results in Fig. 5-4. It is worth noting that Eq. (5.14) is an overall better fit for the experimental results than Eq. (5.13).

The models presented here are very attractive when control is implemented, since despite their simplicity they can capture the observed features in the experimental measurements including growth rate, limit-cycle amplitude and the phase-change mechanism that causes limit cycles as discussed in Sec. 5.1.

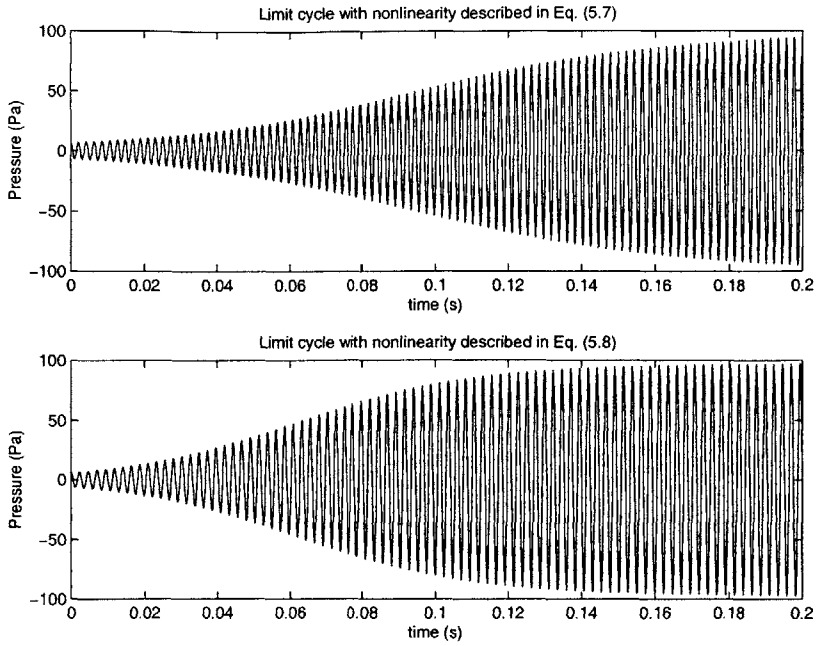

Figure 5-13: Pressure response with the nonlinear dynamics in Eqs. (5.13) and (5.14), respectively

5.6 Control

In this section, we use linear control methods, e.g. LQG (as in Chapter 4), to stabilize the nonlinear system as presented in Section 5.2.

Considering a two-mode combustor model with essentially instability induced by area fluctuations coupled with the velocity oscillations, we design an LQG controller based on the linear model and implement it on the nonlinear model, considering a nonlinearity similar to Eqs. (5.13) and (5.14).

To evaluate the possibility of success of a linear controller with a nonlinear combustor model, we start by expressing the nonlinearity as $f(V_f') = V_f' - g(V_f')$, and making further simplifications, the resulting closed-loop can be described as (see Fig. 5-14)

$$V_f' = W_{cl}(s)\left[-g\left(V_f'\right)\right], \tag{5.15}$$

where W_{cl} represents the closed-loop system with linear controller, and $g(.)$ represents the

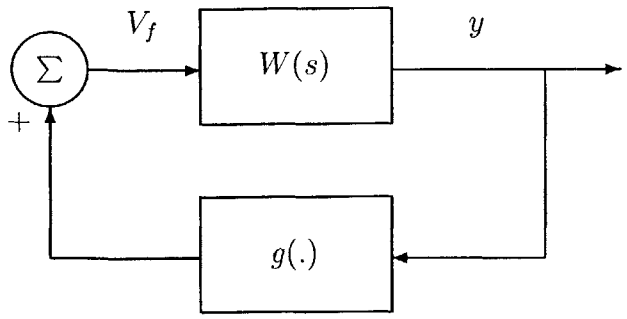

Figure 5-14: Closed-loop nonlinear system.

deviation in f from linearity.

Under some conditions on $W_{cl}(s)$ and $g(.)$, it can be shown that the closed-loop system will be stable. The following arguments summarize these conditions.

If the components in the closed-loop system, described in Fig. 5-14, are such that: (i) $W_{cl}(s)$ is strictly positive real, (ii) $g(x)x > 0$ for all $x \neq 0$, and $g(0) = 0$. Then, the closed-loop is asymptotically stable.

The closed-loop system stability follows in a straightforward manner by showing that $V_l = x^T P x$ is a Lyapunov function where x is the state vector of the linear system, i.e.

$$\dot{x} = Ax + BV_f', \quad y = C^T x$$

and P is the solution of the equations

$$\begin{aligned} A^T P + PA &= -Q, \\ Pb &= C, \end{aligned}$$

where Q is a positive-definite symmetric matrix.

The actuated combustor system using a secondary fuel injector satisfies condition (i), as it is of minimum phase and of relative degree one. Also condition (ii) is satisfied by the nonlinearities in Eqs (5.13) and (5.14), as these are first and third quadrant nonlinearities.

A numerical simulation is shown in Fig. 5-15 where an LQG controller based on two

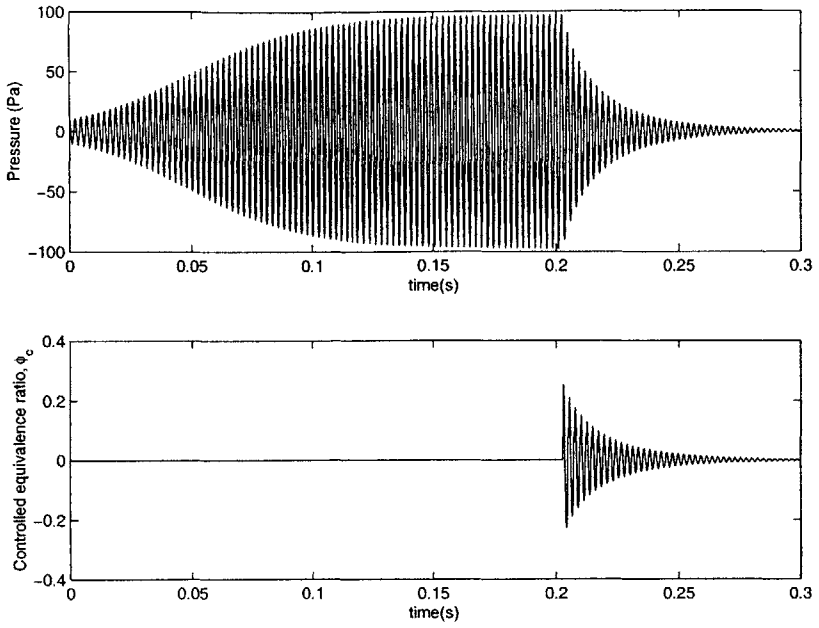

Figure 5-15: Controlled response with an LQG controller, and with a heat release nonlinearity as in Eq. (5.14).

modes (for parameters given in Chapter 4 and in [4]) is shown to stabilize a combustor with the heat release nonlinearity in Eq. (5.14).

5.6.1 Saturation in the Control Input

As discussed before in Chapter 4, injectors are plagued with limited authority causing saturation in the control input. To evaluate the performance of a linear controller with saturation in the control input we simulate the system discussed above imposing a saturation (on-off) block in the secondary fuel input.

Figure 5-16 shows the time response of a controlled combustor. The control is switched *on* and turned em off at different times. We notice that at $t = 0.07s$ the controller is switched *on* and the system is brought to asymptotic stability. Then control is switched *off* and the pressure starts to grow back to the limit cycle. When control is switched *on* again at $t = 0.66s$, the controller is only capable of bringing the pressure down to a smaller limit cycle (controlled limit cycle). Then, control is turned *off* again, and the pressure settles back

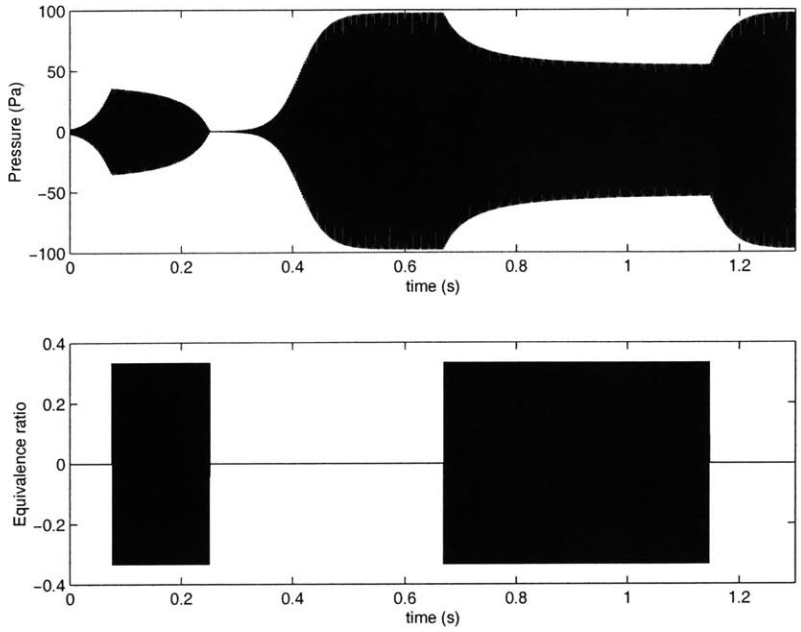

Figure 5-16: Controlled response with on-off nonlinearity in the controlled input.

to the natural (open-loop) limit cycle.

Saturation in the control input creates an unstable limit cycle, enveloping a controllability set that brings the response to asymptotic stability if initial conditions are within this set. If initial conditions are included within this set. Otherwise, the response will go to a second limit cycle as seen in Fig. 5-16.

Figure 5-17 shows how the controllability set increases as the saturation (on-off) limits ($\phi_{max}/\overline{\phi}$) are increased (the dashed line). On the other hand, the controlled limit cycle decreases in amplitude until it collapses to zero (i.e, asymptotic stability) as the $\phi_{max}/$ $ov\phi$ is increased. Any initial conditions below the controllability set line "- -" will result in asymptotic stability, otherwise the pressure will exhibit a limit cycle delineated by the controlled limit cycle line "-". We note that for this example a $\phi_{max}/\overline{\phi} > 0.6$ will always bring the system to asymptotic stability.

Similar observations have been noted in the experiment in [102], where linear control was implemented on a realistic sector rig engine.

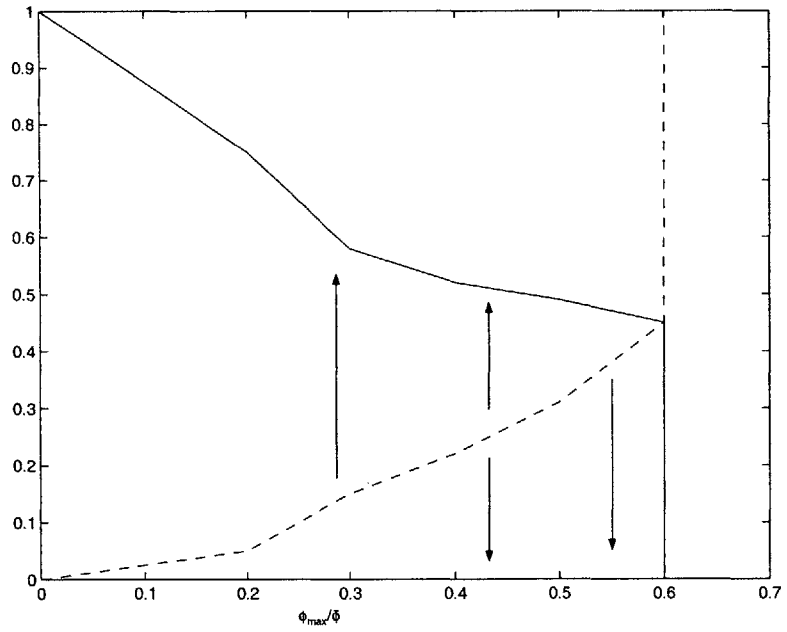

Figure 5-17: Controllability set "- -" and controlled limit cycle "-" with increase in $\phi_{max}/\overline{\phi}$.

Chapter 6

Summary, Conclusions and Future Work

The focus of this thesis is in the modeling and control of combustion systems that exhibit thermoacoustic instability. The latter has been observed to occur in lean-premixed low-emission combustors as well as high-power near-stoichiometry combustors. Applications of the first include commercial aeroengines, land-based, marine-based gas turbines, incinerators, and boilers where low emissions are sought after; whereas for the second, military applications prevail either in the form of aeroengines, afterburners, rockets, etc.

The main goals throughout this work were to model combustion situations as realistically as possible based on the physics and propose reduced-order models which can be implemented in designing control strategies to abate the instability. Herein, we summarize the main results and propose future research that can be be carried out in light of the efforts discussed in the thesis.

6.1 Summary and Conclusions

In Chapter 1, an extensive literature survey of the endeavors carried out for understanding and mitigating combustion instability was presented. The efforts done in experiments, CFD simulations, modeling, sensing, actuation and control of combustion systems were dis-

cussed. While experiments and CFD analyses highlighted the complexity of the mechanisms involved in the combustors, the physical mechanisms pertaining to combustion instability were not fully understood. The lack of accurate predictive models amenable for control design was obvious. Although models of acoustics have been proposed, heat-release models lacked. Control was mostly empirical and has shown to be of the phase-shift type which has been observed to cause resonances at frequencies which were not excited in the uncontrolled combustor [27].

In Chapter 2, a model of the combustor comprising the acoustics as well as the heat-release dynamics is derived. The acoustics model encompassed bulk as well as longitudinal modes, usually observed in actual combustors. Two approaches for deriving the heat-release dynamics are proposed including a flame kinematics approach and a lumped-model approach. Oscillations in the equivalence ratio as well as in the velocity are introduced and their effect on the heat-release rate of a premixed, high-Damkohler number and low to moderately turbulent flame, i.e, wrinkled flame, is studied. The coupling mechanisms between the acoustics and the heat release are shown to be crucial in causing the instability. While velocity perturbations cause instability of a phase-lag nature, equivalence-ratio oscillations introduce a time-delay instability causing the model to be infinite dimensional. These mechanisms have been observed in actual combustors. Comparisons with typical systems in the literature have been carried out, and the models were shown to predict situations in actual combustors. The dynamics in these models are very rich and were shown to encompass a plethora of combustor situations [38, 40, 29]. The models are easily implementable for model-based control [37]. Nonlinearities in the heat release are shown to be easily included in these models as illustrated in Chapter 5 and in [19, 74].

In Chapter 3, the dynamics of typical actuators used in modulating combustors are modeled. A typical flow source, a speaker, and a typical heat source, a fuel injector, are modeled. The impact of the different actuators is investigated. First a speaker is studied. A dynamic analysis reveals how the dissipative component in the model which arises from the controlled actuator is formed and the criteria for stability that depend on the controller parameters, the sensor/actuator locations, and the combustor parameters, are found for different configurations. An energy analysis is then carried out to explain how these dissipative terms

are related to work done by/on the speaker. The speaker is found to exchange work with the acoustic field directly, and indirectly through the flame in the burning zone. One can quantify these energy transfers, define their physical origins, and determine the necessary control signals to the actuators for minimizing the acoustic energy in the combustor. An optimization study for the controller is performed based on the physical insight gained from the dynamic analysis of the combustor. A fuel injector is then analyzed dynamically as well as energetically. The work exchange between the injector and the acoustic field is shown to resemble the indirect work exchange between the speaker and the acoustic field, since both actions affect the acoustics through modulating the heat release in the burning zone. The results shed more light on the physics behind the different actuation effects, and emphasize the importance of using this understanding in designing effective actuators and stabilizing optimal controllers [39].

In Chapter 4, control strategies for different combustors situations as well as actuators are presented. Two categories of combustors are considered depending on the mechanism which leads to instability. The first is caused by phase-lag dynamics, typically due to flame area/acoustics velocity interaction, and the second is caused by time-delay effects due to convection of oscillations in the reactants mixture from the mixing section to the burning zone. Diverse model-based control methodologies are presented for each case. In general, optimal linear control techniques, e.g., LQG, have shown to be successful in situations without convective time delay [37]. For systems with delays, model-based control methodologies which exploit the time-delay nature of the system are employed. A Posi-Cast controller is shown to be successful for multi-mode combustor models with arbitrary location of the fuel injector [40]. The controllers are also shown to stabilize an experimental test-rig as well as explain controlled situations in actual combustors. Limitations in the form of bandwidth and control authority, especially for injectors, have plagued combustion control. Injector's location, bandwidth, nonlinearities in the form of two-position injectors and saturation are investigated and compared to actual combustion system observations.

In Chapter 5, experiments are carried out on a 1 kW combustor rig at MIT to investigate the cause of limit-cycles in the combustion system. Measurements reveal that a change in phase between oscillations in the heat-release and the growing perturbations in the ve-

locity is the cause of the limit-cycling nonlinearity. Nonlinear models based on the flame kinematics are proposed, and nonlinearities causing the limit-cycling behavior are shown to depend on the nonlinear heat-release dynamics rather than on the nonlinear acoustics as suggested in [18]. The nonlinear heat release model introduces phase-lag dynamics between the heat-release and the velocity oscillations similar to the measurements in the experiment. Phenomenological reduced-order nonlinear models amenable for model-based control design are suggested and are shown to predict the change in phase nonlinearity and exhibit limit cycles. Linear control is shown to stabilize the nonlinear combustor through analysis and simulation. Saturation in the controlled input is studied and its effect on the controlled combustor is discussed.

6.2 Current and Proposed Future Work

A natural continuation on the heat-release models presented in this thesis is the inclusion of: (1) liquid-fuel combustion dynamics which is governed by atomization, dispersion, evaporation and burning, and (2) fluid dynamics typical of turbulent propulsion systems accompanied by large-scale vortical structures, recirculation zones, and turbulent mixing. A physical-based modeling as well as system ID experiments can be implemented to derive an accurate model.

A physical understanding of the nonlinearities leading to limit cycles is needed. While experimental measurements have been carried out in this thesis and have shown that a phase change between the heat release and the growing acoustic velocity is a plausible mechanism of nonlinearity, the physics behind it are still to be investigated and modeled. This can be achieved through experiments or full-scale CFD simulations.

Open-loop control techniques which exploit the dynamics in the combustion system are very attractive means for suppressing the instability. Open-loop injection of secondary fuel for control at much lower frequencies than the instability frequency has shown to succeed [82]. Currently, we are investigating the physics causing this procedure to work using the combustor model presented in Chapter 3 [78].

Bibliography

[1] B. D. O. Anderson and John B. Moore. *Optimal Control: Linear Quadratic Methods.* Prentice Hall, Englewod Cliffs, N. J., 1990.

[2] J.D.. Anderson. *Fundamentals of Aerodynamics.* McGraw-Hill, Inc., New York, 1991.

[3] A. M. Annaswamy, O. El-Rifai, M. Fleifil, J. P. Hathout, and A. F. Ghoniem. A model-based self-tuning controller for thermoacoustic instability. *Combustion Science and Technology*, 135:213–240, 1998.

[4] A. M. Annaswamy, M. Fleifil, J. P. Hathout, and A. F. Ghoniem. Impact of linear coupling on the design of active controllers for thermoacoustic instability. *Combust. Sci. Tech.*, 128:131–180, 1997.

[5] A. M. Annaswamy, M. Fleifil, J. Rumsey, R. Prasanth, J. P. Hathout, and A. F. Ghoniem. Thermoacoustic instability: Model-based optimal control and experimental validation. *Submitted to IEEE Control Systems Technology*, 1999.

[6] G.A. Baker and P Graves-Morris. *Padé Approximants.* 2nd edition, Cambridge University Press, 1996.

[7] S. A. Billings, H. B. Jamaluddin, and S. Chen. Properties of neural networks with applications to modelling non-linear dynamical systems. *International Journal of Control*, 55(1):193–224, 1992.

[8] G. Billoud, M. A. Galland, C. Huynh Huu, and S. Candel. Adaptive active control of combustion instabilities. *Combust. Sci. and Tech.*, 81:257–283, 1992.

[9] G. J. Bloxsidge, A. P. Dowling, N. Hooper, and P. J. Langhorne. Active control of an acoustically driven combustion instability. *Journal of Theoretical and Applied Mechanics*, supplement to vol. 6, 1987.

[10] G.J. Bloxsidge, A.P. Dowling, N. Hooper, and P.J. Langhorne. "Active control of reheat buzz.". *AIAA Journal*, 26, No. 7, July 1989.

[11] B. J. Brunell. "A system identification approach to active control of thermoacoustic instabilities". In *S.M. Thesis*, MIT, Cambridge, MA, 2000.

[12] A.E. Bryson, Jr., and Y.C. Ho. *Applied Optimal Control.* Blaisdell Publishing Company, Waltham, Massachusetts, 1969.

[13] S.M. Candel. "Combustion instabilities coupled by pressure waves and their active control". *The twenty-fourth (International) Symposium on Combustion*, pages 1277–1296, 1992.

[14] J. M. Cohen. *Private Communication*, 2000.

[15] J. M. Cohen, N. M. Rey, C. A. Jacobson, and T. J. Anderson. "Active control of combustion instability in a liquid-fueled low-NO_x combustor". *ASME 98-GT-267, ASME/IGTI, Sweden*, 1998.

[16] J. Le Conte. -. *Philosop. Mag.*, page HP. 235, 1958.

[17] L. Crocco and S.L. Cheng. *Theory of combustion instability in liquid propellant rocket motors.* Butterworths Science Publication, 1956.

[18] F.E.C. Culick. "Non-linear growth and limiting amplitude of acoustic oscillations in combustion chambers". *Combustion Science and Technology*, 3:1–16, 1971.

[19] A. P. Dowling. Nonlinear acoustically-coupled combustion oscillations. *2nd AIAA/CEAS Aeroacoustics Conference*, May 6-8 1996.

[20] A. P. Dowling. Nonlinear self-excited oscillations of a ducted flame. *AIAA Aeroacoustics Conference*, State College, PA, 1996.

[21] A.P. Dowling. "Nonlinear self-excited oscillations of a ducted flame". *Journal of Fluid Mechanics*, 1998.

[22] A.P. Dowling. "A kinematic model of of a ducted flame". *Journal of Fluid Mechanics*, 394:51–72, 1999.

[23] A.P. Dowling and J.E. Ffowcs-Williams. *Sound and Sources of Sound.* Ellis Horwood Limited, West Sussex, PO191EB, England, 1983.

[24] M. Faraday. -. *Journal of Science and the Arts*, 5:274, 1918.

[25] M. Fleifil, A. M. Annaswamy, Z. Ghoniem, and A. F. Ghoniem. Response of a laminar premixed flame to flow oscillations: A kinematic model and thermoacoustic instability result. *Combust. Flame*, 106:487–510, 1996.

[26] M. Fleifil, A.M. Annaswamy, J.P. Hathout, and A.F. Ghoniem. A model-based active control design for thermoacoustic instability. Technical report, Adaptive Control Laboratory, MIT, Cambridge, MA, 1996.

[27] M. Fleifil, J. P. Hathout, A. M. Annaswamy, and A. F. Ghoniem. The origin of secondary peaks with active control of thermoacoustic instability. *Combustion, Science, and Technology*, 133:227–265, 1998.

[28] M. Fleifil, J.P. Hathout, Annaswamy A.M., and A.F. Ghoniem. "The origin of secondary peaks with active control of thermoacoustic instability". In *Proceedings of the AIAA Joint Propulsion Conference*, Seattle, WA, July 1997.

[29] M. Fleifil, J.P. Hathout, A.M. Annaswamy, and A.F. Ghoniem. "Reduced order modeling of heat release dynamics and active control of time-delay instability". *AIAA 2000-0708, 38th AIAA Aerospace Sciences Meeting, Reno, NV, 10-13 January 2000.*

[30] M. Fleifil, J.P. Hathout, S. Park, A.M. Annaswamy, and A.F. Ghoniem. "Nonlinear flame dynamics and limit cycles in combustion instability". *Combustion and Flame, (In preparation)*, 2000.

[31] Y-T. Fung and V. Yang. Active control of nonlinear pressure oscillations in combustion chambers. *Journal of Propulsion and Power*, Vol. 8, No. 6:1282–1289, 1992.

[32] Y.-T. Fung, V. Yang, and A. Sinha. Active control of combustion instabilities with distributed actuators. *Combust. Sci. and Tech.*, 78:217–245, 1991.

[33] A. Gulati and R. Mani. "Active control of unsteady combustion-induced oscillations". In *28th Aerospace Sciences Meeting*, pages AIAA–90–0270, Washington, D.C., January 1990. American Institute of Aeronautics and Astronautics.

[34] A. Gulati and R. Mani. Active control of unsteady combustion-induced oscillations. *Journal of Propulsion and Power*, 8(5):1109–1115, 1992.

[35] E. Gutmark, T. P. Parr, K. J. Wilson, D. M. Hanson-Parr, and K. C. Schadow. Closed-loop control in a flame and a dump combustor. *IEEE Control Systems*, 13:73–78, April 1993.

[36] C. Hantschk, J. Hermann, and D. Vortmeyer. "Active instability control with direct drive servo valves in liquid-fuelled combustion systems". In *Proceedings of the International Symposium on Combustion*, Naples, Italy, 1996.

[37] J. P. Hathout, A. M. Annaswamy, M. Fleifil, and A. F. Ghoniem. Model-based active control design for thermoacoustic instability. In *Combustion Science and Technology*, volume 132, pages 99–138, 1998.

[38] J. P. Hathout, A. M. Annaswamy, and A. F. Ghoniem. Control of combustion instability using fuel injection. In *AVT Nato Conference*, Braunschweig, Germany, May 8-12 2000.

[39] J. P. Hathout, M. Fleifil, A. M. Annaswamy, and A. F. Ghoniem. Role of actuation in combustion control. In *1999 IEEE CCA/CACSD*, Hawai'i, August 22-27 1999.

[40] J. P. Hathout, M. Fleifil, A. M. Annaswamy, and A. F. Ghoniem. Heat-release actuation for control of mixture-inhomogeneity-driven combustion instability. In *28th International Symposium on Combustion*, Edinburgh University, Scotland, July 30 - August 4 2000.

[41] J.P. Hathout, A.M. Annaswamy, M. Fleifil, and A.F. Ghoniem. "A model-based active control design for thermoacoustic instability". In *ASME International Mechanical Engineering Congress and Exposition*, Dallas, Texas, November 1997.

[42] J.P. Hathout, M. Fleifil, A.M. Annaswamy, and A.F. Ghoniem. Experimental investigation of hysteresis and its potential for control in the mit combustor. Technical Report 9901, Adaptive Control Laboratory/Reactive Gas Dynamics Laboratory, Department of Mechanical Engineering, M.I.T., 1999.

[43] K. Ichikawa. Frequency-domain pole assignement and exact model-matching for delay systems. *Int. J. Control*, 41:1015–1024, 1985.

[44] K. Kailasanath, J. H. Gardner, E. S. Oran, and J. P. Boris. "Numerical simulation of unsteady reactive flows in a combustion chamber". *Combustion and Flame*, 86:115–134, 1991.

[45] J.O. Keller, L. Vaneveld, D. Koochlet, G.L. Hubbard, A.F. Ghoniem, J.W. Daily, and A.K. Oppenheim. "Mechanisms of instabilities leading to flashback". *AIAA Journal*, 20:254–262, 1982.

[46] D.W. Kendrick, T.W. Zsak, and E.E. Zukowski. *"An Experimental and Numerical Investigation of Premixed Combustion in a Vortex in a Laboratory Dump Combustor"- Unsteady Combustion.* Kluwer Academic Publishers, 1996.

[47] P. Knoop, F.E.C. Culick, and E. E. Zukoski. Extension of the stability of motions in a combustion chamber by nonlinear active control based on hysteresis. *Short Communication, Combustion, Science, and Technology*, 123:363–376, 1997.

[48] W. Lang, T. Poinsot, and S. Candel. Active control of combustion instability. *Combustion and Flame*, 70:281–289, 1987.

[49] P. J. Langhorne, A. P. Dowling, and N. Hooper. Practical active control system for combustion oscillations. *Journal of Propulsion and Power*, 6(3):324–333, 1990.

[50] T. Lieuwen, Y. Neumeir, and B.T. Zinn. "The role of unmixedness and chemical kinetics in driving combustion instabilities in lean premixed combustors". *Combustion Science and technology*, 135:193–211, 1998.

[51] T. Lieuwen and B.T. Zinn. "The role of equivalence ratio oscillations in driving combustion instabilities in low NO_x gas turbines". *The Twenty Seventh International Symposium on Combustion*, pages 1809–1816, 1998.

[52] Lennart Ljung. *System Identification: Theory for the User.* Prentice-Hall, Englewood Cliffs, NJ, 1987.

[53] J.C. Magill, M. Bachmann, and K.R. McManus. Combustion instabilitydynamics and control in liquid-fueled direct injection systems suppression in liquid-fueled combustors. *38th Aerospace Sciences Meeting and Exhibit*, AIAA-2000-1022, 2000.

[54] A.Z. Manitius and A.W. Olbrot. Finite spectrum assignement problem for systems with delays. *IEEE Transactions on Automatic Control*, AC-24 no. 4, 1979.

[55] K. R. McManus and J. C. Magill. Control of thermo-acoustic instabilities using pulse width modulation. *Proceedings of the 1997 IEEE Int'l Conf. on Control Applications*, pages 824–829, 1997.

[56] K. R. McManus, U. Vandsburger, and C. T. Bowman. Combustor performance enhancement through direct shear layer excitation. *Combustion and Flame*, 82:75–92, 1990.

[57] K.R. McManus, T. Poinsot, and S.M. Candel. A review of active control of combustion instabilities. *Progress in energy and combustion science*, 19(1):1–30, 1993.

[58] L. Meirovitch. *Elements of Vibration Analysis (Second Edition).* McGraw-Hill, Inc., NY, 1986.

[59] S. Menon and W.-H Jou. Simulation of ramjet combustor flow fields. Part 1 - Numerical model, large scale and mean motions. AIAA-87-1421, 1987.

[60] R. Mongia, R. Dibble, and J. Lovett. "Measurement of air-fuel ratio fluctuations caused by combustor driven oscillations". *ASME paper 98-GT-304*, 1998.

[61] R. M. Murray, C. A. Jacobson, A. I Khibnik, Jr. C. R Johnson, R. Bitmead, A. A Peracchio, and W. M. Proscia. "System identification for limit cycling syatems: A case study for combustion instabilities". *ASME Gas Turbine and Aerospace Congress*, 1998.

[62] S. Murugappan, S. Acharya, E. Gutmark, and T. Messine. "Active control of combustion instabilities in spray combustion with swirl". *AIAA-2000-1026, 38th AIAA Aerospace Sciences Meeting, Reno, NV*, 2000.

[63] S. Murugappan, S. Park, A.M. Annaswamy, and A.F. Ghoniem. "Optimal control design for a swirl-stabilized combustor using system identification methods". Technical report, MIT, Cambridge, MA, April 2000.

[64] H.M. Najm and A.F. Ghoniem. "Modeling pulsating combustion in vortex stabilized pre-mixed flames". *Combustion Sci. Tech.*, 94:259–278, 1993.

[65] P.A. Nelson and S.J. Elliott. *Active Control of Sound.* Academic Press, London, England, 1994.

[66] Y. Neumeier and B.T. Zinn. Active control of combustion instabilities using real time identification of unstable combustor modes. In *Proceedings of the IEEE Conference on Control Applications*, pages 691–698, Albany, NY, 1995.

[67] S. I. Niculescu. Some remarks on second order system including restoring delays. In *Private communication*, 1999.

[68] S. I. Niculescu and A. M. Annaswamy. A simple adaptive controller for positive-real systems with time-delay. In *The American Control Conference in Chicago, IL., (to appear)*, February 2000.

[69] S. I. Niculescu, A.M. Annaswamy, J.P. Hathout, and A.F. Ghoniem. Control of time-delay induced instabilities in combustion systems. In *IEEE, CDC conference (in review)*, 2000.

[70] S. I. Niculescu, E. I. Verriest, L. Dugard, and J. M. Dijon. Stability and robust stability of time-delay systems: A guided tour. In *Stability and Control of Time-Delay Systems*, London, 1997. (L. Dugard and E.I. Verriest, Eds.), LNCIS, Springer-Verlag.

[71] K. Ogata. *Modern Control Engineering.* Third Edition, Prentice Hall, Inc., NJ, 1997.

[72] R. Ortega and R. Lozano. Globally stable adaptive controller for systems with delay. *International Journal of Control, Vol. 47, No. 1, pp 17-23*, 1988.

[73] Rijke P. -. *Ann. phys.*, Lpz 107:339, 1959.

[74] A. A. Peracchio and W. Proscia. Nonlinear heat release/acoustic model for thermoacoustic instability in lean premixed combustors. In *ASME Gas Turbine and Aerospace Congress*, Sweden, 1998.

[75] T. Poinsot, F. Bourienne, S. Candel, and E. Esposito. Suppression of combustion instabilities by active control. *Journal of Propulsion and Power*, 5(1):14–20, 1989.

[76] T. J. Poinsot and S. M. Candel. A nonlinear model for ducted flame combustion instabilities. *Combustion Science and Technology*, 61:121–153, 1988.

[77] T. J. Poinsot, A. C. Trouve, D. P. Veynante, S. M. Candel, and E. J. Esposito. Vortex-Driven acoustically coupled combustion instabilities. *Journal of Fluid Mechanics*, 177:265–292, 1987.

[78] R. Prasanth, A.M. Annaswamy, J.P. Hathout, and A.F. Ghoniem. "When do open-loop strategies for combustion control work?". (In preparation), 2000.

[79] A.A. Putnam. *Combustion Driven Oscillations in Industry.* American Elsevier Pub. Co., NY, 1971.

[80] J.W.S. Rayleigh. "The explanation of certain acoustical phenomena". *Nature*, 18:319–321, 1878.

[81] J.W.S. Rayleigh. *The Theory of Sound*, volume 2. Dover, New York, 1945.

[82] G. A. Richards, M. C. Yip, and E. H. Rawlins. Control of flame oscillations with equivalence ratio modulation. *Journal of Propulsion and Power*, 15:232–240, 1999.

[83] G.A. Richards, M.C. Yip, E. Robey, L. Cowell, and D. Rawlins. Combustion oscillation control by cyclic fuel injection. *Journal of Engineering for Gas Turbines and Power*, 119:1–4, 1997.

[84] G.A. Richards and M.J. Yip. Oscillating combustion from a premix fuel nozzle. *The Combustion Institute/American Flame Research Committee Meeting, San Antonio TX*, 1995.

[85] J. Rumsey, M. Fleifil, A.M. Annaswamy, and A.F. Ghoniem. "Low order nonlinear models for thermoacoustic instability". In *Proceedings of the Conference on Control Applications*, Trieste, Italy, August 1998.

[86] H. Schlichting. *Boundary-Layer Theory.* McGraw-Hill Book Company, 1968.

[87] J.R. Seume, N. Vortmeyer, W. Krause, J. Hermann, C.-C Hantschk, P. Zangl, S. Gleis, and D. Vortmeyer. "Application od active combustion instability control to a heavy duty gas turbine". In *Proceedings of the ASME-ASIA*, Singapore, 1997.

[88] S. Sivasegaram and J. H. Whitelaw. Active control of oscillations in combustors with several frequency modes. In *Proceedings of the ASME Winter Annual Meeting*, Anaheim, CA, 1992.

[89] J.-J. E. Slotine and W. Li. *Applied Nonlinear Control.* Prentice Hall, Englewood Cliffs, NJ, 1991.

[90] O.J. Smith. "A controller to overcome dead time". *ISA Journal*, 6, 1959.

[91] G. Stein and M. Athans. The LQG/LTR procedure for multivariable feedback control design. *IEEE Transactions on Automatic Control*, 32:105–114, 1987.

[92] D. Thibaut and S. Candel. "Numerical study of unsteady turbulent premixed combustion: Application to flashback simulation". *Combustion and Flame*, 113:53–65, 1998.

[93] J. E. Tierno and J. C. Doyle. Multimode active stabilization of a Rijke tube. In *DSC-Vol. 38.* ASME Winter Annual Meeting, 1992.

[94] T.Y. Toong. *Combustion Dynamics: The Dynamics of Chemically Reacting Fluids.* McGraw-Hill Book Company.

[95] J. Tyndal. *Sound.* D. Appleton & Company, New York, 1897.

[96] K.K. Venkataraman, L.H. Preston, D.W. Simons, B.J. Lee, J.G. Lee, and D.A. Santavicca. "A study of the mechanism of combustion instability in a lean premixed dumb combustor". *Submitted to the Journal of Power and Propulsion*, 1998.

[97] B. Widrow and S.D. Stearns. *Adaptive signal processing.* Prentice-Hall, Inc., Englewood Cliffs, N.J., 1985.

[98] F.A. Williams. *Combustion Theory.* Addison-Wesley Co., Reading, MA, 1965.

[99] W.A. Wolovich. *Linear Multivariable Systems.* Springer Verlag, Berlin, 1974.

[100] V. Yang, A. Sinha, and Y.-T. Fung. State feedback control of longitudinal combustion instabilities. *Journal of Propulsion and Power*, 8, 1992.

[101] K. Yu, K.J. Wilson, and K.C. Schadow. Active combustion control in a liquid-fueled dump combustor. In *35th Aerospace Sciences Meeting and Exhibit*, pages AIAA 97–0462, Reno, NV, 1997.

[102] K. Yu, K.J. Wilson, and K.C. Schadow. Scale-up experiments on liquid-fueled active combustion control. In *34th AIAA/ASME/SAE/ASEE Joint Propulsion Conference*, pages AIAA 98–3211, Cleveland, OH, 1998.

[103] B.T. Zinn. *Pulsating combustion. Advanced Combustion Methods.* Academic Press Inc. (London) LTD., London, 1986.